UNIVERSITÀ
DEGLI STUDI
DI PADOVA

Sede Amministrativa: Università degli Studi di Padova

Dipartimento di Ingegneria Civile, Edile e Ambientale (ICEA)

SCUOLA DI DOTTORATO DI RICERCA IN:
SCIENZE DELL'INGEGNERIA CIVILE ED AMBIENTALE
XXVII CICLO

CATCHMENT TRANSPORT AND TRAVEL TIME DISTRIBUTIONS: THEORETICAL DEVELOPMENTS AND APPLICATIONS

Direttore della Scuola: Ch.mo Prof. Stefano Lanzoni

Supervisori: Ch.mo Prof. Andrea Rinaldo

Ch.mo Prof. Gianluca Botter

Dottorando: Paolo Benettin

30 Gennaio 2015

Abstract

The fate of water and solutes introduced into a watershed and sampled at the catchment outlet depends on a number of factors that include the underlying climatic forcing and the heterogeneity of subsurface environments. After a storm event, the hydrologic response of a watershed is known to rapidly displace large amounts of water that had been contained in the system storage prior to the arrival of the storm. The actual time spent by non-event water particles within the catchment spans a large range of timescales and typically exceeds the characteristic times of the hydrologic response by at least two orders of magnitude. Inferring water age is crucial for our understanding of streamflow generation and catchment-scale dispersion processes. Water travel time distributions can be used to address a number of environmental challenges, such as modeling the dynamics of river water quality, quantifying the interactions between shallow and deep flow systems and understanding nutrient loading persistence. The need for robust yet simple mathematical tools to describe water age dynamics is here addressed using a catchment-scale approach. In this context, water particles can be seen as a dynamic population whose evolution can be described through suitable partial differential equations. Novel theoretical solutions are here proposed, with extensive applications to real-world case studies that include the transport of chloride, isotopic content and silica. Coupling transport models to high-quality hydrochemical datasets allows for inferences on water age distributions and proves able to explain different features of measured water quality dynamics. The applications allowed an improved understanding of the underlying transport processes and many further developments can be foreseen along the path here pursued, inching towards a watershed theory.

Sommario

Le dinamiche dell'acqua e dei soluti introdotti nei bacini idrografici e campionati alle rispettive sezioni di chiusura dipende da numerosi fattori, tra cui l'influenza del clima e l'eterogeneità dell'ambiente sotterraneo. In seguito a un evento di precipitazione, la risposta idrologica di un bacino innesca lo spostamento di volumi di acqua che in gran parte si trovavano già immagazzinati nel sottosuolo prima dell'inizio della precipitazione. Il tempo da cui tali particelle d'acqua si trovavano nel bacino può variare su un ampio intervallo di scale temporali e tipicamente supera i tempi caratteristici della risposta idrologica di almeno due ordini di grandezza. La stima dell'età dell'acqua ricopre notevole importanza nella comprensione dei meccanismi di deflusso e di dispersione alla scala di bacino. Le distribuzioni dei tempi di residenza, utilizzate in questa tesi, possono essere utilizzate per affrontare numerosi problemi ambientali, tra cui la modellazione idrochimica dei corsi d'acqua, la quantificazione degli apporti di deflusso superficiali o profondi e la stima della persistenza dei nutrienti nelle acque. La necessità di disporre di strumenti matematici semplici e robusti viene qui affrontata utilizzando un approccio a scala di bacino. In tale contesto, le particelle d'acqua si possono vedere come una popolazione dinamica che evolve nel tempo e descrivibile mediante opportune equazioni differenziali. Questa tesi propone nuovi sviluppi teorici e molteplici applicazioni a casi di studio reali, tra cui il trasporto di cloruri, deuterio e silice. Associando modelli di trasporto a misure idrochimiche è possibile ottenere una stima delle distribuzioni dei tempi di residenza, permettendo di spiegare diverse caratteristiche delle dinamiche dei soluti nei corsi d'acqua. Le applicazioni hanno consentito una migliore comprensione dei processi di trasporto a scala di bacino e segnano la strada verso ulteriori sviluppi orientati a una teoria generale del bacino.

Contents

List of Figures

List of Tables

Chapter 1

Introduction

This thesis investigates novel developments in the formulation of transport by travel time distributions and proposes theoretical advances (Chapters 2 and 3) as well as applications to real-world transport problems (Chapters 4, 5 and 6).

Travel time distributions (TTDs) are key descriptors of catchment-scale transport processes as they provide fundamental information on water storage dynamics, flow pathway heterogeneity, sources of water in space and time within a catchment and on the chemistry of water flows through the outlet. The early formulation of the so-called old-water paradox first recognized that a notable part of the streamflow released in response to a given rainfall event is supplied by water volumes already in storage within the catchment prior to the event. Since that time, the issue of the age of runoff water has attracted many theoretical and observational studies [*Rinaldo and Marani*, 1987; *Rinaldo et al.*, 1989; *Beven*, 2010, 2012; *Weiler et al.*, 2003; *Kirchner*, 2003] and the spate of papers dedicated to the subject was justified by the true paradigm shift implied by the role of non-event water.

The age of streamflow strongly impacts the chemical composition of river flows as it reflects the memory of hydrologic systems to rainfall or soil moisture compositions and is thus crucial for our understanding and modeling of the chemical composition of runoff waters. The issue has long been disregarded by hydrologists dealing with the quantification of input/output water fluxes, and has now rightfully become a cornerstone of hydro-chemical studies. Typical applications include both atmospheric compounds entering the catchment through precipitation [*Shaw et al.*, 2008; *Godsey et al.*, 2010] or anthropogenic compounds injected onto the catchment e.g. due to farming activities [e.g. *Basu et al.*, 2010; *Rouxel et al.*, 2011; *Kennedy et al.*, 2012]. The emerging need for tracking the time spent by water particles traveling through a catchment brought mul-

tifaceted implications, including the identification of flow pathways, catchment storage capacity, water quality and bio-geochemistry [*McGlynn et al.*, 2003; *Liu et al.*, 2004; *McGuire and McDonnell*, 2006; *McGuire et al.*, 2007; *McDonnell et al.*, 2010].

While early studies focused on data-driven, parametric identifications of average travel time distributions, the recent developments explicitly incorporated the time-variability of climatic conditions [*Hrachowitz et al.*, 2010; *Brooks et al.*, 2010], topographic controls [*McGuire et al.*, 2005] and the spatial heterogeneity of soil properties [*Fiori and Russo*, 2008; *Russo and Fiori*, 2009]. The need for new tools that can capture the dynamic nature of catchments has led to the development of novel theoretical formulations [*Botter et al.*, 2010, 2011; *Rinaldo et al.*, 2011; *van der Velde et al.*, 2012; *Hrachowitz et al.*, 2013; *Benettin et al.*, 2013a; *Harman*, 2014] and a number of time-variant approaches for estimating water age in real-world applications [*van der Velde et al.*, 2010a; *Birkel et al.*, 2012; *McMillan et al.*, 2012; *Davies et al.*, 2013; *Benettin et al.*, 2013b; *Harman and Kim*, 2014]. One of the key results of these new approaches is that instantaneous travel time distributions are intrinsically non-smooth curves. Their erratic character stems from the vagaries of nature in injection, retention and leaching to streamflow, and could be captured by analytic descriptions that employ in- and out-fluxes as forcings.

The increased availability of hydrochemical data, jointly with the improved measurement accuracy, makes it feasible to overcome the simplistic modeling of long-term transport features, allowing to focus on transient dynamics and fluctuations taking place at multiple time-scales, from single storm events to inter-annual timescales. The methodological procedure comparing chemical and hydrological data with the novel conceptual framework represents an interesting advancement of our understanding of catchment-scale transport processes.

Chapter 2

A Novel kinematic framework

2.1 Introduction

In recent years, several papers contributed to the development and clarification of key theoretical issues underlying the formulation of transport by travel time distributions. In this context, important theoretical and practical implications arise from a proper distinction between backward or forward age distributions, which are based on the definition of diverse reference variables. The 'age' of a water particle represents the time elapsed since a previous injection, and as such it is intrinsically a backward concept. A forward approach, instead, requires the introduction of the particle's 'life expectancy', which quantifies the time a water particle will spend within the system before being sampled by one of the outflows. The sum of age and life expectancy is the particle's travel time.

Despite forward and backward approaches are different, and only coincide in the special case of stationary systems, a proper distinction of these formulations has been sometimes overlooked in the literature. In this contribution, the recent backward formulations is reviewed using a unified notation and a novel forward formulation is discussed. The note illustrates how age and life expectancy distributions naturally evolve in response to unsteady hydrologic fluxes.

The concept of travel time distributions (TTDs) was initially developed for chemical reactors [*Danckwerts*, 1953; *Nauman*, 1969; *Chen*, 1971; *Niemi*, 1977] using both forward and backward TTDs, but the approach mostly focused on the distributions that characterize the outflows of a system, leaving the time distributions of the water storage unexplored. The forward-backward issue was later refined by *Cornaton and Perrochet* [2006], who defined the governing age and life expectancy equations for spatially-explicit

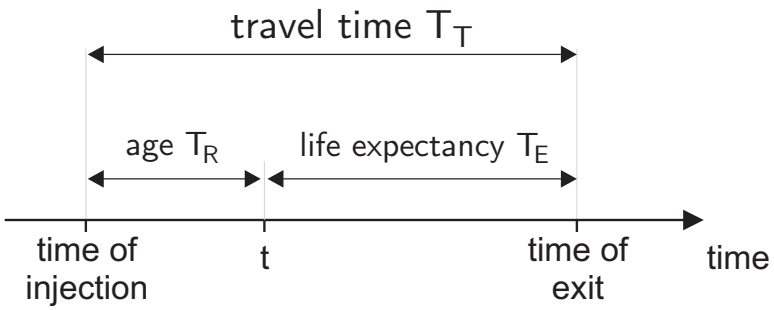

Figure 2.1: Definition of the time variables.

frameworks governed by advection and dispersion. At catchment scales, the relationship between backward and forward distributions has remained mostly unexplored (for notable exceptions see [e.g. *Cvetkovic et al.*, 2012]). A coherent formulation which makes use of catchment-scale forward distributions is still missing in the literature and is here addressed by coupling age to life expectancy for the water particles that reside within the catchment storage. This theoretical clarification is necessary to properly interpret tracer/solute data, and can be useful to develop models and drive experimental design.

2.2 Tracking age and life expectancy

The evolution of a water population within a catchment intimately depends on the forcing in- and out-fluxes and on the (complex) structure of the velocity field that characterizes the system at any time. Time tracking is useful to identify water particles with common features (e.g. those that enter/leave the catchment at the same time) and requires the use of precise definitions and notation. Absolute time is here indicated with the lowercase symbol t, while time intervals are all indicated with capital T. Let us follow a water particle that enters the catchment at a time $t = t_{in}$ and exits at a later time $t = t_{ex}$. At any time t the parcel is characterized by two fundamental properties: its age (or residence time), indicated as T_R, which is defined as the time elapsed since the entrance, and its life expectancy (or time to destination), indicated as T_E, which is the time remaining before getting to an outlet. The sum of age and life expectancy is the particle's travel time (or transit time) through the system (Figure 2.1):

$$T_T = T_R + T_E \,. \tag{2.1}$$

It follows from these definitions that the travel time can be seen either as the life expectancy at the entrance (when T_R=0) or as the age at the exit (when T_E=0). Age

is intrinsically a backward concept, as it is defined with respect to a previous time. Life expectancy, instead, is intrinsically a forward concept [*Nauman*, 1969; *Cvetkovic et al.*, 2012], as it is computed with respect to a later time. As the travel time can be either seen as a special case of age or life expectancy, it can be seen from both a forward and a backward perspective.

Hydrologic fluxes and storage are defined with respect to a control volume (CV). The CV definition can be sometimes uncertain because the subsurface environment is partially unknown and the flow field can change with time. Typical examples of hydrologic CVs can be a hillslope draining to a stream, a soil column in a lysimeter or an entire catchment defined by no-flow borders (Figure 2.2).

When the CV can be satisfactorily defined, the elementary water balance reads:

$$\frac{dS(t)}{dt} = J(t) - ET(t) - Q(t) \tag{2.2}$$

where S is the water in storage and J, ET and Q are precipitation, evapotranspiration and discharge fluxes, respectively. Deep losses are here neglected for simplicity, but can be included in the formulation as well as any other hydrologic in/out flux.

Age and life expectancy can be handled as a property that is transported along with water. Note that the property is not conservative because age increases with time (e.g. every day water particles get one-day older), while life expectancy decreases with time (e.g. every day particles get one-day closer to destination), according to:

$$\frac{dT_R}{dt} = 1\,, \qquad \frac{dT_E}{dt} = -1\,. \tag{2.3}$$

The terms of Eq. (2.3) can be seen as a celerity c with unit value, whose sign determines which property is described. If we denote the probability distribution of a property T (either age or life expectancy) with $p(T,t)$, every term of equation (2.2) can be associated with its distribution: $S \mapsto Sp_S(T,t)$, $J \mapsto Jp_J(T,t)$, $ET \mapsto ETp_{ET}(T,t)$, $Q \mapsto Qp_Q(T,t)$. Once the distributions are introduced, the total derivative at lhs of eq. (2.2) can be developed as:

$$\frac{d\,[S(t)\,p_S(T,t)]}{dt} = \frac{\partial[S(t)\,p_S(T,t)]}{\partial t} + \frac{dT}{dt}\,\frac{\partial[S(t)\,p_S(T,t)]}{\partial T} \tag{2.4}$$

where the term dT/dt at rhs represents the celerity c of propagation of the property and can only assume unit values with positive or negative sign, as prescribed by eq. (2.3). The evolution of the property distribution in the water balance is then completely described by the following equation:

$$\begin{aligned} &\frac{\partial[S(t)\,p_S(T,t)]}{\partial t} + c\,\frac{\partial[S(t)\,p_S(T,t)]}{\partial T} = \\ &J(t)\,p_J(T,t) - ET(t)\,p_{ET}(T,t) - Q(t)\,p_Q(T,t) \end{aligned} \tag{2.5}$$

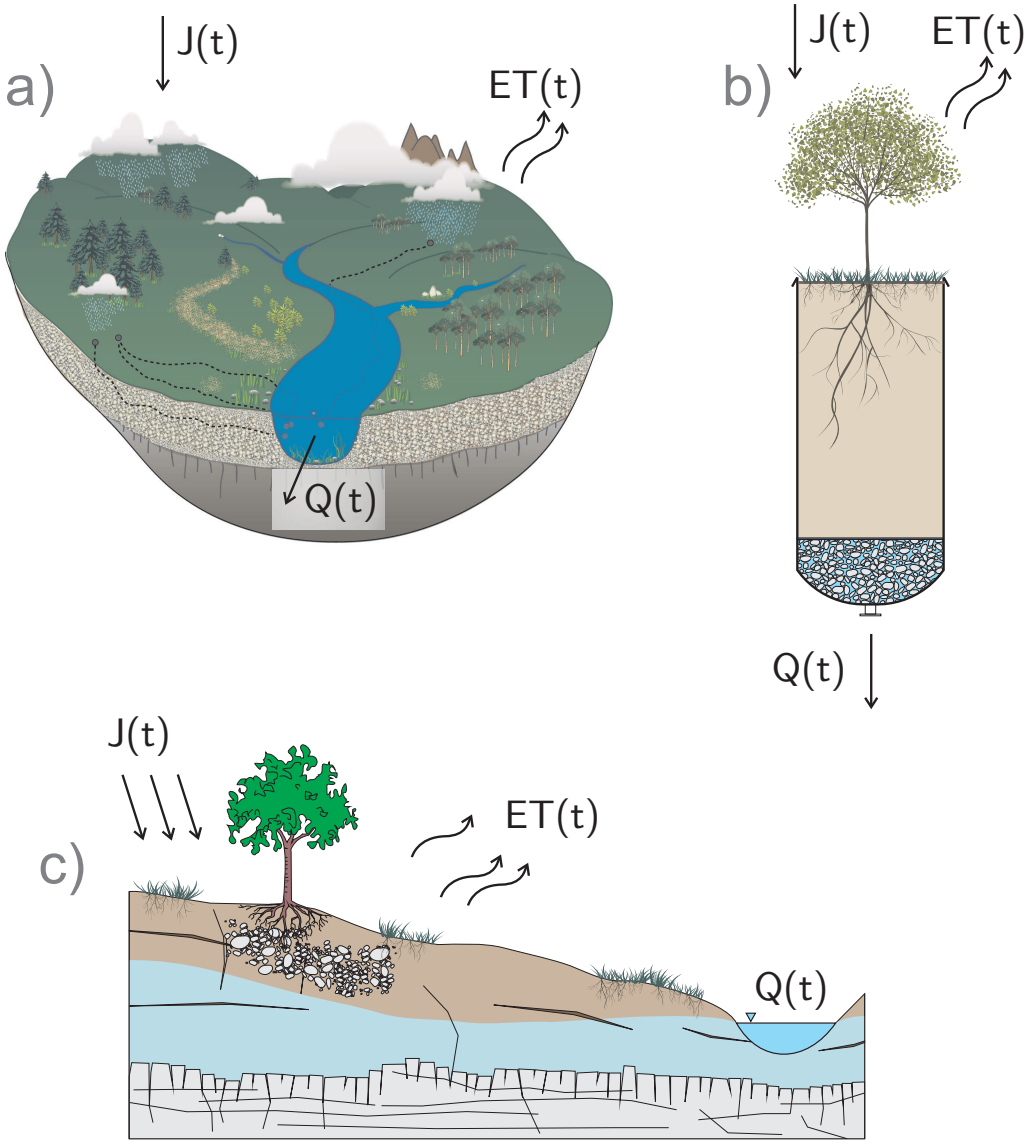

Figure 2.2: Examples of typical control volumes.

Note that a more general form of the equation can be written, where $F_i(t)$ can be any mass flux with its positive or negative sign (possibly including reactive terms) and $p_{F_i}(T,t)$ its property distribution:

$$\frac{\partial[S(t)\,p_S(T,t)]}{\partial t} + c\,\frac{\partial[S(t)\,p_S(T,t)]}{\partial T} = \sum_i F_i(t)\,p_{F_i}(T,t) \tag{2.6}$$

Other forms of eq. (2.6) can be formulated, that use cumulative distributions and do not need an explicit determination of the storage [*Harman*, 2014], but the meaning of the equation remains unchanged.

So far, the most general formulation was used to stress the general character of the processes, and to show that the evolution of ages and life expectancies in a hydrologic system can be described through the same equation. In the following, age and life expectancy equations will be treated separately and focus will be placed on applied concepts.

2.2.1 Backward distributions

The use of backward distributions complies with the problem of how a sample of water taken at a time t is the result of transport processes that involve inputs generated from all previous times.

The mathematical formulation is obtained from equation (2.5) by using $c = 1$ and $T = T_R$. In the notation, a left arrow is added to the distributions to denote their explicit backward character [see *Harman*, 2014]. In most cases precipitation comprises by definition water particles with age zero, hence $\overleftarrow{p}_J(T_R,t)$ turns into a Dirac-delta function centered in $T_R = 0$ which can be removed from the equation to be used as a Dirichlet Boundary Condition. The resulting Master Equation, as first introduced by *Botter et al.* [2011], reads:

$$\frac{\partial[S(t)\,\overleftarrow{p}_S(T_R,t)]}{\partial t} + \frac{\partial[S(t)\,\overleftarrow{p}_S(T_R,t)]}{\partial T_R} = -ET(t)\,\overleftarrow{p}_{ET}(T_R,t) - Q(t)\,\overleftarrow{p}_Q(T_R,t) \tag{2.7}$$

The equation has been extensively studied in the last years [*Botter et al.*, 2011; *Botter*, 2012; *van der Velde et al.*, 2012; *Hrachowitz et al.*, 2013; *Benettin et al.*, 2013b,a; *Harman and Kim*, 2014; *Harman*, 2014] and its physical interpretation is rather intuitive: water particles enter the system through precipitation (BC of the equation) and are gradually depleted by the outflows removal (rhs of eq. 2.7) while they get older (second term at lhs). The equation is illustrated in Figure 2.3.

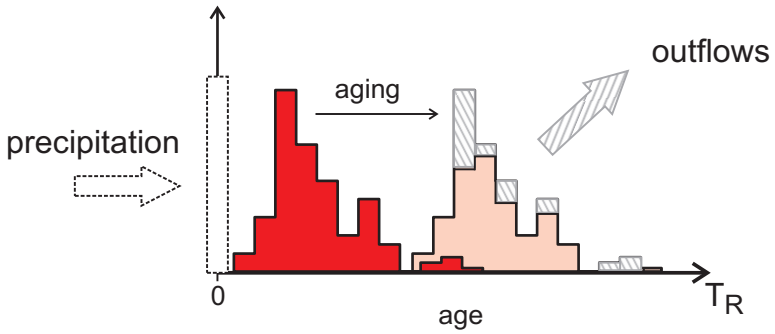

Figure 2.3: Illustration of the Master Equation for the backward TTDs. Water particles enter the system through precipitation (age $T_R = 0$) and move rightwards along the age axis. While ageing, particles are selected by discharge and evapotranspiration and removed from the system.

One implication of Eq. (2.7) is that the age distribution $\overleftarrow{p}_S$ is primarily controlled by the precipitation forcings i.e., mathematically, the BCs. For this reason, the distribution resembles the precipitation timeseries (suitably modulated by the outflows removal) and contains gaps corresponding to dry periods (see Figure 2.3).

A great advantage of using backward distributions is that they allow for a direct representation of tracer concentration in the outflows:

$$C_{out}(t) = \int_0^\infty C_S(T_R)\, \overleftarrow{p}_{out}(T_R, t)\, dT_R \tag{2.8}$$

where the subscript *out* refers to a general outflow (e.g. discharge) and $C_S(T_R)$ is the concentration of particles in storage with age T_R. Eq. 2.8 shows that the outflowing concentration is the result of a composition of parcels of different ages (as evidenced by the TTD) and that every particle brings its own solute contribution. In many cases of interest, the concentrations $C_S(T_R)$ of the resident parcels can be related to their initial concentration C_{in} as $C_S(T_R) = f(T_R)\, C_{in}$ where $f(T_R)$ can be any function of time (e.g. a decay). The particular case of a conservative tracer implies $f(T_R) = 1$, and Eq. 2.8 can be expressed as:

$$C_{out}(t) = \int_0^\infty C_{in}(t - T_R)\, \overleftarrow{p}_{out}(T_R, t)\, dT_R \tag{2.9}$$

Equations (2.8) and (2.9) can be used to compute solute chemographs and to assess the memory of discharge for previous injections of the solute (e.g. fertilizations in agricultural catchments). Note that such memory can be change with time because the trace of older injections might be visible in dry periods only. This behavior can be reproduced by using time-varying backward TTD $\overleftarrow{p}_{out}(T_R, t)$. A numerical example that makes use of Eq. (2.9) is proposed in section 2.4.1.

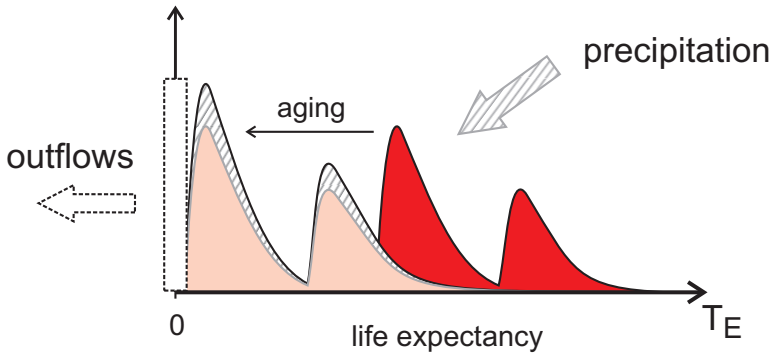

Figure 2.4: Illustration of the Master Equation for the forward TTDs. Water particles with different life expectancies are introduced in the system through new precipitations and move leftwards along the life expectancy axis. When particles reach their destination (hence $T_E = 0$) they are removed from the system by the outflows.

2.2.2 Forward distributions

The forward formulation focuses on life expectancy concepts and complies with the problem of how each water input is transported and dispersed through the system after its injection.

The governing equation is obtained from equation (2.5) by using $c = -1$ and $T = T_E$. In this case a right arrow is used to recall the forward character of the distributions. It is reasonable to assign a null life expectancy $T_E = 0$ to parcels leaving the system, so discharge and evapotranspiration can be removed from eq. (2.5) and be inserted as Dirichlet Boundary Condition, (analogous to precipitation in eq. (2.7)). The resulting Master Equation reads:

$$\frac{\partial[S(t)\,\overrightarrow{p}_S(T_E,t)]}{\partial t} - \frac{\partial[S(t)\,\overrightarrow{p}_S(T_E,t)]}{\partial T_E} = J(t)\,\overrightarrow{p}_J(T_E,t) \tag{2.10}$$

Equation (2.10) represents a rather new concept because it shows that the system evolution can be completely described by forward distributions. The equation can be intuitively interpreted as follows: water particles enter the system with different life expectancies (rhs of Eq. 2.10) because, owing to dispersion processes, particles will reach the system boundaries at different times. While transported along the system, particles' time to destination constantly decreases because all particles get older (second term at lhs, which has negative sign). When the particles reach the outlet, their life expectancy drops to zero as they are removed by the outflows (BC of Eq. 2.10). A graphical representation of Eq.2.10 is provided in Figure 2.4.

Analogous to the age distributions, the life expectancy distribution $\overrightarrow{p}_S(T_E,t)$ is

primarily controlled by the BCs of Eq. (2.10), which in this case correspond to the out-flux $Q(t) + ET(t)$. Hence, the distribution resembles the outflows timeseries and only contains gaps in case evapotranspiration and discharge are null (see Figure 2.3).

The forward travel time distribution can be used to build a tracer breakthrough curve, which is the concentration signal produced at the outlet after the tracer injection. In the case of a conservative solute, the curve reads:

$$C(t) = \frac{M(t)}{Q(t)} = J_0\, C_0 \frac{\overrightarrow{p}_Q\,(t - t_0, t_0)}{Q(t)} \tag{2.11}$$

where t_0 is the time of injection, $M(t)$ the mass flux at the outlet and $J_0\, C_0$ the mass input. The breakthrough curve can be interpreted as the relative contribution of the input J_0 to discharge. As such, it is very different from a TTD (which is the absolute contribution) unless $Q(t)$ is constant in time. The breakthrough curve is easily measurable in a tracer experiment and can be useful to test the theoretical apparatus.

The formulation is somehow more complicated in case one wants to make an explicit distinction among particles that leave the system through different exits. In such a case the problem can be formulated (and solved) by introducing proper partitioning terms $\theta(T_E, t)$ as shown by *Botter et al.* [2010] and *Harman* [2014].

2.2.3 Formulation symmetries

The forward and backward approaches exhibit interesting symmetries, as one formulation can be obtained from the other by simply reversing time and thus the flow field direction [see *Cornaton and Perrochet*, 2006, Figure 1]. Just like pressing a rewind button, in the reversed picture output fluxes become inputs and exit times become entrance times.

Whereas each of the Master Equations (eq. (2.7) and (2.10)) either deals with forward or backward distributions, some relationships can be developed that involve both forward and backward distributions. A first relationship stems from the fact that the travel time of a water particle is the sum of its age and life expectancy (eq. (2.1) and Figure 2.1), which are independent variables. Hence, each distribution of travel times can be obtained from a convolution of age and life expectancy distributions, as:

$$\overrightarrow{p}_Q(T_T, t_{in}) = \int_0^{T_T} \overleftarrow{p}_S(T_R, t_{in} + T_R)\, \overrightarrow{p}_S(T_T - T_R, t_{in} + T_R)\, dT_R \tag{2.12}$$

$$\overleftarrow{p}_Q(T_T, t_{ex}) = \int_0^{T_T} \overrightarrow{p}_S(T_E, t_{ex} - T_E)\, \overleftarrow{p}_S(T_T - T_E, t_{ex} - T_E)\, dT_E \tag{2.13}$$

Equations (2.12) and (2.13) show that i) the convolution structure is the same for the two equations and each integral includes both a backward and a forward distribution, ii) the role played by age in eq. (2.12) is the same as that played by life-expectancy in eq. (2.13), iii) the symmetry between the formulations is preserved and one equation can be obtained from the other by reversing time and the flow direction (t_{in} becomes t_{ex} and T_R becomes T_E).

A useful relationship that links forward and backward travel time distributions is the so-called "Niemi relation" [*Niemi*, 1977; *Botter et al.*, 2010; *Harman*, 2014], which follows from continuity:

$$J(t)\overrightarrow{p}_Q(T,t) = Q(t+T)\overleftarrow{p}_Q(T,t+T) \tag{2.14}$$

Equation (2.14) shows that, in case the system is stationary ($J(t) = Q(t) = const.$), the forward and backward formulations coincide.

2.3 Linking fluxes to storage

The Master Equations (eq. (2.7) and (2.10)) could be solved if distributions in the fluxes were known or could be reasonably assumed. However this is almost impossible in real-world applications because the system evolution is primarily forced by hydrologic fluxes which are naturally erratic and time-variant [*Botter et al.*, 2010]. Moreover, in/outflowing and resident distributions are hardly independent (e.g. if an age is not present in the system, say after a dry period, it cannot be present in the outflows), inducing the need for establishing a dependence of in/outflowing classes of particles on the resident ones. This problem has been solved for backward distributions following two equivalent approaches [*Botter et al.*, 2011; *van der Velde et al.*, 2012], and is here extended to a more general case, which is valid for forward distributions also.

The first approach introduces a functional relation between the distributions (either age or life expectancy) in the fluxes and those in the storage [*Botter et al.*, 2011], expressed by:

$$p_F(T,t) = \omega_F(T,t)\, p_S(T,t)\,, \tag{2.15}$$

where $\omega(T,t)$ are called 'StorAge-Selection' (SAS) functions and can be given any shape provided that they are normalized according to the non-linear constraint:

$$\int_0^\infty p_F(T,t)\, dT = \int_0^\infty \omega_F(T,t)\, p_S(T,t)\, dT = 1 \tag{2.16}$$

which is necessary to ensure that p_F is a probability density function (pdf).

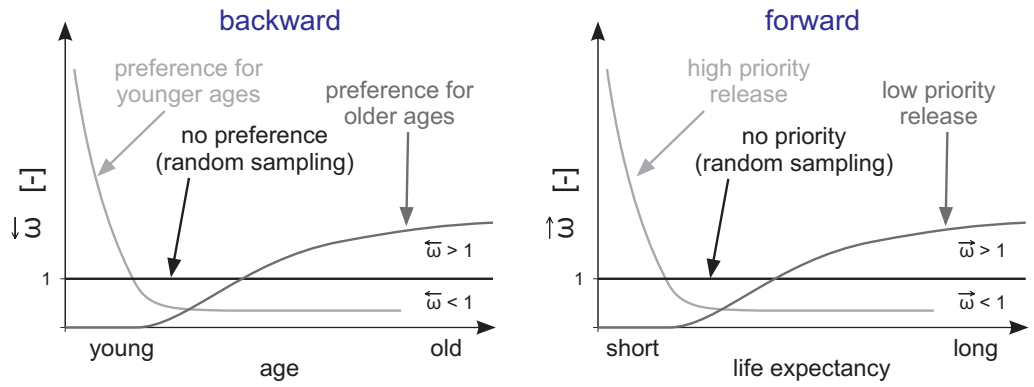

Figure 2.5: Backward and forward StorAge-Selection functions.

The use of Eq. (2.15) has several advantages because it makes the approach consistent with the system mass balance [*Botter*, 2012], basically ensuring that outflows cannot extract more than what is available. The irregular shape of the TTDs is automatically taken into account through the term $p_S(T,t)$, hence one can impose a shape on the SAS function using a smooth curve that is representative of the transport processes involved (see below). Figure 2.5 shows how to interpret different shapes of the SAS functions. In the backward case, SAS functions essentially describe how the outfluxes remove particles among those available within the storage [*Botter et al.*, 2011]. The selection of the particles, based on their age, can have three characteristic shapes: i) preference for younger ages (as e.g. due to preferential pathways like macropores), ii) no preference (random sampling, occurring when mixing and dispersion are enhanced [*Benettin et al.*, 2013a]), iii) preference towards older ages (as e.g. when younger water is present but is hydrologically far from the outlet). In the forward case, instead, the role of the fluxes is switched and the relevant hydrologic flux that is considered is precipitation. The SAS functions are to be interpreted in terms of life expectancy and they basically describe the priority that is given to the particles of the new inputs with respect to the resident particles. The same three shapes that were described for the backward approach can now be interpreted as follows: i) high priority to the new input, which is soon released to the outlets, ii) no priority (random sampling) meaning that the new input and the resident particles are discharged at the same rate, iii) low priority, meaning that the new input has to wait before being released. Note that the name 'StorAge Selection' was originally designed for the backward approach [*Harman*, 2014] and in the forward approach there is no 'selection' anymore, but the term is kept here for simplicity.

The second approach derives suitable TTDs by introducing a transformed domain.

A convenient transformation proposed by *van der Velde et al.* [2012] uses the cumulative storage distribution:

$$T \mapsto P_S(T,t) = \int_0^T p_S(\tau,t)d\tau\,, \tag{2.17}$$

which maps T from its absolute position (e.g. age 5 days or life expectancy 1.2 years) to its relative position in storage (e.g. age that is not exceeded by the 1% of the resident particles or time to destination that is not exceeded by the 70%). The new domain is bounded in $[0,1]$ as implied by the cumulative pdf. The resulting transformed TTD is a derived distribution, hence in the new domain it keeps the properties of a pdf:

$$p_F(T,t)\,dT = p_F^*(P_S,t)\,dP_S \tag{2.18}$$

The transformed domain introduces two major advantages: i) it is focused on the relative position in the storage, which is not affected by the ageing of the particles and allows for a continuous P_S domain even when the absolute T domain contains gaps; ii) all the natural variability of the distributions is accounted for in the change of variables, and p_F^* can be easily parametrized by using smooth pdf's over a bounded domain (e.g. the beta distributions [*van der Velde et al.*, 2012, 2014]). In some circumstances [*Harman*, 2014] even a pdf defined over a semi-infinite domain (like a gamma) can be employed.

The two approaches are fully equivalent because, if the change of variables is applied to the SAS functions, one gets:

$$p_F(T,t)\,dT = \omega_F(T,t)\,p_S(T,t)\,dT = \omega_F^*(P_S,t)\,dP_S \tag{2.19}$$

which implies:

$$p_F^*(P_S,t) \equiv \omega_F^*(P_S,t) \tag{2.20}$$

Hence, the only practical difference between the two approaches relies on the use of a regular or transformed domain for the SAS functions. For this reason and to simplify the notation, I will always refer to SAS functions as ω and will indicate the different domain in the argument of the functions. Alternatively, one can use the terminology aSAS, fSAS and rSAS to refer to the different possible domains, as described by *Harman* [2014]. The meaning of Figure 2.5 applies to all the approaches.

2.4 Numerical examples and implications for water-age modeling

In the following, two simple numerical applications are shown to illustrate some practical consequences of the theory described so far.

2.4.1 Tracer injection experiment

Any tracer injection into a control volume can be seen as a forward experiment where the (forward) travel times of the solute mass can be measured at the system outlet. Typical real-world examples are conducted in fully controlled systems [*Stumpp et al.*, 2009; *Harman and Kim*, 2014] but can be applied to catchment scales in case a distributed injection can be marked with a distinctive tracer.

A synthetic hydrologic system is here modeled where, for the sake of simplicity, discharge is the only outflow. Two different injections are simulated, to evaluate the potential time-variance of the response and the dependence on the climatic forcings. The mass response of the tracer at the system outlet is computed by solving the life-expectancy Master Equation (Eq. (2.10)). The three emblematic types of SAS function described in Figure 2.5 are tested.

The simulation details are as follows. 2000 days of hourly precipitation J were taken from the USGS Four Mile Run weather station (Alexandria, VA, USA). A virtual hydrologic balance $dS/dt = J - Q$ was computed by assuming a non-linear storage-discharge relationship $Q(t) = a\, S_n(t)^b$ where S_n is the storage S normalized by a reference volume of 500 mm, $a = 100$ mm/h, $b = 12$. A further residual storage $S_0 = 200$ mm was added to the system to account for the volume of water in storage that is not visible in the hydrologic response [*Kirchner*, 2009]. Two injections of 100 grams of conservative solute per squared meter were introduced in the system at days 300 and 395. The Master Equation was solved with a finite differences scheme using stationary SAS functions taken from a beta distribution with parameter β constantly equal to unity and α parameters equal to 0.5 (high priority), 1 (random sampling) and 2 (low priority).

The results of the simulation are reported in Figure 2.6. The top panel shows the hydrologic fluxes timeseries and the three fSAS functions used in the simulation. The different mass behaviors induced by the SAS functions are mostly visible for both the injections in the early part of the response and can be summarized as follows: high priority means high release rate in the upcoming storms (and hence high mass peaks). However, as soon as other storms arrive and receive the new priority, the remaining part of mass injection is highly retarded causing long delays in the late mass recovery. This can be representative of a system with important preferential pathways (e.g. large fractures or macropores), where most of the response is drained by the macropores and a little component moves slowly through the soil matrix. Low priority is the opposite. Solute particles have to wait before being released, but then they are discharged in relatively short time interval. This resembles systems with dominant

convective conditions as e.g. the purely vertical flow in a lysimeter. Random sampling represents a situation in-between, where the injected solute is sensitive to the subsequent storm events on a large range of times, indicating a sort balance between fast and slow response components.

The dependence on the climatic forcings is visible in both the injections because the peaks in the mass flux correspond with the peaks in the discharge (the more the discharge, the more the particle removal). Moreover, as injection **a** takes place right before a very wet period, its mass response (for all three SAS functions) is faster. This also shows that, even using a stationary SAS function, the resulting solute response can be very time-variant as it depends on time-variable fluxes.

This numerical exercise can be easily adapted to real-world injection experiments, where fluxes and storages can be measured or computed. A number of different SAS functions (which can be made time-variant and dependent on the system's wetness as shown by *Harman* [2014]) can be tested, making the approach suitable to capture the relevant transport processes in a broad range of problems.

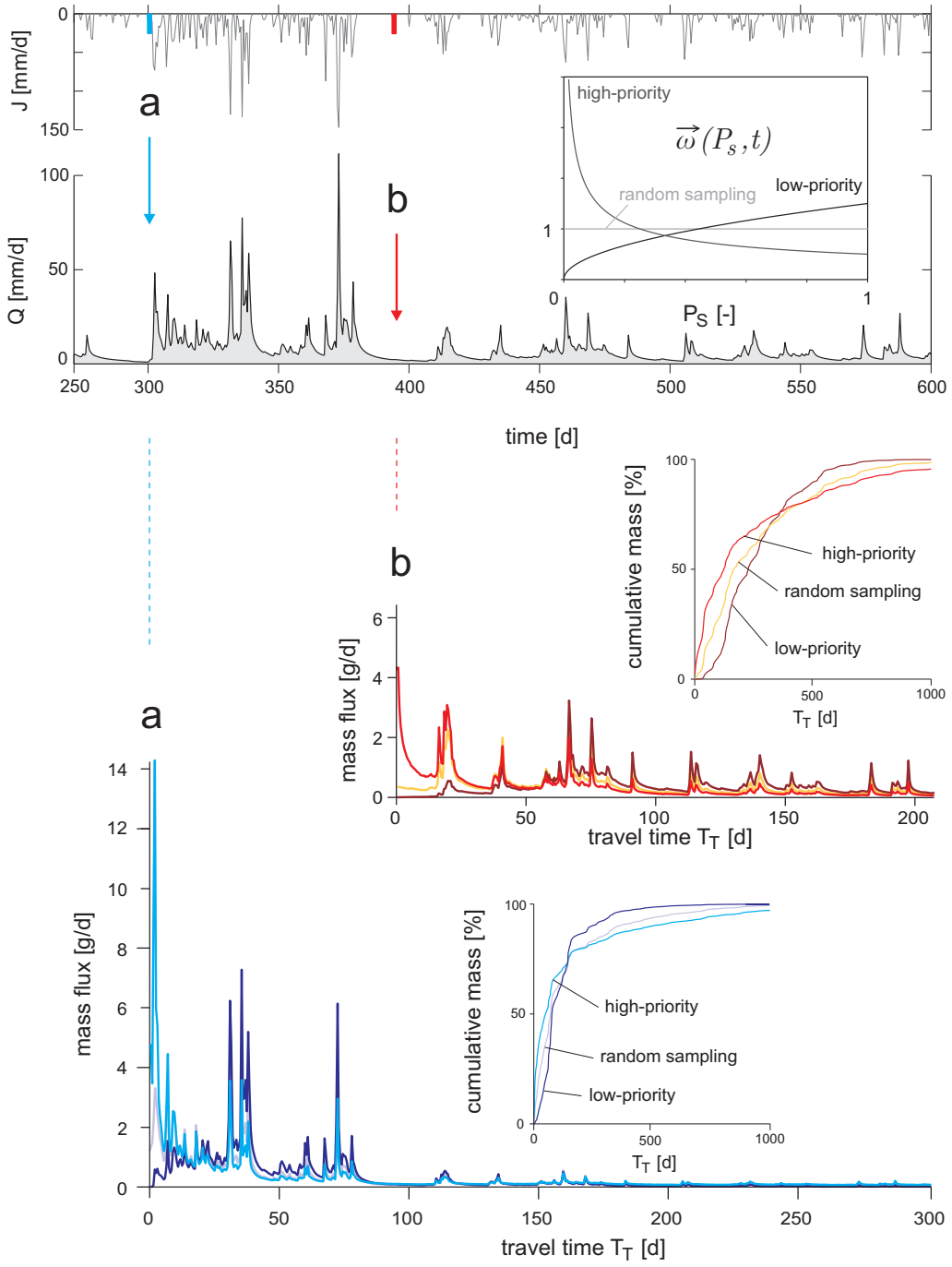

Figure 2.6: Forward experiment - tracer injection simulations according to different SAS functions.

2.4.2 Tracer sampling at an outlet

This second numerical experiment deals with concentration samples at a catchment (or lysimeter) outlet. Each sample is a collection of solute parcels that entered the system in previous injections and can thus be described by modeling backward TTDs. It will be shown how different choices of the SAS functions affect the concentration signal in the streamflow.

The same hydrologic system as the previous exercise was used for this simulation, with the addition of a solute concentration C_{in} to each input flux. Input concentration was randomly distributed among the injections but was inversely related to precipitation intensity, to simulate the effect of atmospheric washouts. Discharge concentration was computed through Eq. 2.9, using the backward TTDs resulted from the solution of the backward Master Equation (2.7) using different SAS functions.

The simulation is illustrated in Figure 2.7. The top axis shows the rainfall concentration timeseries and the bottom axis reports the discharge during the synthetic experiment. The simulated concentration corresponding to each SAS function shows the role of the age selection concept. The high-frequency fluctuations in stream concentration are closely related to the selection of the youngest water particles in the storage ($P_S \approx 0$), corresponding to the latest precipitation events. Hence, when discharge preferentially samples younger particles (blue and green curves in Figure 2.7), the stream concentration is very sensitive to precipitations. In the simulation, this causes a dilution of the baseflow during high discharge because rainfall concentration is lower. The random sampling scheme (red curve) is characterized by a neutral affinity for all the ages, hence some younger particles are sampled and the signal shows a moderate sensitivity to new precipitation events. The opposite holds when older ages are mainly selected (yellow and orange curves). The yellow curve, in particular, is close to zero for the youngest ages, hence it only reacts to longer term (e.g. seasonal) variations. Note that even when the signals are strongly influenced by recent precipitations, the majority of the water, at any time, is "old" and mean travel times always exceed 50 days.

The age-selection concept can be given a physical interpretation. The affinity for the youngest ages quantifies the presence of preferential pathways and overland flow processes, that can quickly convey an input to the outlet. The random sampling is representative of highly heterogeneous environments and dense drainage networks, that enable the stream (or the plant roots) to collect water particles from the whole catchment. The affinity for older water particles portrays the cases where advective processes are dominant, such as in a lysimeter. The ability of the SAS functions to reproduce a

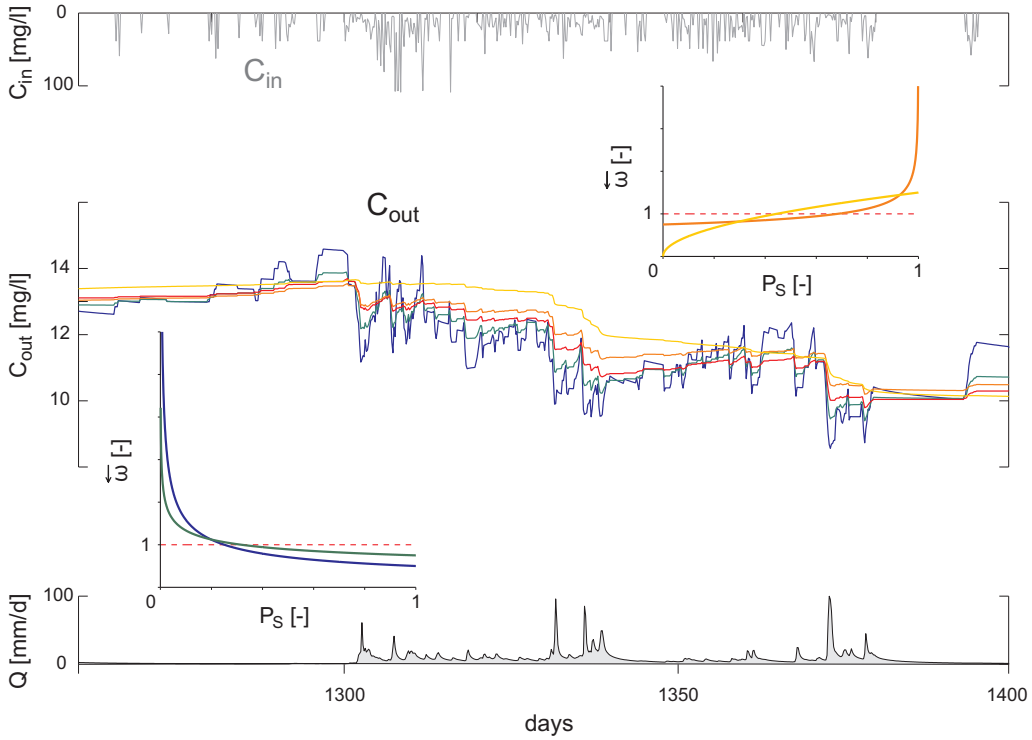

Figure 2.7: Backward experiment - modeled outlet concentration using different SAS functions (inset). The colors are used to associate each timeseries with its SAS function.

broad range of processes at different time-scales makes the approach easily applicable to catchment water-quality measurements, particularly where high-frequency timeseries are available [e.g. *Neal et al.*, 2012; *Aubert et al.*, 2013].

2.5 Final remarks

- Tracking the age (time since injection) and life expectancy (time to exit) of labeled water parcels allows for a coherent and comprehensive description of the fate of rainfall injections at catchment scales. Two complementary formulations, based on mass conservation, allow age and life expectancy to be treated as a scalar property that is transported along with water. Notably, the sum of the age and life expectancy is the particle's travel time through the system;

- The backward formulation tackles how a sample of water taken at any time within the outflows relates to the transport processes experienced by the system in all previous times. The forward formulation stems from the concept of life expectancy concepts and addresses how each water pulse disperses through the system after its injection. Exact symmetries are established between the two formulations;

- While the backward formulation had already been described in terms of the master equation relating particles in storage with particles that cross the exit surfaces, a novel description has been identified in this contribution for the forward problem focusing on life expectancy concepts. The related master equation shows that the system evolution can be completely described in terms of forward distributions only inasmuch as the backward approach had proved. Moreover, the relationship between backward and forward formulations has been analyzed.

- StorAge Selection functions have finally been introduced in various forms to propose a closure suited for general applications to catchment transport. Examples of application show the flexibility and potential of the approach for hydrologic practice, where both forward and backward formulations can be used to contrast tracer experiments.

Chapter 3

Kinematics of Age Mixing in Advection-Dispersion Models

3.1 Introduction

Advection-dispersion models have received massive attention in the geosciences. Their ubiquitous applicability stands from the generality of the underlying continuum- and statistical-mechanical foundations [e.g. *Allen et al.*, 1988; *Gardiner*, 1983], the only requirement being continuity of the trajectories. An appealing property of dispersion mechanisms is the additive nature of dispersion processes operating at different scales, which allows for the definition of a hierarchy of macro-dispersion coefficients (say, from molecular diffusion to turbulent, hydrodynamic and geomorphological dispersion) embedding the relevant heterogeneity of flow pathways through the underlying displacement covariances [*Dagan*, 1989; *Rodríguez-Iturbe and Rinaldo*, 1997]. Such property makes advection-dispersion models a tool suited to handle large-scale settings like those involved in the transport of chemicals across river basins, whose dispersive features are primarily related to geomorphologic and kinematic properties [*Rinaldo et al.*, 1991; *Snell and Sivapalan*, 1994; *Rinaldo et al.*, 1995; *Robinson et al.*, 1995; *Botter and Rinaldo*, 2003; *Saco and Kumar*, 2004]. However, even though first passage times in dispersive models are a well known mathematical problem [*Gardiner*, 1983; *Cox and Miller*, 1978], generalized applications to environmental systems are far from straightforward owing to the effects of complex geometries and boundary conditions.

Tracking the age of water (or solute) particles in the context of advection-dispersion models first interested chemical engineers [*Danckwerts*, 1953] and soon spread into the geosciences, where traditionally it has been pertaining to marine and groundwater stud-

ies. In ocean science, the basic theoretical apparatus was introduced in early works by *Delhez et al.* [1999] and *Deleersnijder et al.* [2001]. In groundwater studies, the general framework introduced by *Dagan* [1989] for describing transport in porous media by means of age distributions has been extensively adopted in later works [e.g. *Rinaldo et al.*, 1991; *Fiori*, 1996; *Cvetkovic and Dagan*, 1994]. The foundation of a general age theory for groundwater, instead, originated from *Ginn* [1999], who derived a groundwater age equation by augmenting the physical space with an additional dimension (the age). The theory was revisited and complemented in later papers [*Cornaton and Perrochet*, 2006; *Ginn et al.*, 2009] which posed the basis for a range of applications [e.g. *Cornaton*, 2012; *Cvetkovic et al.*, 2012; *Engdahl et al.*, 2012, 2013; *Gomez and Wilson*, 2013].

Based on these premises, this chapter investigates age mixing processes arising in advection-dispersion models, where spatially-integrated travel and residence time distributions can be derived from the local velocity field, thereby unraveling the kinematic origin of age mixing. This emblematic problem yields theoretical and practical implications for solute transport through geophysical systems, where the velocity field is typically unknown and explicit mixing hypotheses need to be introduced.

3.2 Age dynamics in advection-dispersion models

The transport and mixing of conservative solutes is investigated within a control volume V, which represents a generic set of hydrologic pathways involved in the terrestrial part of the hydrologic cycle. Examples are the root zone of a plot where infiltration occurs, a hillslope transect fed by rainfall, a gaining channel reach, a small headwater catchment or a combination of hillslopes arbitrarily arranged around a complex river network (Figure 3.1).

Following a setting analogous to that employed by *Dagan* [1989], solutes are introduced into the control volume through a given atmospheric or hydrologic carrier, and are then temporarily stored into V until they eventually leave the control volume through its boundaries ∂V. The portion of ∂V through which the water particles are allowed to leave is termed ∂V_{out}. Other portions of ∂V, instead, can be characterized by a no-flux boundary condition which incorporates the effect of physical barriers and/or confining units (e.g., deep impervious surfaces or divides for hillslopes/catchments, regoliths and bedrocks). The input/output solute fluxes ($\phi_{in}(t)$ and $\phi_{out}(t)$) are linked to the solute storage $M(t)$ through the mass balance equation, which in the absence

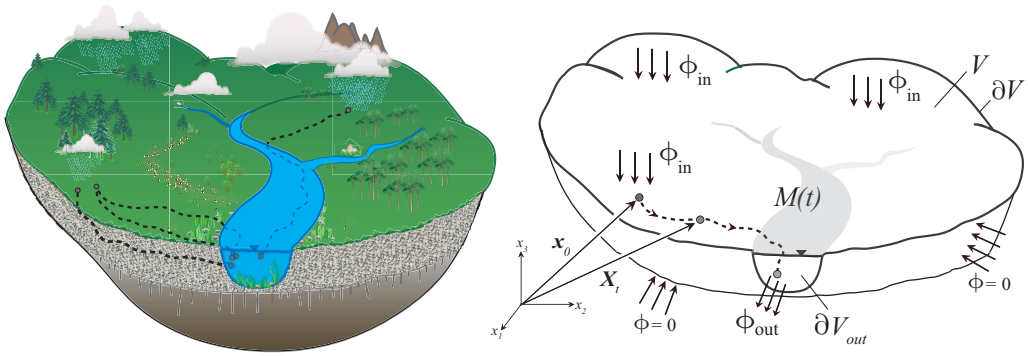

Figure 3.1: Sketch and Lagrangian representation of a catchment control volume.

of reaction/degradation processes can be written as: $dM(t)/dt = \phi_{in}(t) - \phi_{out}(t)$. In what follows, reactive transport is not considered, in order to focus on mixing processes. Moreover, the mass input to the system is assumed to be known, whereas the time-variable solute storage and the mass outflow can be computed from the underlying Eulerian velocity field $\mathbf{v}(\mathbf{x}, t)$, which is in general dependent on a $3D$ space coordinate $\mathbf{x}$ and time t. The Lagrangian equation for the trajectory $\mathbf{X}_t(t)$ of a single particle injected in t_0 from a prescribed initial position $\mathbf{x}_0$ thus obeys the implicit equation [see *Cvetkovic and Dagan*, 1994]: $d\mathbf{X}_t/dt = \mathbf{v}(\mathbf{X}_t, t)$, with $\mathbf{X}_t = \mathbf{x}_0$ for $t = t_0$ (where the dependence of $\mathbf{X}_t$ on t_0 and $\mathbf{x}_0$ has been omitted for simplicity). The velocity field can be suitably decomposed into a mean advection $\mathbf{u}$, resulting from the integration of $\mathbf{v}$ over a given time-lag and within prescribed regions of V, plus some fluctuations $\mathbf{u}'$. The vector $\mathbf{u}'$ represents the variability of the velocity field at spatial and temporal scales smaller than those employed to define the mean advection. When the mean flow $\mathbf{u}$ is the (constant) long-term expectation of $\mathbf{v}$ over the whole control volume, the fluctuations are in general both space- and time-dependent and incorporate the dispersive effect of all processes contributing to the spreading of the solute plume within V. This includes molecular diffusion, pore-scale dispersion, turbulence in channels, space-time patterns of velocity as well as catchment-scale geomorphologic and kinematic dispersion [*Rinaldo et al.*, 1991; *Rodríguez-Iturbe and Rinaldo*, 1997]. Typically, however, due to the hierarchical nature of dispersive processes, the effect of large-scale mechanisms overwhelms the ones produced by smaller-scale velocity fluctuations. In other circumstances, instead, the mean advection $\mathbf{u}$ may be a local (spatially and temporally distributed) velocity field resulting from the integration of $\mathbf{v}$ over smaller-scale representative elementary volumes (REVs), and the fluctuations $\mathbf{u}'$ embed the local diffusion within each REV, which bears a negligible effect on large-scale transport properties in most cases [*Fiori*,

1996; *Jankovic et al.*, 2009].

In hydrologic pathways, the spatially distributed nature of injections (which typically occur over entire catchment areas through precipitation, or along the course of complex river networks through lateral subsurface flow), jointly with the heterogeneity of the trajectories, determines the spreading of the solute plume within V, which is here quantified through the displacement distribution for the solute particles $g(\mathbf{x}, t|t_0)$ $[L^{-3}]$. The distribution is here intended as a probability density function (pdf), such that $g(\mathbf{x}, t|t_0)d\mathbf{x}$ quantifies the probability for solute particles injected in the control volume in t_0 to be at time t within the infinitesimal volume $d\mathbf{x}$ around $\mathbf{x} \in V$. The conditioning of the pdf on t_0 highlights the general transient character of the formulation, but will be hereafter avoided in the notation unless strictly necessary.

In the presence of continuous particles' trajectories, the displacement pdf g obeys the Forward Fokker-Planck equation [e.g. *Gardiner*, 1983], which can be written as:

$$\frac{\partial g(\mathbf{x}, t)}{\partial t} + \nabla \cdot [\mathbf{u}(\mathbf{x}, t)\, g(\mathbf{x}, t)] = \nabla \cdot [\mathbf{D}(\mathbf{x}, t)\ \nabla g(\mathbf{x}, t)] \tag{3.1}$$

where $\mathbf{D}(\mathbf{x}, t)$ is a space-time dependent dispersion tensor related to the covariance matrix of the velocity fluctuations $\mathbf{u}'$ with respect to the mean convection (see, for a hydrologic perspective, *Rinaldo and Rodriguez-Iturbe* [1996]). According to the advection-dispersion model given in equation (3.1), the output flux is given by the integral through the boundaries ∂V_{out} of convective and dispersive flux:

$$\phi_{out}(t) = \int_{\partial V_{out}} [\mathbf{u}(\mathbf{x}, t)\, g(\mathbf{x}, t) - \mathbf{D}(\mathbf{x}, t)\ \nabla g(\mathbf{x}, t)] \cdot \mathbf{n}\ d\sigma\,, \tag{3.2}$$

where $\mathbf{n}$ is the unit vector normal to ∂V. For passive solutes which are simply advected by the flow field, solute molecules are only dispersed by the heterogeneity of the velocity field. Hence, the concentration field is directly related to the displacement distribution. In particular, the solute concentration observed in $\mathbf{x}$ at time t, $C(\mathbf{x}, t)$, due to an impulsive input in t_0, is proportional to the relative number of particles residing in x at time t: $C(\mathbf{x}, t) = m\, g(\mathbf{x}, t|t_0)$, where m is the solute mass injected in t_0 and g the displacement distribution, derived by solving equation (3.1) with a delta-Dirac initial condition. In case of continuous mass input, instead, the linearity of the equation allows the overall concentration field to be expressed as the convolution between the displacement distribution of a single pulse injection ($g(\mathbf{x}, t - t_0|t_0)$) and the underlying input forcing ($\phi_{in}(t)$):

$$C(\mathbf{x}, t) = \int_{-\infty}^{t} \phi_{in}(t_0) g(\mathbf{x}, t - t_0|t_0) dt_0\,. \tag{3.3}$$

The primary focus of this work is on the age of solute particles moving within the control volume, which can be quantified by means of their residence time, T_R. The residence time of each particle stored in V is defined as the time spent by the particle inside V since its entry up to current time. Hence, the residence time of the stored particles grows in time due to aging. In the case of a single instantaneous injection taking place at t_0, the age of the particles traveling through V is uniform and independent of the position, thereby implying that $T_R = t - t_0$ for all stored particles. In case of a continuous mass input, however, particles with different ages are found in the same position at a given time. In this instance, a proper characterization of the age distribution of the particles residing in a prescribed position at a given time can be achieved using the mass age density, $\rho(\mathbf{x}, T_R, t)$ $[M\,L^{-3}\,T^{-1}]$, first introduced by *Ginn* [1999]. Formally, $\rho(\mathbf{x}, T_R, t)\,d\mathbf{x}\,dT_R$ quantifies the solute mass with age $T_R \in (T_R, T_R + dT_R)$ contained at time t in the infinitesimal volume $d\mathbf{x}$ around the position $\mathbf{x} \in V$. Here, to stress the link with solute particles displacement, ρ is seen as a time-dependent bivariate distribution of residence times and (stochastic) displacements, hence investing ρ with a probabilistic meaning as well. The link between ρ and g is provided by the following equation:

$$\rho(\mathbf{x}, T_R, t) = \phi_{in}(t - T_R) g(\mathbf{x}, t | t - T_R)\,, \tag{3.4}$$

which states that the particles residing around $\mathbf{x}$ at time t have an age nearly equal to T_R if and only if they entered V in $t - T_R$. Equation (3.4) represents the fundamental link between the formulation of transport proposed by *Dagan* [1989] and the water age theory developed by *Ginn* [1999]. In fact, combining equations (3.1) and (3.4), after some manipulation (Appendix A.1), yields:

$$\frac{\partial \rho(\mathbf{x}, T_R, t)}{\partial t} + \frac{\partial \rho(\mathbf{x}, T_R, t)}{\partial T_R} + \nabla \cdot [\mathbf{u}(\mathbf{x}, t)\, \rho(\mathbf{x}, T_R, t)] = \nabla \cdot [\mathbf{D}(\mathbf{x}, t)\ \nabla \rho(\mathbf{x}, T_R, t)]\,. \tag{3.5}$$

which takes the same mathematical form as the water age equation derived by *Ginn* [1999]. Equation (3.5) defines the combined dynamics of age and position of solute particles moving within V by means of continuous trajectories (thus obeying Fokker-Plank equation). This equation has a form similar to the advection-dispersion equation, the major difference being that an extra-dimension (the residence time) is added to the problem, requiring the introduction at the left-hand side of a convective term with unit speed in the age domain which accounts for the aging of the stored particles. Note also that, owing to the general transient formulation, the same equations are suitable to describe the age dynamics of water (instead of solutes), provided that solute mass fluxes are replaced with water mass fluxes.

3.3 Travel/residence time distributions and age selection

The formulation described in the previous section quantifies in a spatially explicit setting the coupled dynamics of solute (or water) age and displacement based on the knowledge of the velocity field, which induces solute dispersion and age mixing. Such a framework proves useful in tracking the spreading of solute plumes in groundwater and oceans. However, in some circumstances one may not be interested in the pointwise specification of the underlying concentration field, the primary focus being the identification of large-scale patterns. This can be done by shifting the focus from the age distribution of the particles residing at any point $\mathbf{x} \in V$, to the age distribution of particle samples belonging to prescribed large-scale regions of V, which thus represent spatially-integrated descriptors of the underlying transport processes.

Hydro-chemical studies usually focus on two different types of large-scale sampling of the solute storage: i) the whole collection of particles stored within V at a given time, and ii) the fraction of particles leaving the system as ϕ_{out} at a given time t. In the first case, we are interested in quantifying the distribution of the ages in storage within the control volume V at a given time, independently on their specific position. This distribution is typically indicated in catchment hydrology as the residence time distribution, $p_S(T_R, t)$ [*Botter et al.*, 2011]. The distribution of residence times at a given time t can be obtained from the integration of ρ over V as:

$$p_S(T_R, t) = \frac{1}{M(t)} \int_V \rho(\mathbf{x}, T_R, t) d\mathbf{x}\,. \tag{3.6}$$

where the overall solute storage $M(t)$ represents the proper normalization constant, which allows to comply with condition $\int_0^\infty p_S(T_R, t) dT_R = 1$. In the latter case, instead, the considered sample is constituted by those particles leaving the system at a given time t. In this case, sampled particles cannot grow any older because they leave the system. Hence, their residence time at time t (the time of exit) is their maximum residence time in V, which is usually termed travel (or transit) time (T_T) in catchment hydrology. The travel time is thus the time elapsed from entrance to exit of a given solute particle in the control volume V. The distribution of travel times for the particles leaving the system at time t, hereafter termed (backward) travel time pdf $p_Q(T_T, t$, quantifies the ages sampled by the output flux through the control surface ∂V_{out}. $p_Q(T_T, t)$ can be obtained by integrating over ∂V_{out} the age distribution associated with the (convective and dispersive) output fluxes at time t (see equation (3.2)):

$$p_Q(T_T, t) = \frac{1}{\phi_{out}(t)} \int_{\partial V_{out}} [\mathbf{u}(\mathbf{x}, t)\, \rho(\mathbf{x}, T_T, t) - \mathbf{D}(\mathbf{x}, t)\, \nabla \rho(\mathbf{x}, T_T, t)] \cdot \mathbf{n}\, d\sigma, \tag{3.7}$$

where $\phi_{out}(t)$ represents the size of the sample and acts as a time-variant normalizing constant. Note that, based on the link between g and ρ given by eq. (3.4), travel and residence time distributions can be equivalently expressed as function of g (Appendix A.2). These alternative expressions will be later used for the computation of travel and residence time distributions shown in Section 3.5.

The family of time variant residence and travel time distributions are key descriptors of large-scale transport properties and can be used to calculate the mean solute concentration of the storage and the concentration of the output fluxes, based on the knowledge of the solute input [*Rinaldo et al.*, 2011, equations (2) and (5)]. From a kinematic viewpoint, these distribution provide important integral information on the age of the solute particles residing within V and near its boundaries.

If equation (3.5) is integrated over the whole control volume V (similarly to *Chen* [1971] in chemical reactors context), after using the divergence theorem and equations (3.6) and (3.7), we obtain the so called Master Equation for the residence time distribution, which reads [*Botter et al.*, 2011]:

$$\frac{\partial[M(t)p_S(T_R,t)]}{\partial t} + \frac{\partial[M(t)p_S(T_R,t)]}{\partial T_R} = -\phi_{out}(t)\, p_Q(T_R,t) \tag{3.8}$$

Equation (3.8) has the same meaning of equation (3.5), the only difference being its spatially integrated nature. Note that, by definition, particles composing the input flux are characterized by $T_R = 0$ at the moment of their entrance. Hence, differently from what happens in a spatially distributed setting, the input flux is only involved in the boundary conditions on the residence time domain of eq. (3.8). The Master Equation for the residence time distribution provides a robust linkage between the temporal evolution of the ages stored and those removed from the system by the output fluxes. Equation (3.8) shows that the travel and residence time distributions are mutually dependent, and that their shape is strongly affected by the dynamical nature of the underlying fluxes and storages.

A second independent linkage between residence and travel time distributions can be deduced directly from the kinematic relationship defining p_T and p_S (equations (3.6) and (3.7)). Whenever at time t there exists an age τ for which all over the control volume $\rho(\mathbf{x}, T_R = \tau, t) = 0$ (i.e., the age τ is not represented in the storage, e.g. because $\phi_{in}(t-\tau) = 0$), then $p_S(\tau, t)$ shall be be necessarily null, which in turn implies $p_Q(\tau, t) = 0$. The ages sampled by the output flux must be indeed chosen among those available in the storage. The above ansatz can be mathematically expressed as [*Botter*

et al., 2011]:

$$p_Q(\tau, t) = p_S(\tau, t)\, \omega(\tau, t) \tag{3.9}$$

where ω is called StorAge Selection (SAS) function, and represents the preference of the output flux toward the different ages τ potentially available in V. Equation (3.9) states that the chance that any age has of being sampled by ϕ_{out} at a given time t can be thought of as the product between the availability of that age (expressed by p_S) and the preference of the output for sampling that age (expressed by the SAS function ω). Either low availability or low preference thus imply that a given age should be poorly represented in the output flux. In cases where $\mathbf{u}$ and $\mathbf{D}$ are known, the SAS functions ω can be explicitly linked to the underlying flow field. If we divide both sides of equation (3.9) by p_S, and we make use of equations (3.6) and (3.7) to specify p_S and p_Q as a function of ρ, the following result is obtained:

$$\omega(\tau, t) = \frac{p_Q(\tau, t)}{p_S(\tau, t)} = \frac{M(t)}{\phi_{out}(t)} \frac{\int_{\partial V_{out}} \left[\mathbf{u}(\mathbf{x}, t)\, \rho(\mathbf{x}, T_R, t) - \mathbf{D}(\mathbf{x}, t)\, \nabla\rho(\mathbf{x}, T_R, t)\right] \cdot \mathbf{n}\, d\sigma}{\int_V \rho(\mathbf{x}, T_R, t) d\mathbf{x}}\,. \tag{3.10}$$

Equation (3.10) (which holds for $p_S(\tau, t) \neq 0$) explicitly shows that the SAS functions are linked to the heterogeneity of the mass age density. In particular, equation (3.10) suggests that even though ρ is not spatially uniform, whenever the surface integral at the numerator is well representative of the volume integral at the denominator, the resulting SAS functions can be nearly constant with τ, implying that the age distribution of the particles leaving V is similar to that of the whole storage ($p_Q(\tau, t) \simeq p_S(\tau, t)$). In the following, the relationship between the kinematics of the flow field and the mixture of ages in the output fluxes is analyzed through the underlying SAS functions ω.

Besides theoretical importance, practical implications of the kinematics of age mixing should not be underestimated. The emergence of universal behaviors for the SAS functions under simplified controlled settings, can significantly improve our ability to model complex hydrologic pathways where the spatial distribution of the velocity field is typically unknown and the underlying SAS functions need to be specified based on some assumptions. Simplified geometries and kinematic fields of the type investigated here clarify the link between dispersion and age selection and may ultimately lead to general analytical expressions for the SAS functions (eq. (3.9)). This would allow to solve equation (3.8), yielding the related residence/travel time distributions, which could eventually be tested against hydrochemical observations in different real-world hydrologic settings [*van der Velde et al.*, 2012; *Bertuzzo et al.*, 2013; *Benettin et al.*, 2013b].

The advantage of this general procedure is threefold. First, robustness to impact of heterogeneity and computational efficiency is significantly improved with respect to standard distributed modeling approaches, owing to the spatially integrated setting and the use of analytical expressions. Second, differently from standard approaches where the shape of the underlying travel time distribution is pre-specified, the temporal fluctuations of residence and travel time distributions and their reciprocal consistency (equation (3.8)) are automatically taken into account. Third, the SAS functions can be easily interpreted on physical grounds, giving insight on age selection processes taking place in catchments e.g. by facing even scanty hydrochemical observations. For instance, $\omega \simeq const(\tau)$ implies no selective preferences for the different ages available, while increasing (or decreasing) SAS functions would imply enhanced preference toward older (or younger) ages in storage.

3.4 Application to 1D advection-dispersion models

In this section, an illustrative example of the theory described in Sections 3.2 and 3.3 is provided. As the purpose is that of revealing some leading age dynamics, equation (3.1) is solved over a one-dimensional spatial domain and under the assumption of uniform and constant velocity and dispersion. This is a common assumption in catchment hydrology for the description of single hillslopes or channels [e.g. *Beven et al.*, 1993; *Kirchner et al.*, 2001], even though to develop a diffusive regime with constant D in any heterogeneous flow field, one has to travel several correlation lengths of heterogeneous properties [*Dagan*, 1989]. Nevertheless, more involved solutions could be derived numerically for the desired domains and velocity fields [see e.g. *Soltani and Cvetkovic*, 2013]. Note that as the carrier flows steadily, travel time analysis is only allowed for carried solutes. Within this setting, the solution for $g(x,t)$ is a function of two variables and equation (3.1) simplifies to:

$$\frac{\partial g}{\partial t} + u\frac{\partial g}{\partial x} = D\frac{\partial^2 g}{\partial x^2} \quad . \tag{3.11}$$

Analytical expressions for the displacement distribution $g(x,t)$ are thus derived for suitable initial and boundary conditions and then used to calculate all related travel/residence time distributions. The classic solution to equation (3.11) refers to the case of an impulse injection of mass into $x = x_0$ advected and diffused over an infinitely-long domain, where the solution goes to zero at the boundaries. The basic

solution $g_0(x,t)$ reads:

$$g_0(x,t) = \frac{1}{\sqrt{4\pi Dt}} \exp\left[-\frac{(x-x_0-ut)^2}{4Dt}\right] \tag{3.12}$$

Equation (3.12) is derived for an infinite domain and may not be appropriate for most practical applications, where the solution needs to be confined (say, to $[0, L]$) due to the finite size of the control volume. Moreover, the computation of travel times is only meaningful in the presence of a first-passage time boundary at the domain outlet [*Cox and Miller*, 1978]. The choice of proper boundary conditions (BC) for finite domains is discussed in the literature [see *Kreft and Zuber*, 1978; *Delhez et al.*, 2004; *Charbeneau*, 2006], but it is often overlooked in catchment hydrology. Here, a no-flux condition is imposed in $x = 0$ to represent any upstream physical impediment. This reflecting barrier condition can be neglected in case of high advection compared to dispersion (i.e. Péclet numbers $Pe > 10$) [*Rinaldo et al.*, 1991], but becomes crucial in case of $Pe \leq 1$, a likely occurrence in subsurface environments. If no reflecting barrier is used, a considerable mass loss occurs at low Pe due to the upstream dispersive flux, which can be quantified by integrating g_0 over $[0, +\infty]$. The boundary condition at $x = L$, instead, must be representative of the outlet where the outflows are typically measured. This BC is here described introducing an absorbing barrier in $x = L$. Such a condition is the necessary basis for a proper identification of travel times [see *Dagan*, 1989; *Rinaldo et al.*, 1991] because if particles were allowed to re-enter the volume after they left, travel time would be indeed undetermined. The effects of the absorbing barriers are relevant at any Péclet number.

The initial condition (IC) that will be explored is the impulse injection in $x = x_0 = 0$ at $t = t_0$ (with $t_0 = 0$, for simplicity). This IC forms the basis for successive extensions to continuous and/or spatially distributed injections. The problem that will be addressed is then defined by the following set of IC and BCs:

$$g(x,0) = \delta(0); \quad ug(0,t) - D\frac{\partial g(0,t)}{\partial x} = 0; \quad g(L,t) = 0. \tag{3.13}$$

The solution to this linear problem is fully developed in Appendix A.3.

Based on the solution $g(x,t)$, the breakthrough curve (or normalized mass flux at the outlet) can be calculated for each injection [see *Dagan and Nguyen*, 1989]. The stationarity of the flow field implies that each mass injection is transported towards the outlet regardless of the specific injection time. Indeed, the solution g is stationary and each input produces the same (normalized) mass flux, which is a function of $t - t_0$ only. Normalized mass fluxes are shown in Figure 3.2 for different Péclet numbers ($Pe =$

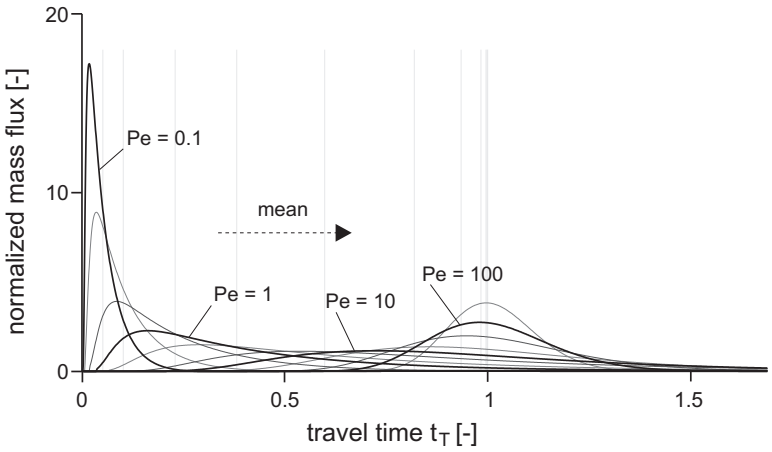

Figure 3.2: Breakthrough curves of the system described in section 3.4, for different Péclet numbers. The x-axis is scaled to mean advection time L/u.

Lu/D). Note that, due to the specific boundary conditions used in the simulation, in case of low Pe particles are rapidly dispersed throughout the domain, so they rapidly reach the absorbing barrier resulting in early breakthrough curves.

3.5 Results

The setting described in section 3.4 allows for the analytical solution of $g(x,t)$. Hence, the corresponding travel and residence time distributions can be readily calculated by using expressions from Appendix A.2. Stationarity of the normalized mass flux (shown in the previous section) does not imply, in general, stationary travel time distributions p_Q , as the latter depend not only on the flow field but also on the sequence of injections and the implied temporal evolution of the storage [*van der Velde et al.*, 2010a; *Rinaldo et al.*, 2011; *Heidbuechel et al.*, 2012; *Hrachowitz et al.*, 2013]. Stationary distributions are instead obtained in case of stationary injection ($\phi_{in} = const$), where p_Q equals the normalized mass flux (equation A.5). This is emphasized in figure 3.3a, where different distributions are calculated at different times in a conceptual experiment where mass input varies according to a damped oscillation in time. The shape of p_Q is strongly influenced by the sequence of previous mass inputs, thereby resembling a sinusoidal shape. Moreover, as soon as stationarity is reached (i.e. when outflows balance inflows, implying constant mass within the volume), distributions collapse into the stationary breakthrough curve of the system. Residence time distributions, p_S (eq. (A.4)), behave similarly because the relative abundance of each age within the control volume is driven

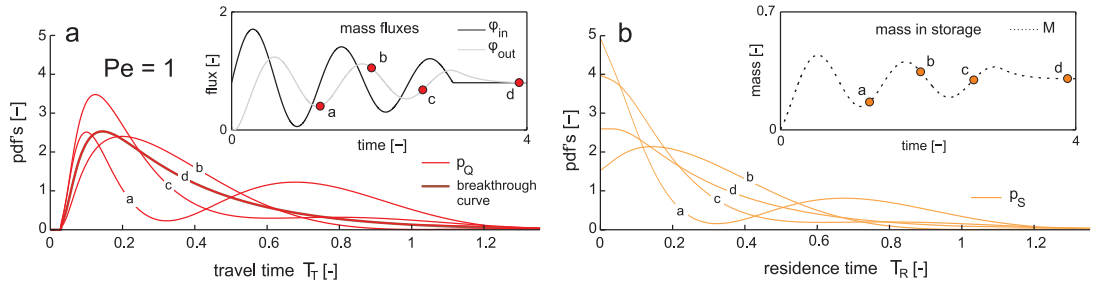

Figure 3.3: Travel (a) and residence (b) time distributions evaluated at different times for a system characterized by $Pe = 1$ and forced by oscillating non dimensional input. Insets show fluxes/storage evolution during the entire simulation and indicate the four instants at which distributions were extracted.

by mass inputs, thus making the distributions highly time-variant (Figure 3.3b).

The shape of the ω-functions can be tracked by comparing the behavior of p_Q and p_S at the same times (eq. (A.6)). Note that, as the dependence on the input flux vanishes, the shape of the functions is only driven by $g(x,t)$, which is time- independent in this case. The presence in eq. (A.6) of both resident and outflowing mass only acts as a scaling factor and in most of the analyzed cases it displays a small range of variation, making ω almost stationary. This is clearly shown in Figure 3.4, where travel/residence time distributions and SAS functions are calculated for different types of input fluxes. The Figure evidences how the same SAS functions can underlie radically different travel time distribution shapes. Indeed, as SAS functions are governed by the characteristics of the flow field (namely, the stationary solution g), their shape depends on the relationship between dispersion and advection which is quantified by the Péclet number. This concept is further reinforced by the plots shown in Figure 3.5, where the functions p_Q, p_S and ω corresponding to different Pe numbers are reported in case of Poissonian injections of mass. At any Pe, the youngest resident ages are not sampled by the outflows because of the time-lag required to travel from injection point x_0 to the absorbing barrier. Therefore, the youngest ages contribute to the residence time distribution (as they are available in the storage), but are not represented in the travel time distribution because they are poorly sampled by ϕ_{out}. For high dispersion (say, $Pe \leq 1$), the range of ages where this discrepancy is significant is narrowed. For higher Pe, the shift between the two distributions increases, resulting in ω functions that are progressively shifted to the right and markedly peaked, indicating preferential affinity for older resident particles.

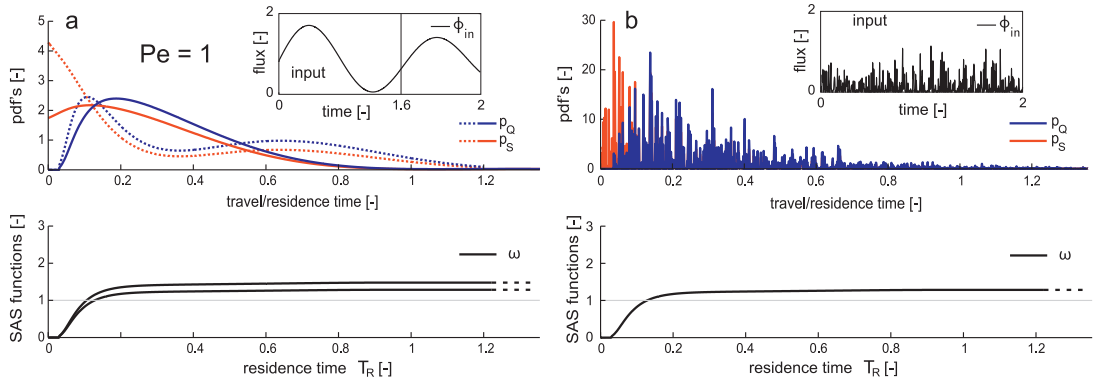

Figure 3.4: Travel/residence time distributions and SAS functions for a system characterized by $Pe = 1$ and forced by oscillating (a) and poissonian (b) input. Insets show input sequence up to sampling times ($t = 1.6$ and $t = 2$ in (a), $t = 2$ in (b))

3.6 Discussion

The results shown in Section 3.5 indicate that the structure of age selection emerging in advection-dispersion models is primarily controlled by the relative magnitude of the dispersion coefficient, quantified by the underlying Péclet number. Figure 3.6 summarizes the pattern exhibited by the SAS function defined through equations (3.9) and (3.10) for selected representative values of Pe. The ages along the x-axis are normalized to a reference timescale, corresponding for each case to the time required to recover 99% of the solute mass. The plot has been obtained under steady state conditions ($\phi_{in} = \phi_{out}$), implying that the age-selection functions are time-invariant, but a similar pattern can be observed also in transient input conditions. The horizontal line $\omega = 1$ corresponds to the random sampling [see *Benettin et al.*, 2013b, par. 18] where all ages are sampled according to their relative abundance in the control volume. Figure 3.6 evidences that convection processes dominate for high Pe, such that the age selection is reduced. Under such circumstances, only the oldest solute particles in storage are flushed out of the control volume, as implied by the sharp increase of the age function ω (in analogy to what happens in piston-flow conditions [*Botter*, 2012]). Conversely, for decreasing Pe numbers, the shape of the SAS functions flattens, and most of the ages available in the control volume are sampled in the same proportion as their availability (with the exception of the youngest ages, which are systematically undersampled due to the distance between the injection point and the absorbing barrier). Figure 3.6 thus shows that the assumption according to which residence and travel time distributions have the same shape - first introduced by *Botter et al.* [2010] and later used in *Bertuzzo et al.* [2013] and

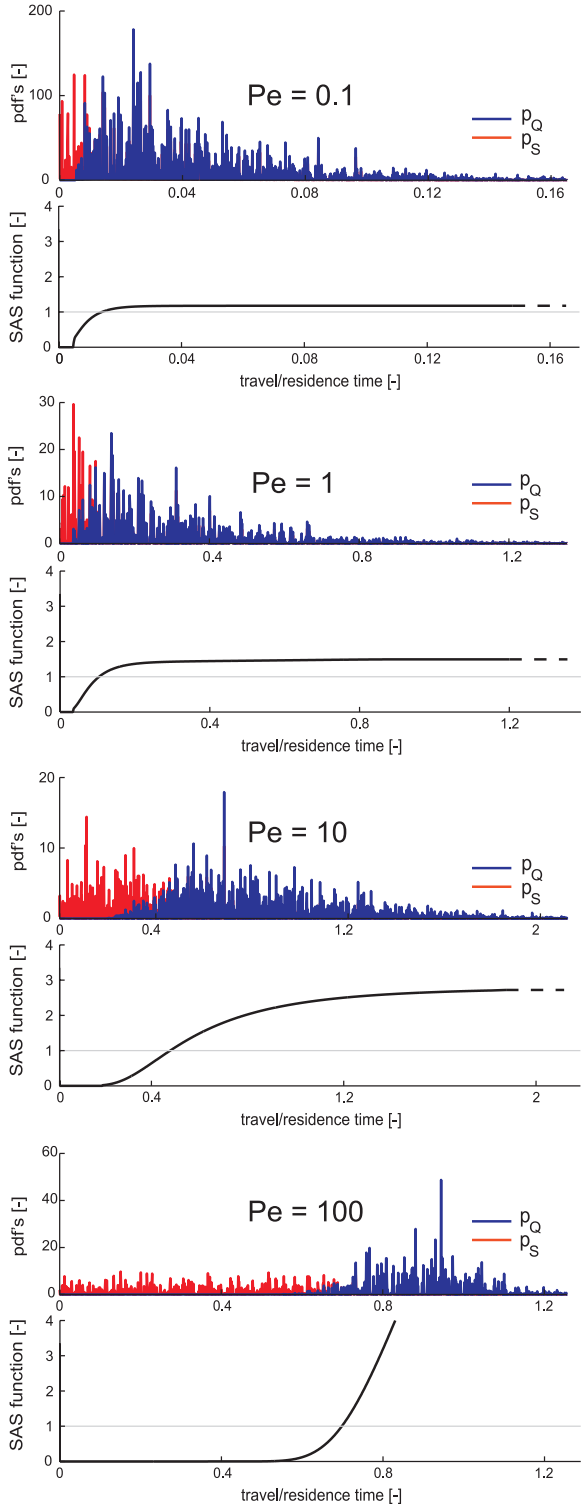

Figure 3.5: Travel/residence time distributions and SAS functions for different Péclet numbers, forced by poissonian inputs.

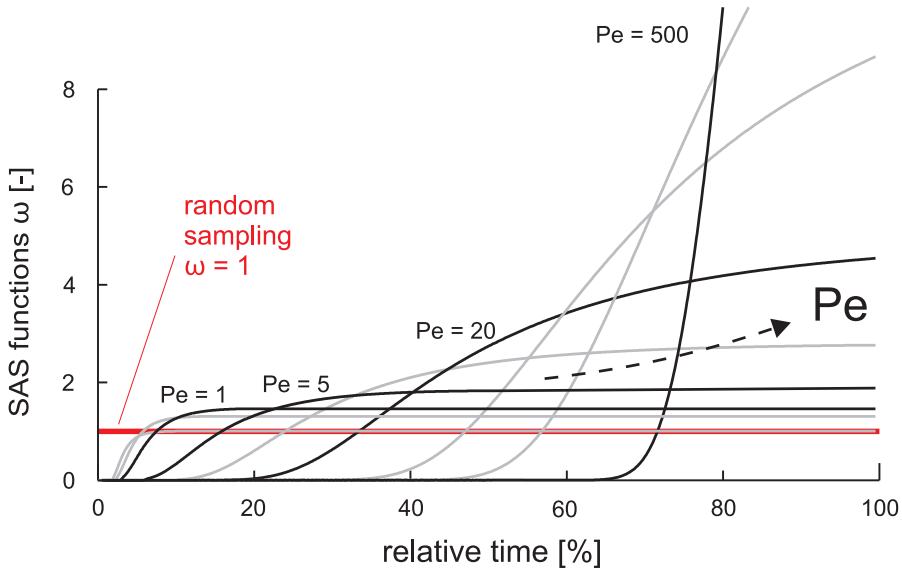

Figure 3.6: SAS functions for different Péclet numbers. To allow comparisons, residence times were rescaled to the relative time required to recover 99% of the solute mass.

Benettin et al. [2013b] - may be a reasonable approximation for advection-dispersion models with enhanced dispersivity (say, $Pe < 5$).

A second point worth clarifying relates to the key differences found between the random-sampling scheme mentioned above and an idealized well-mixed reactor where the spatial gradients of solute concentration are disregarded and the output concentration is equal to the average concentration in the control volume. A well-mixed system of the latter type behaves by definition as a random sampler. Nevertheless, outflows may sample stored ages proportionally to their relative abundance even in systems far from resembling well-mixed reactors. Hydrologic media with enhanced dispersion (e.g. a hillslope) represent a noteworthy example [*Rinaldo et al.*, 2011]. Indeed, even though for $Pe < 5$ the age-selection functions ω become almost uniform (suggesting that most of the available ages in the control volume are randomly sampled by the output flux), the concentration profile $C(x, t)$ is not uniform at all (Figure 3.7) owing to the temporal variability of the mass input and to the effects of boundary conditions. The similarity of residence and travel time distributions in time-variant flow systems, hence does not imply at all the existence of a single perfectly-mixed compartment where the solute inputs are instantaneously mixed into the pre-existing storage. This is the essence of the kinematics of age mixing.

In all the simulations discussed above, solute injection is assumed to take place pointwise, at a given location along the considered hydrologic pathway. This setting may

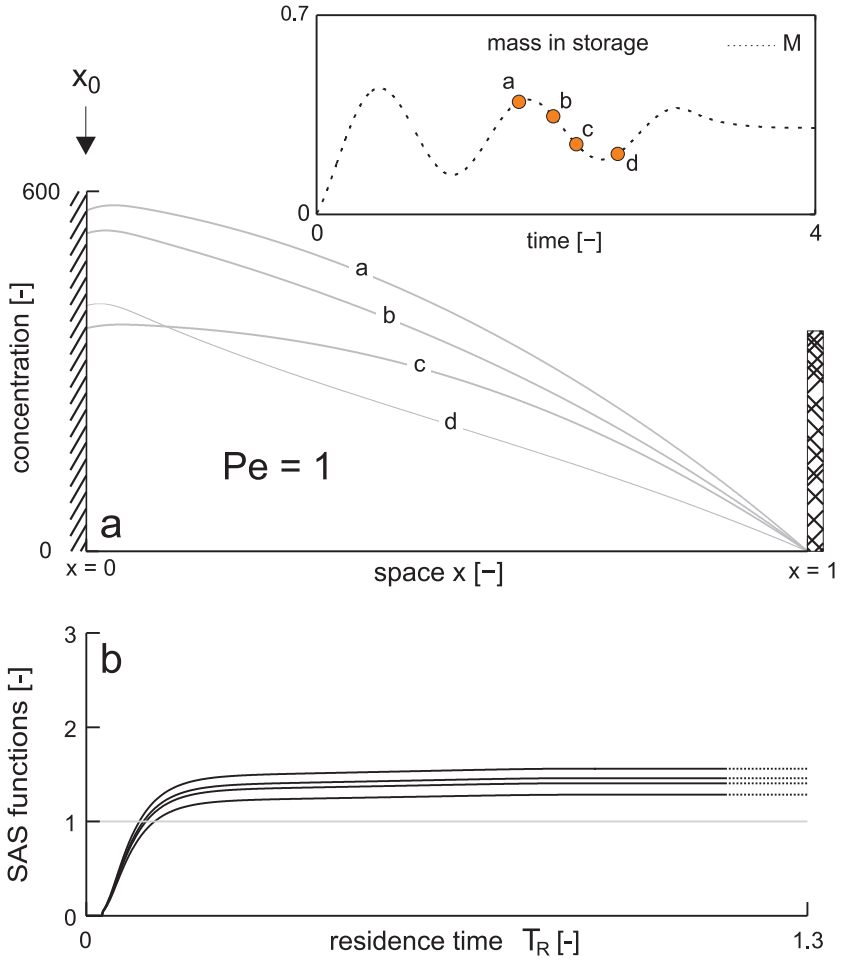

Figure 3.7: Concentration profiles (a) over a normalized spatial domain. Profiles are calculated at different times, in case of oscillating input. The inset shows the evolution of stored mass. For the same times, SAS functions (b) are also reported. The simulation is run at $Pe = 1$.

be appropriate to describe the sub-vertical movement of solutes in the root-zone (where the solute injection takes place in correspondence to the soil surface), or to model the spreading of solutes/contaminants originating from a point source [e.g. *Harman et al.*, 2011]. However, in other circumstances (like e.g. for the sub-horizontal displacement of solutes in groundwater receiving inputs as leakage from a root-zone, or for in-stream transport of chemicals originating from diffuse sources along a complex river network) the appropriate setting is a spatially distributed injection along the entire domain. To investigate the impact of spatially distributed solute inputs on the shape of the SAS functions, a sequence of conceptual experiments was performed in which the mass input is provided to the system along the entire simulation domain according to a set of representative patterns (insets of Figure 3.8). For a uniform injection along the domain (Figure 3.8a) the resulting age-selection function exhibits an evident affinity for the younger ages, while intermediate and old ages are quite uniformly removed by the output, exactly as in a random sampling scheme. The observed preference for younger ages is due to the fact that a fraction of the solute input is introduced into the control volume very close to the outlet, implying reduced residence times for a significant fraction of solute mass injected. Indeed, when the specific (per unit length) mass flux is made linearly increasing along with x (Figure 3.8b), the preference for younger ages is enhanced, due to the increased number of particles injected in proximity of the absorbing barrier. Conversely, when the specific mass input is linearly decreasing with x (Figure 3.8c), the resulting SAS function is remarkably uniform, implying that the various ages are flushed in the same proportion as they are available in the storage, with the exception of a limited range of young ages. The most appropriate setting that needs to be considered in real-world hydrologic applications is strongly dependent on the physical and morphologic properties of the control volume, and on the nature of the considered processes (e.g. channel routing, surface/subsurface flow). For instance, several previous studies have linked the spatial variability of the input to the hillslope geometry in simple first-order catchments [e.g. *Kirchner et al.*, 2001]. In Figure 3.8d, instead, the solute spreading along a complex river network is considered, where the input is uniformly originating from the whole catchment surface. The resulting mass flux along the river is represented by the downstream increment of total contributing area whose distribution is known and universal [*Rodríguez-Iturbe and Rinaldo*, 1997]. This distributed input function (calculated through a Digital Elevation Map of the upper portion of the Piave river, Italy) exhibits a complex pattern, with a number of spikes in correspondence of the major tributaries to the main reach. However, such

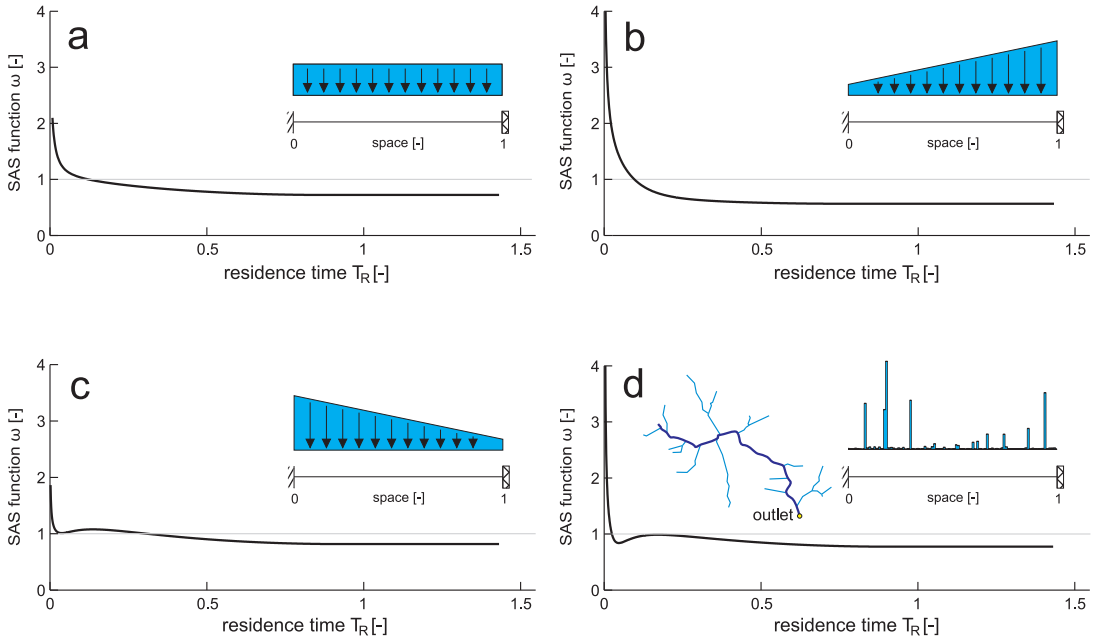

Figure 3.8: SAS functions resulting from the application of distributed mass inputs over the whole domain length. Insets show spatial distributions. Simulations are run for $Pe = 1$.

heterogeneous inputs are not mirrored by the underlying SAS function, which appears to be remarkably uniform except for the smallest residence times, which are flushed out in a larger proportion with respect to their availability due to the presence of a tributary close to the outlet.

This last example is deemed to be especially relevant to complex catchments where the overall dispersion is linked to morphological and kinematic heterogeneity [*Rinaldo et al.*, 1991; *Snell and Sivapalan*, 1994; *Rinaldo et al.*, 1995; *Robinson et al.*, 1995; *Saco and Kumar*, 2004; *Botter and Rinaldo*, 2003]. The large-scale effect of such heterogeneity can be tackled through nested convolutions, which mirror the geomorphic arrangement of diverse landscape elements around the river network.

3.7 Final remarks

The outlined formulation bridges previous theoretical results from diverse fields, namely i) the Lagrangian travel time formulation of transport in heterogeneous porous formations [*Dagan*, 1989]; ii) the Eulerian groundwater age theory [*Ginn*, 1999]; and iii) the Master Equation for spatially integrated residence and travel time distributions [*Botter et al.*, 2011]. Travel/residence time distributions and age-selection functions have been

explicitly linked to the kinematics of the flow field, thereby unraveling the nature of large-scale age mixing in domains where solutes are advected and dispersed.

In spite of the enhanced non-stationarity of travel and residence time distributions implied by unsteady solute inputs, the type of mixing was found to be markedly invariant, and independent on the temporal evolution of the mass input and the storage. The resulting SAS functions are controlled by the relevant Péclet number. For $Pe < 5$, despite the significant spatial gradients of solute concentration along the entire domain, the resulting mixing functions were found to be substantially uniform, implying that the different ages available in the control volume are removed at a rate which is nearly proportional to their relative abundance (random sampling).

The theoretical tools have been illustrated through the application to a simplified one-dimensional domain characterized by constant advection and dispersion. The same approach however can be adapted to heterogenous 3D models, to seek characteristic shapes of the age-selection functions arising from complex (and more realistic) domains.

The observed trends of age mixing dynamics originated in dispersive processes provide clues for the development of general catchment-scale transport models for heterogeneous geophysical systems (like hillslopes, catchments or entire watersheds), where the velocity field is typically unknown and the definition of explicit, large-scale mixing assumptions could significantly improve our ability to characterize observed hydrochemical patterns.

Chapter 4

Modeling the Hupsel Brook Catchment (NL)

4.1 Introduction

In this chapter, analytical, time-variant travel time distributions are used to model the leaching of chloride from a small and well-instrumented agricultural catchment in the Netherlands. The aim of the study is twofold: i) demonstrate the suitability of the general formulation of transport by travel time distributions to describe a real-world case study where empirical hydrologic and chemical information is simultaneously available; ii) identify the uncertainty in the model structure/parameters, and the additional information gathered when chemical data are added to the hydrologic data during calibration. The key role played by the time-variance of transport processes (emerging at different temporal scales) is also highlighted.

4.2 The Random Sampling (RS) scheme

Among the possible age-selection schemes (see Chapter 2), a noteworthy case is the one where ages are randomly sampled by the output fluxes in the same proportion as they are stored in the control volume (random sampling). Under this hypothesis, the age distribution of the outflows is fully representative of the age distribution of the whole storage, and the solution to the master equation gets particularly simple and instructive [*Botter*, 2012]. This framework has been previously called *complete mixing* (or *well-mixed case*), which is however a misleading term in that it seems to imply spatially uniform concentrations in the control volume, as a byproduct of the instantaneous

mixing of each input with the existing storage. Instead, even though a well-mixed system behaves by definition as a random sampler, yet there exist systems far from being completely mixed where the output fluxes may still sample stored ages proportionally to their relative abundance. Hence, this mixing scheme is termed *random-sampling* (RS), to emphasize that spatial gradients of resident ages (or solute concentrations) are not necessarily neglected. Physically, the situation is representative of control volumes where mixing of ages and macro-dispersion are significant. The assumption of random sampling was proved to be quite robust in single hillslopes characterized by heterogeneous soils [*Rinaldo et al.*, 2011]. Moreover, the non-point source nature of the inputs and the integrative nature of the network geometry [*Rinaldo et al.*, 1991] seem to favor the robustness of this assumption also in larger catchments with complex network structures.

Mathematically, the RS assumption implies that the distributions p_Q and p_{ET} coincide with p_S (i.e. $\omega_Q = \omega_{ET} = 1$), leading to a major simplification in eq. (2.7) that gives:

$$\frac{\partial p_S(T_R,t)}{\partial t} + \frac{\partial p_S(T_R,t)}{\partial T_R} = -\frac{J(t)}{S(t)}\, p_S(T_R,t) \tag{4.1}$$

and whose general solution is readily available [*Rinaldo et al.*, 2011]. Though relatively simple, the random-sampling hypothesis has a broad range of applications, especially when the catchment is schematized as a combination of different water storages in series or in parallel (as customary on conceptual modeling of the interactions of, say, the root zone and groundwater). The RS scheme could then be applied to each compartment, providing an overall non-RS storage. The overall travel time pdf's would be obtained from those pertaining to each sub-storage by means of weighted averages (parallel reservoirs) or convolutions (in-line reservoirs). This makes the scheme flexible to different types of applications. In relatively small lowland catchments of the type considered in this paper, reasonable results can be obtained through the use of two storages, as shown in Section 4.4.

An advantage of applying RS schemes pertains the computation of the flux concentration of solutes transported through the hydrologic cycle. The equivalence between travel and residence time distributions implied by the RS hypothesis allows the use of p_S as the convolution operator in equation (2.8). Thus the flux concentration in the runoff is given by the composition of the different water particles' concentrations that are stored within the catchment at any time, yielding:

$$C_Q(t) = \int_0^\infty C(t - T_R, t) p_S(T_R, t) dT_R = \bar{C}(t) \tag{4.2}$$

where $\bar{C}(t)$ is the average storage concentration. This brings notable simplifications in the calculations because the outflowing concentration can now be computed as $\bar{C}(t) = M_S(t)/S(t)$, where M_S is the solute mass contained within the storage and can be obtained, as well as $S(t)$, from a mass balance. Equation (4.2) shows that behind such an apparently easy scheme there is a rather complex process, driven by time-variant TTD's. Therefore, the use of the mean concentration does not imply that all the water particles have the same concentration, but rather that the global concentration can be used to characterize the outflows. This makes transport modeling easier from a computational point of view, because all mass leaving a RS storage can be computed as the product between the output water flux $Q(t)$ and the average storage concentration $\bar{C}(t)$. Were this approach extended to a multi-storage system, each compartment would be characterized by a different average concentration that also characterizes the corresponding outflows.

4.3 The Hupsel Brook Catchment

The *Hupsel Brook* catchment is a small lowland watershed of about 6.5 km^2 located in the eastern part of the Netherlands (Figure 4.1). Due to its geological and hydrogeological characteristics it has been used as a research catchment since the 1960's [*Wosten et al.*, 1985; *van Ommen et al.*, 1989; *van der Velde et al.*, 2009, 2010a,b; *Brauer et al.*, 2011]. Data series regarding rainfall, discharge, solar radiation, temperature, chemical concentration, water levels, etc. are available at different time scales. In particular, more than 25 years of hourly discharge data at the outlet are available.

Typical of much of the Netherlands, the climate of the study area is semi-humid (annual rainfall about 700-1000 mm) with rare snowfall events in winter. Seasonality is quite marked. Summers are relatively dry and evapotranspiration is predominant, while winter is wet and characterized by a soil water content that is close to saturation. Intense agricultural use dominates the hydrologic and biochemical characteristics of the catchment. The crop fields are densely drained by ditches and almost 50% of the land is artificially drained via a tile drain network. Overland flow is mainly due to saturation excess, which is frequently observed in winter and it is estimated to contribute, depending on the period, between 25% and 40% of total catchment discharge [*van der Velde et al.*, 2010c, 2011]. The response of the catchment is quickened also by the high efficiency of the tile drainage network. Due to the small size of the catchment, discharge is relatively low (average flow is about 0.070 m^3/s) with highest peaks rarely reaching

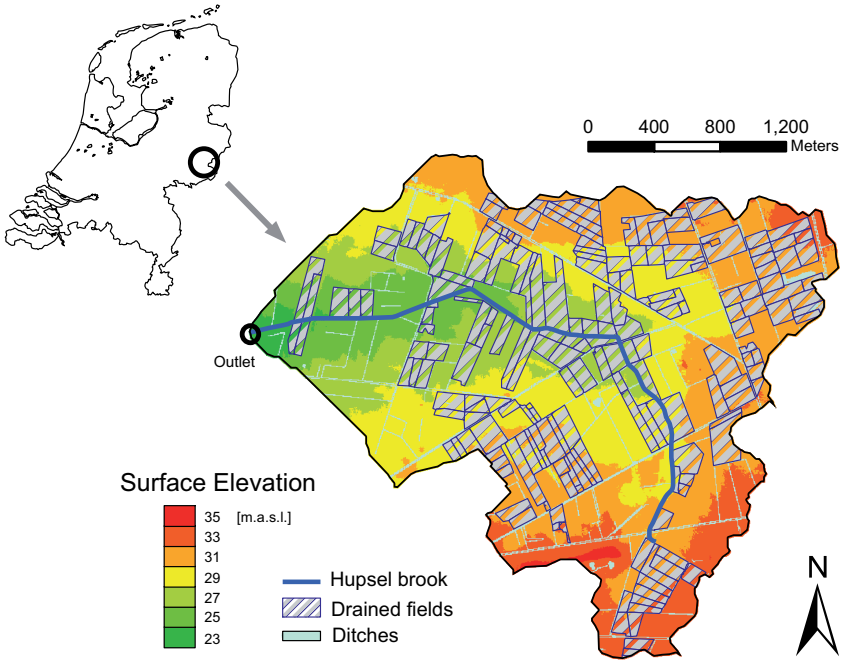

Figure 4.1: Sketch of the Hupsel Brook catchment.

2 m^3/s. Nutrients like nitrates, phosphates and chlorides are introduced into the soil in the form of manure and fertilizers during the fertilization period (March to October). Regional estimates of the inputs clearly show a decreasing trend in agricultural loads: chloride decreased from about 250 kg/ha in 1983 to less than 130 kg/ha in 2008 (-48%) [*van der Velde et al.*, 2010a]. Chlorides stemming from atmospheric sources are expected to be around a few mg/L, providing a negligible contribution if compared to uncertainty in anthropogenic loads.

In this study, one year of available chloride measurements in the discharge, from May 2007 to May 2008, are considered. Therein, samples have been taken with irregular frequencies of about one week. The mean over the measured period is about 30 mg/L, which is higher than the estimated input concentration during the preceding five yers (about 18 mg/L). Since chlorides are known to be non-reactive, the apparent imbalance between input and output is to be first addressed. This is a classical problem when dealing with chlorides [*Neal et al.*, 1988] and can be caused by a set of different reasons such as dry and occult deposition [*McMillan et al.*, 2012; *Page et al.*, 2007], presence of forested areas [*Guan et al.*, 2010; *Oda et al.*, 2009] or evapoconcentration during dry seasons. In the Hupsel Brook Catchment, forests are almost absent and as

wet deposition is very low (1-2 mg/l), also dry deposition is expected to be of the same order of magnitude, thus not sufficient to explain the 12 mg/l gap between output and input. The presence of some chloride concentration in soil waters can have a positive influence on vegetation [*Xu et al.*, 1999], but a potential toxicity is expected at such high concentrations. Under stress conditions, the plant metabolism can cause the transpiration of chlorides at a lower rate than water, resulting in a global increase of stored water concentration. Given annual water balance, according to which approximately 50% of annual rainfall goes into evapotranspiration, if plants uptake concentration were on average not higher than 10 mg/l, discharge concentration would increase up to approximately 30 mg/l, which would be amply sufficient to close the mass balance. Following similar conjecture, a successful approach was adopted by *van der Velde et al.* [2010a] who assumed plants to uptake chlorides at a fixed concentration, whose value was derived through calibration. Resulting value was significantly lower than discharge concentration and allowed balance closure. On a similar approach, a time-dependent uptake rate was used here to simulate time-variant evapoconcentration dynamics, as explained in section 4.4. In addition to its theoretical basis, such an approach can be an effective tool to take into account the uncertainties in input estimation.

Observed concentration, besides flat long-term mean, shows short-term fluctuations that, compared with discharge, suggest a negative correlation between Q and C (Figure 4.2). This is a typical behavior of chlorides in case water injections have lower concentration than baseflow [see *Neal et al.*, 2012], indicating that most of the discharge right after intense rainfall events is comprised of event water contributions. This further confirms the general affinity of lowland catchment responses for relatively new water suggested by *van der Velde et al.* [2012]. Finally, it is noted that concentration remains high even in winter period when fertilizations are suspended and discharges (that result in solute depletion) are higher.

4.4 Model

4.4.1 Hydrologic Model

A key-feature of the test catchment is the strongly non-linear dependence of the outflows on soil moisture content [*Brauer et al.*, 2011]. A soil moisture balance for the root zone [*Rodriguez-Iturbe et al.*, 1999; *Laio et al.*, 2001] was set up as :

$$nZ_r \frac{ds(t)}{dt} = I(t) - L(s(t)) - ET(s(t), t) \tag{4.3}$$

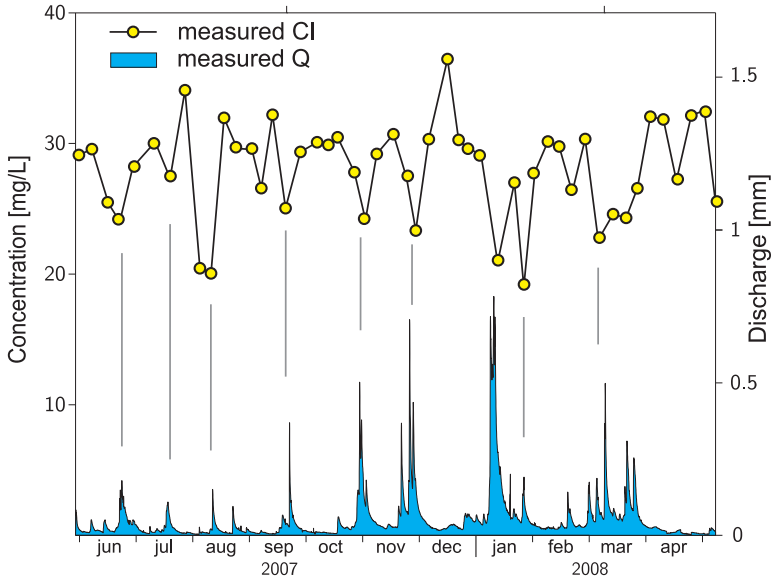

Figure 4.2: Measured discharge and chloride concentration from May 2007 to May 2008. Vertical bars highlight the matching between discharge peaks and flux concentration troughs

where n is porosity, Z_r the root zone depth [L], s the soil moisture content, I is infiltration into the root zone [L/T], L is the leakage to lower horizons [L/T] and ET is evapotranspiration flux [L/T]. The notation for L and ET stresses the dependence on s. The stored volume in the root zone ($nZ_r s$) is named Srz hereafter. As described in Section 4.3, fast hydrological response is due to artificial tile drainage network and to overland flow (mainly driven by soil water saturation excess). In both these two processes, water flux can be associated with soil moisture content, so all runoff contributions flowing out of the root zone were grouped together in a single non-linear leakage term, that was modeled through the Clapp-Hornberger equation [*Clapp and Hornberger*, 1978]. The redundancy of a separate modeling of the overland flow was confirmed by preliminary numerical experiments. Infiltration flux I was then set equal to rainfall intensity J.

Starting from eq. (4.3), four different models with increasing degree of non-linearity were tested (Figure 4.3). Model (a) is made of a single root zone storage that directly leaks into discharge. The other three models include deep storage that accounts for groundwater flow. This is obtained by partitioning the leakage from the root zone into two components: one producing the subsurface discharge Q_{rz} and one feeding the groundwater storage. Slow flows Q_{gw} originating from groundwater are modeled according to the linear reservoir scheme: $Q_{gw} = kS_{gw}$, while the overall discharge is the

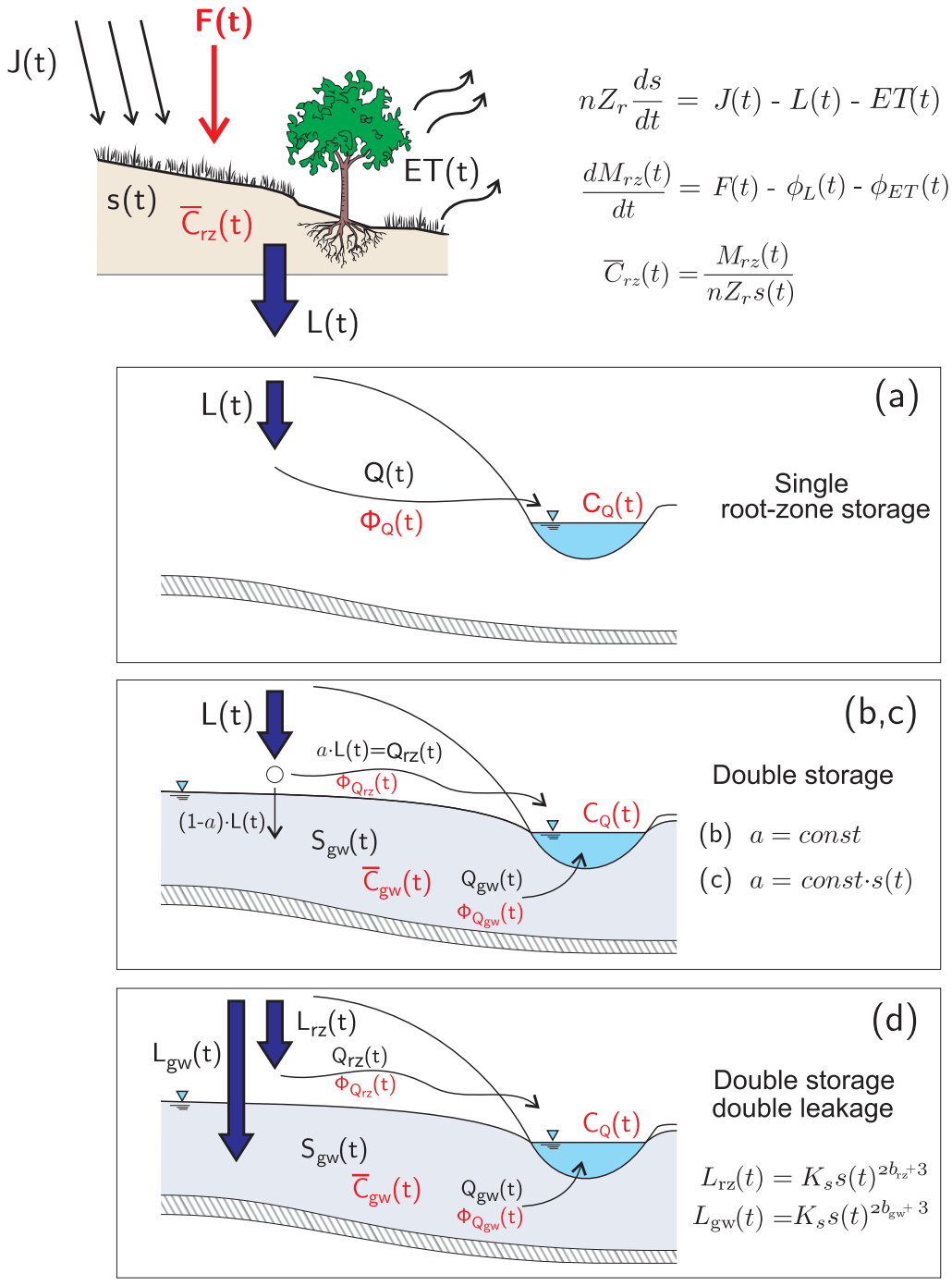

Figure 4.3: Tested models representation. Mass terms are colored in red. Mass fluxes are always associated with a corresponding water flux (e.g. ϕ_{rz} is mass flux corresponding to Q_{rz}).

		root zone storage	groundwater storage	
		all models	models (b,c)	model (d)
storage equations	av. conc.	$\overline{C}_{rz}(t) = \frac{M_{rz}(t)}{nZ_r s(t)}$	$\overline{C}_{gw}(t) = \frac{M_{gw}(t)}{S_{gw}(t)}$	$\overline{C}_{gw}(t) = \frac{M_{gw}(t)}{S_{gw}(t)}$
	water	$nZ_r \frac{ds(t)}{dt} = J(t) - L(t) - ET(t)$	$\frac{dS_{gw}(t)}{dt} = L_{gw}(t) - Q_{gw}(t)$	$\frac{dS_{gw}(t)}{dt} = L_{rz}(t) - Q_{gw}(t)$
	mass	$\frac{dM_{rz}(t)}{dt} = F(t) - \phi_L(t) - \phi_{ET}(t)$	$\frac{dM_{gw}(t)}{dt} = \phi_{Lgw}(t) - \phi_{Qgw}(t)$	$\frac{dM_{gw}(t)}{dt} = \phi_{Lgw}(t) - \phi_{Qgw}(t)$
water	inflows	J	$L_{gw}=(1-a)L$ *	$L_{gw}= K_s s(t)^{2b_{gw}+3}$
	outflows	$ET=ET_{max}\frac{s(t) - s_w}{s^* - s_w}$ $L = K_s s(t)^{2b+3}$	$Q_{gw} = kS_{gw}$	$Q_{gw} = kS_{gw}$
mass	inflows	F	$\phi_{Lgw}(t) = \overline{C}_{rz} L_{gw}$	$\phi_{Lgw}(t) = \overline{C}_{rz} L_{gw}$
	outflows	$\phi_L=\overline{C}_{rz} L$ $\phi_{ET}=\alpha \overline{C}_{rz} ET$	$\phi_{Qgw} = \overline{C}_{gw} Q_{gw}$	$\phi_{Qgw} = \overline{C}_{gw} Q_{gw}$

* leakage separation is constant $a= ls_1$ in model (b), while it is time-variant $a= ls_2 \cdot s(t)$ in model (c)

Figure 4.4: Summary of model equations for the 4 models tested in this paper

sum of subsurface and deep components $Q(t) = Q_{rz}(t) + Q_{gw}(t)$. The key difference between the three multi-storage models lies in leakage partitioning. Model (b) uses a constant partition, while model (c) uses a time-variant partition that is a function of the soil moisture content. Finally, model (d) has two separate leakages from the root zone, to separate the processes giving birth to fast response flows (preferential pathways, drainage network, etc) from those that produce deep percolation and groundwater flow. The main equations implemented within each model are summarized in Figure 4.4.

4.4.2 Transport Model

A transport model for chloride was coupled to the hydrologic model on the following premises. Solute main input to the catchment is the mass introduced through fertilization. Mass loads were calculated by dividing annual estimates into the total number of hours characterizing fertilization season. Loads were introduced during every hour of the fertilization season but were assumed to remain immobile in the topsoil until a new rainfall pulse mobilized them through infiltration. Therefore, the concentration of a new rainfall pulse was obtained as the total mass loaded since previous precipitation, divided by rainfall depth. An additional constant chloride concentration in rainfall (wet deposition), though very low compared to uncertainty in fertilization loads, was accounted for and set to 1.5 mg/L [*van der Velde et al.*, 2010a].

The main assumption of the transport model is that both root zone and groundwater storage are random sampled. This allows the numerical computation of the outflowing

concentrations to be simplified by the introduction of mass balances that implicitly incorporate the time-variant structure of the convolution operations, as shown in eq (4.2). Such a convenient implementation is used throughout the calibration process (see Section 5). Travel time distributions are then calculated on the calibrated model, to infer their time-variant properties.

Under the RS hypothesis, the two modeled storages can be characterized by average concentrations $\bar{C}_{rz}(t)$ (root zone) and $\bar{C}_{gw}(t)$ (groundwater) respectively. Chlorides are assumed to be conservative (no reaction takes place along with the transport), but they are assumed to be only partially uptaken by plants because of their potential toxicity on plants metabolism [*Xu et al.*, 1999; *Taiz and Zeiger*, 2010]. Plants are assumed to sample particles from the root zone with concentration C_{ET} that is proportional to the average concentration of soil moisture: $C_{ET}(t) = \alpha\bar{C}_{rz}(t)$, with $\alpha \in [0, 1]$. During evapotranspiration, solutes leave the system at a lower rate than water, resulting in an increase of the average storage concentration. This yields a higher flux concentration in the runoff offering a possible explanation to the apparent chloride imbalance, as discussed in Section 4.3.

Mass balance in the root zone yields:

$$\frac{dM_{rz}(t)}{dt} = \phi_J(t) - \phi_L(t) - \phi_{ET}(t) \tag{4.4}$$

where M_{rz} is the chloride mass contained in the root zone and the terms ϕ_J, ϕ_L and ϕ_{ET} are mass flows attached to rainfall, leakage and evapotranspiration respectively. All mass fluxes in eq. (4.4) can be expressed as water fluxes times the corresponding flux concentrations. Recalling the random-sampling hypothesis for the leakage flow ($C_L = \bar{C}_{rz}(t)$) and the selective evapotranspiration assumption ($C_{ET} = \alpha\bar{C}_{rz}(t)$) one gets:

$$\frac{d}{dt}(\bar{C}_{rz}(t)S_{rz}(t)) = C_0(t)J(t) - \bar{C}_{rz}(t)L(t) - \alpha\bar{C}_{rz}(t)ET(t) \tag{4.5}$$

where C_0 is the initial concentration of rainfall pulses. By expanding the derivative of the product at left-hand side of equation (4.5) and rearranging the equation, one gets the differential equation that governs the average concentration $\bar{C}_{rz}(t)$ in the root zone storage as:

$$\frac{d\bar{C}_{rz}(t)}{dt} = \frac{J(t)}{S_{rz}(t)}(C_0 - \bar{C}_{rz}(t)) + \frac{ET(t)}{S_{rz}(t)}(1 - \alpha)\bar{C}_{rz}(t) \tag{4.6}$$

Equation (4.6) shows that average storage concentration is increased/decreased when initial concentration of rainfall pulses is higher/lower than the resident concentration $\bar{C}_{rz}(t)$ (first term at right-hand side). Moreover, selective evapotranspiration (second

Table 4.1: Constant parameters of the four tested models

Parameter	Symbol	model (a)	model (b)(c)(d)
soil porosity [-]	n	0.35	0.35
root zone depth $[mm]$	Z_r	750	750
soil moisture at wilting point [-]	s_w	0.11	0.11
soil moisture for runoff triggering [-]	$s*$	0.35	0.35
saturated soil conductivity $[mm/h]$	K_{sat}	100	100
initial groundw. saturated depth $[mm]$	S_{gw_0}/n	–	1000
initial groundw. conc. $[mg/L]$	$\bar{C}_{gw_0}$	–	40

term at right-hand side) induces an increase in $\bar{C}_{rz}(t)$ (recall $(1-\alpha) > 0$) which is stronger when evapotranspiration is more intense.

Models (b), (c), and (d) also employ a groundwater storage that is assumed to be randomly-sampled with no evapotranspiration occurring within the groundwater compartment. Provided that output fluxes do not change the storage concentration, the evolution of average concentration in the groundwater storage is due only to the leakage input:

$$\frac{d\bar{C}_{gw}(t)}{dt} = \frac{L_{gw}(t)}{S_{gw}(t)}(\bar{C}_{rz}(t) - \bar{C}_{gw}(t)) \tag{4.7}$$

and the final flux concentration is the weighted average of subsurface and groundwater flow concentrations:

$$C_Q(t) = \frac{Q_{rz}(t)}{Q_{rz}(t)+Q_{gw}(t)}\,\bar{C}_{rz}(t) + \frac{Q_{gw}(t)}{Q_{rz}(t)+Q_{gw}(t)}\,\bar{C}_{gw}(t) \tag{4.8}$$

The related water travel time distributions are derived in detail in Appendix A.4.

4.5 Parameters, Calibration and Ranking Methods

Each of the four models tested in this paper requires the determination of the related parameters. Some of these parameters, common to all the models, were chosen according to previous works and are summarized in table 4.1. The remaining free parameters (hydrologic ones plus the selective evapotranspiration factor α) are in number 5 in model (a) and 6 in models (b, c, d) and have been derived through calibration.

To fully explore the parameters space, a Montecarlo approach is employed [*Beven and Freer*, 2001]. For each model, 10^7 simulations were run with combinations of random parameters sampled from a uniform prior distribution. The length of the simulation

Table 4.2: Setup of Montecarlo calibration (CH = Clapp-Hornberger, LS = leakage separation; GW = groundwater)

Parameter	Symbol	Parent model	min	max
max ET warm periods $[mm/h]$	ET_{maxw}	a-d	0.05	0.15
max ET cold periods $[mm/h]$	ET_{maxc}	a-d	0.01	0.06
plants selectivity coeff. [-]	α	a-d	0	0.6
CH parameter $[mm/h]$	b	a, b, c	8	18
CH parameter $[mm/h]$	b_{rz}	d	5	15
CH parameter $[mm/h]$	b_{gw}	d	10	20
LS coefficient [-]	ls_1	b	0.1	0.9
LS coefficient [-]	ls_2	c	0.5	1.5
GW coefficient $[h^{-1}]$	k	b, c, d	0.1×10^{-4}	3×10^{-4}

period is 350 days (from May 2007 to May 2008), which, at an hourly timescale, results in 8400 simulated timesteps for each run. Initial groundwater average concentration $\bar{C}_{gw_0}$ was derived from preliminary simulations starting approximately 22 years before the start of the measurements. The resulting value (40 mg/l) was observed to be quite stable under different reasonable model settings and initial conditions. Other details about the setup of the calibration procedure are summarized in table 4.2. In order to rank model performances, the Nash-Sutcliffe model efficiency was first evaluated for discharge ($NS_Q = 1 - \sum_{i=1}^{n}(Q_{i,meas} - Q_{i,calc})^2 / \sum_{i=1}^{n}(Q_{i,meas} - \overline{Q_{meas}})^2$) over 8400 discharge measurements. The Residual Sum of Squares was used instead for chloride concentration in discharge ($RSS_C = \sum_{i=1}^{n}(C_{i,meas} - C_{i,calc})^2$) over the 50 available chloride concentration measurements.

Models and parameters were accepted if $NS_Q > 0.75$, and the accepted models were then ranked according to their RSS_C score (the lowest RSS_C corresponds to the best performance). The *behavioral* subset of simulations for the sensitivity analysis was defined by the first 100 performances of the ranking.

4.6 Results

After calibration, each of the four models was associated with a ranking of the 100 best RSS_C scores. This makes it easy to compare the models in order to select the most suitable one. A representation of the scores versus the ranking position is shown in Figure 4.5.

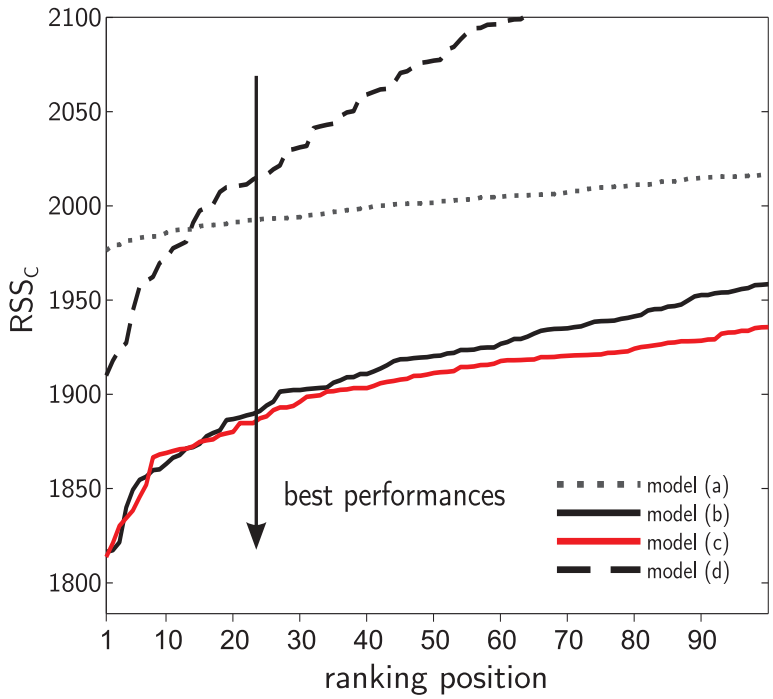

(a) single randomly-sampled (RS) storage
(b) double RS storage (constant leakage separation)
(c) double RS storage (time-variant leakage separation)
(d) double RS storage with two leakage sources

Figure 4.5: Ranking of model performance according to first 100 Residual Sum of Squares scores.

Model (a) performed the worst (i.e. possessed the highest RSS scores), especially for the first positions of the ranking, showing that the single storage proves too rough a scheme to correctly reproduce the main mechanisms responsible for the measured concentration data. Moreover, the score function shown in Figure 4.5 is quite flat, meaning that the differences in score among different parameter combinations is low, thus implying that optimal parameter identification is uncertain. Remarkably, were the focus limited to discharge alone, model (a) would be as performant as the double storage models. This issue is further discussed in Section 3.6. Models (b) and (c) have similar performances and clearly outperform the single random-sampling (a) and the double-leakage (d) models. The pronounced slope of the score function in the region of the first positions of the ranking indicates that optimal parameter identification is reliable. Model (d) allows for a clear identification of its parameters, but the performances are not satisfactory. After the first twenty positions of the ranking it is even worse than the single random-sampling model. Even though the double leakage was designed to be flexible enough to simultaneously capture fast and slow subsurface flow processes, the number of free parameters proved inadequate to meet this purpose. As model (c) has, on average, the best scores, it is selected as the choice model to describe the hydrochemistry of the Hupsel Brook catchment.

The posterior parameter distribution of the selected model is represented in Figure 4.6, suggesting the robustness of the identification procedure in this case. The corresponding discharge and chloride concentration series from the best 100 model parameterizations are then compared to observations in Figure 4.7 and Figure 4.8. Modeled discharge series shows a general agreement with the measurements. For low flows ($O(10^{-2})$ mm/h, approximately equivalent to 20 l/s) the model tends to underpredict discharge, with no significant effect on its chemical composition and travel time distributions, because of the negligible impact of low flows on the storage and residence time distributions. Modeled chloride concentration (Figure 4.8) is able to reproduce the two main observed features, that are the general fluctuations pattern and the mean value of about 30 mg/l. The mean value is a direct consequence of the employed evapoconcentration scheme, which proved effective in simulating the observed difference between input and output concentrations. The model is less accurate during periods where separation between fast and slow flow contributions to discharge is more uncertain. This is visible in the period June-July 2007, as also underlined by the larger deviations of model simulations among each others.

The reliability of the model allowed a meaningful analysis of the travel time distri-

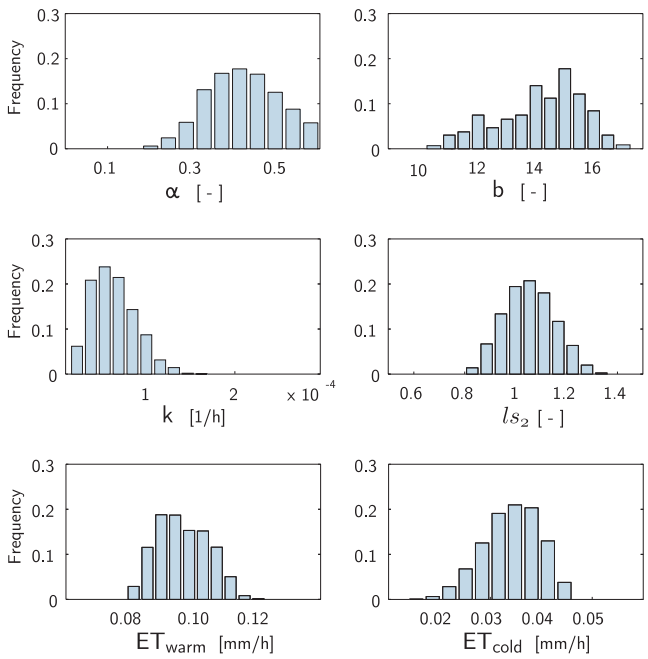

Figure 4.6: Sensitivity plots for 100 best performances of the selected model. Parameter description and range is described in table 4.2.

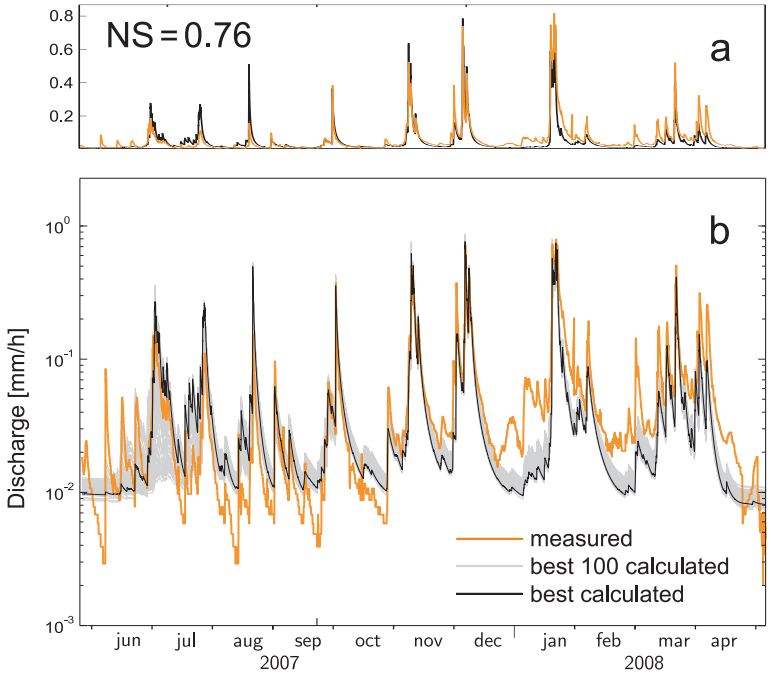

Figure 4.7: Discharge series modeled according to the selected model (model C). All simulations have Nash-Sutcliffe (NS) score ≥ 0.75. Figure (4.7a) shows best performance in natural axis while figure (4.7b) shows 100 best performances in semi log-scale

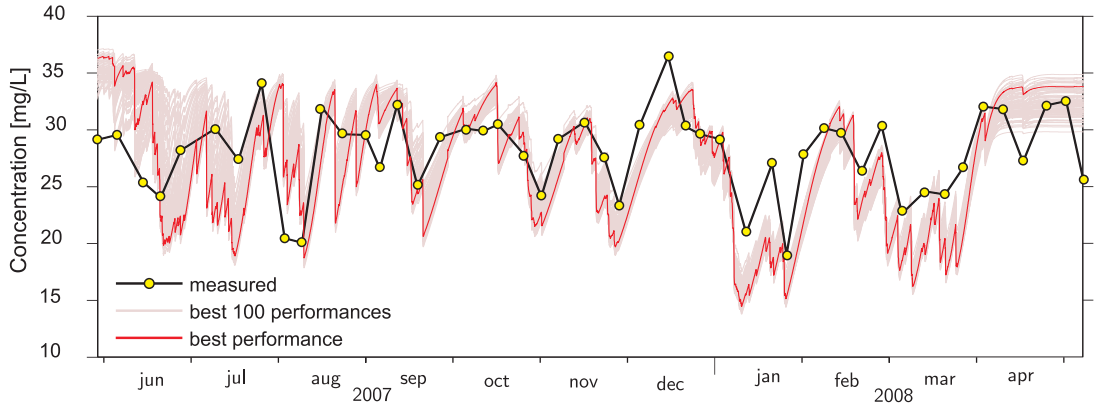

Figure 4.8: Modeled chloride concentrations for the 100 best performances of the selected model.

butions that enabled to match the observed concentrations. TTD's were first calculated for the two storages separately, and then combined together to get the overall distributions (eq. (A.17)). As each distribution retains the memory of the hydrologic history of the system for years, the calibrated model was started 20 years before the beginning of the available measurements, to ensure the tails of the distributions were properly calculated. A startup period of 16 years was observed before discharge was made for more than 99% by water injected into the system after the start of the simulation. This assured that, over the period 2004-2008, TTD's were computed over more than 99% of their age-domain. For this period, the mean value of each distribution was used for further analysis.

A look into the temporal evolution of mean travel times in the two storages allows an assessment of the difference in the corresponding characteristic time-scales (Figure 4.9). The root zone is characterized by a low ratio between storage and flows, meaning that it is relatively dynamic. Therefore, the storage has short memory of past rainfall events and mean travel times are easily affected by single events, producing high frequency fluctuations in the transport features, including the mean (Figure 4.9). Groundwater, on the contrary, has a much larger ratio between storage and flows, meaning that it is only affected by long term variability of climate conditions and it is likely to be characterized by seasonal and inter-annual fluctuations.

The TTD's of the root-zone and groundwater storages were then combined together to yield the overall travel time distributions. The mean of the overall TTD shows a rather irregular behavior, reflecting the continuous interplay between fast and slow flow contributions to discharge. In contrast with stationary distributions, that are

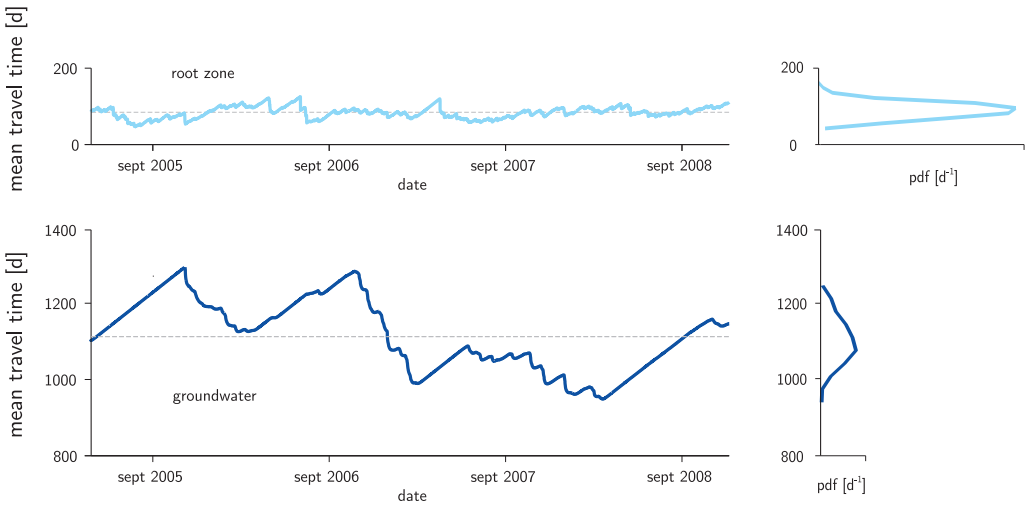

Figure 4.9: Mean travel time computed over a four-year period.

characterized by a single mean value, a whole pdf of mean travel times is note here, with a Coefficient of Variation CV of 0.77 (Figure 4.10). The two peaks of the pdf of the mean travel times recall the fact that streamflows are a suitable combination of young ($O(100\ d)$) water from the root zone and old ($O(1000\ d)$) water from groundwater. The average travel time, though not representative of the actual travel time of the transported water particles (its frequency is practically zero), is of the order of 1.45 years. This turns out to be slightly lower but very similar to the value of 1.8 years estimated by *van der Velde et al.* [2010a]. This difference is due to the different model structures and to the non-stationarity of the distributions over the years, (TTD's were calculated here during a shorter time window with respect to *van der Velde et al.* [2010a]).

The highly non-stationary behavior renders rather meaningless, for transport computations, the characterization of catchment travel times through stationary distributions, as frequently pursued in the literature. Nevertheless, stationary distributions are entirely meaningful in the context of peak discharges and where no basin-scale transport is attached to the hydrological component (as the age paradox is immaterial as long as only the quantity of the runoff water is pursued).

4.7 Discussion

The analysis of TTD's allows for proper understanding of large-scale, multi-state control volumes hosting transport processes. Here, it was shown that root zone (i.e. near-

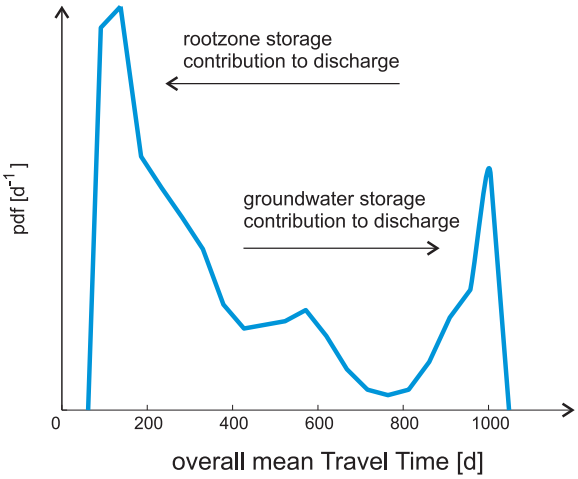

Figure 4.10: Empirical probability distribution function of the mean travel time in the Hupsel Brook catchment.

surface) residence times are affected by short-term events, leading to the relatively fast release of solutes associated with regimes entailing transport times ranging from weeks to months. Moreover, solutes in the root zone (or whatever is conveniently modeling the behavior of a near-vertical water and solute circulation) are likely to be quickly diluted in case of intense rainfall events and almost completely removed in periods with no fertilization. On the contrary, solutes that reach groundwaters are released at lower rates and tend to accumulate and persist for much longer times. The combination of these separate behaviors, together with the time-variant partitioning between discharge contributions, fully captures the behavior of solutes transported along the catchment. The framing of this particular model into the general scheme of the Master Equation for residence and travel time distributions clarifies a mathematical position that may seem arcane unless dressed by a proper physical meaning.

After intense rainfall events, large amounts of new water enter the root zone. In this case new water is almost solute-free (even in the presence of fertilization because solutes get largely diluted), so it causes the average concentration in the root zone outflows $\bar{C}_{rz}$ to suddenly decrease. According to the model(s), because the main discharge component right after rainfall events is subsurface flow, solute concentrations in the global discharge also quickly decreases. This corresponds rather well with the observed concentration decreases (recall Figure 4.2). Note that this dilution mechanism could be simulated by a single storage model. However, in such a case, concentration would remain low until solutes are replenished by new fertilizations. Even so, this would take a long time to occur and would not happen at all in periods with no fertilization.

What makes it possible for the model to allow re-growth of the flux concentration is the presence of deep storage. Solutes in the groundwater tend to persist and accumulate, so at any time chlorides mainly belong to older fertilizations from many years before. Also, during wet winter periods the average groundwater concentration remains high (around 40 mg/L) because past fertilizations are speculated to be more intense [*van der Velde et al.*, 2010a]). As soon as subsurface contribution to discharge is depleted, the main discharge source is groundwater flow, which increases solute concentration again.

The use of travel time distributions fosters a deeper understanding that can be of practical use. It often happens in rural catchments [*Aquilina et al.*, 2012; *Ruiz et al.*, 2002] that stopping fertilization loads for one or more years does not result in a significant permanent decrease of average stream concentrations. According to these results, the same would occur in the Hupsel Brook catchment. Ceasing fertilizations would affect the root zone storage, mainly because of its short hydrologic memory as underlined by its relatively short mean travel times. For the same reason, groundwater storage would hardly be affected. As the average concentration is the byproduct of long-term dynamics, it is mainly governed by the groundwater storage which hardly responds to just one or two non-fertilized seasons.

The single-storage model was able to reproduce measured discharge with the same accuracy as double-storage models. This means that it is appropriate, as commonly held, in describing the hydrological response but not in describing transport, making clear the different nature of the two problems. Hence, the ability of the model to reproduce measured concentration data lies in the double-storage schematization. It seems reasonable for relatively small and densely drained catchments to schematize both the root zone and groundwater as separate but randomly-sampled storages. Then the non-linear and non-stationary partitioning among the storages makes the overall system strongly non randomly-sampled. In hydrologic practice, however, more storages could be employed (e.g a "saturated area" storage which can capture the very fast response of the catchment). This would potentially yield better model performance, but it is unclear whether improved performance would be justified by the added complexity, say via Akaike testing. It is remarked, however, that this goes beyond the scope of this study, centered, as it is, on the inferences of non-stationary travel time tools and comparative field data analysis on the basic transport mechanisms operating in a typical catchment setting.

4.8 Final remarks

The Master Equation for the residence time distribution, keeping track of the temporal evolution of the ages in storage, has the central role of generator of all the other involved distributions. What is needed for application is a reasoned choice of input-output flows, possible chemical reactions and an age-selection scheme. The random-sampling assumption employed in this study is one of the many possible choices having some key operational advantages. Results can be tested with different hydro-chemical models and mixing schemes, at no loss of generality.

Besides theoretical aspects, the theory has found in the Hupsel Brook catchment a broad space for application. Modeling chloride concentration in discharge led to understanding and reproducing long term and short term transport dynamics. The schematization of the catchment by separate randomly-sampled compartments is computationally easy and proved reliable in reproducing measured signals.

As one of the first applications to real catchments, the model was tested on simple non-reactive solutes. Future applications can be extended to solutes that undergo different transport processes, by including proper chemical, physical or biological reactions.

Chapter 5

Modeling the Hafren Catchment (UK)

5.1 Introduction

High-frequency datasets prove particularly important for understanding event-scale dynamics which may cause rapid fluctuations in stream concentrations [*Kirchner and Neal*, 2013]. High-frequency measurements allow the identification of shifts in catchment behavior associated with variations in catchment connectivity caused by drying and wetting [*Tetzlaff et al.*, 2014; *Smith et al.*, 2013]. Similarly, stream hydro-chemistry can be used to investigate the role of non-linearities and thresholds in runoff generation [*Detty and McGuire*, 2010a; *Gannon et al.*, 2014]. This is especially true in headwater catchments, where geomorphic effects of river networks [*Rinaldo et al.*, 1991] can be disregarded and the critical role of hillslope processes is dominant. Hence, the view on catchments as stochastic dynamical systems [*Kirchner*, 2009; *Botter et al.*, 2009] favors the use of a time-variant approaches [*Botter et al.*, 2010; *Rinaldo et al.*, 2011; *Botter et al.*, 2011; *van der Velde et al.*, 2012; *Benettin et al.*, 2013a; *Harman*, 2014] towards travel time distributions.

The availability of high-quality datasets, jointly with extensive information on soil features and biogeochemistry, make the Plynlimon watersheds an ideal place to test recent advances in water age theory. In particular, the focus here is analyzing and modeling chloride concentrations at the catchment outlet during one year of high-frequency measurements, with a view toward clarifying physical processes.

Chloride has been extensively used to investigate transport processes at the catchment scale [*Kirchner et al.*, 2000; *Page et al.*, 2007; *Shaw et al.*, 2008; *Oda et al.*, 2009;

Godsey et al., 2010; *Kirchner et al.*, 2010; *van der Velde et al.*, 2010a; *Hrachowitz et al.*, 2013; *Benettin et al.*, 2013b], because it can be often considered as a conservative tracer [see *Svensson et al.*, 2012]. At Plynlimon, chloride mainly originates from sea salt in rainfall, cloud water, and aerosol dry deposition, resulting in mean streamflow concentrations of about $5-7$ mg/l [*Neal and Kirchner*, 2000; *Kirchner and Neal*, 2013]. Such a concentration is significantly higher than background noise, but lower than the toxicity threshold for vegetation uptake [*Xu et al.*, 1999], implying some active role of plant uptake in the underlying solute circulation. Still, the impact of vegetation on tracer transport is poorly understood [*Brooks et al.*, 2010; *Penna et al.*, 2013] and catchment mixing processes cannot be quantified directly. Thus, hydrochemical models represent a useful tool to test hypotheses concerning physical processes that drive solute circulation in river basins.

As in the previous chapter, this study is developed using backward travel time distributions under the assumption of multiple randomly-sampled (RS) storages. However, the concept of catchment storage is advanced by introducing the 'residual' storage, which is the portion of storage that does not emerge from simple water balances [*Kirchner*, 2009; *Birkel et al.*, 2011].

5.2 Data and study area

The data of this study are from the Upper Hafren catchment, mid-west Wales (UK), where the Centre for Ecology and Hydrology (CEH) conducted intensive measurement campaigns (2007-2009), aimed at taking high-frequency water quality measurements in precipitation and streamflow, spanning more than 40 elements of the periodic table [*Neal et al.*, 2012, 2013; *Kirchner and Neal*, 2013]. The watershed is part of the Plynlimon catchments, which have been extensively studied for the last 40 years, resulting in a notable body of literature that documents their climatic and morphologic features and explores their hydrological and hydrochemical behavior [see *Kirby et al.*, 1991, 1997; *Neal et al.*, 2001; *Neal*, 2004; *Brandt et al.*, 2004; *Marc and Robinson*, 2007, and references therein].

The Hafren catchment (3.7 km^2) is subdivided into an upper and lower part (Figure 5.1) corresponding to two distinct landscapes [*Neal et al.*, 2010]. The Lower Hafren (LH) is a Sitka spruce forest plantation underlain by peaty podzol soils, whereas the Upper Hafren (UH) is a relatively undisturbed moorland catchment with some wetland areas. Both UH and LH catchment outlets were monitored during the measurement

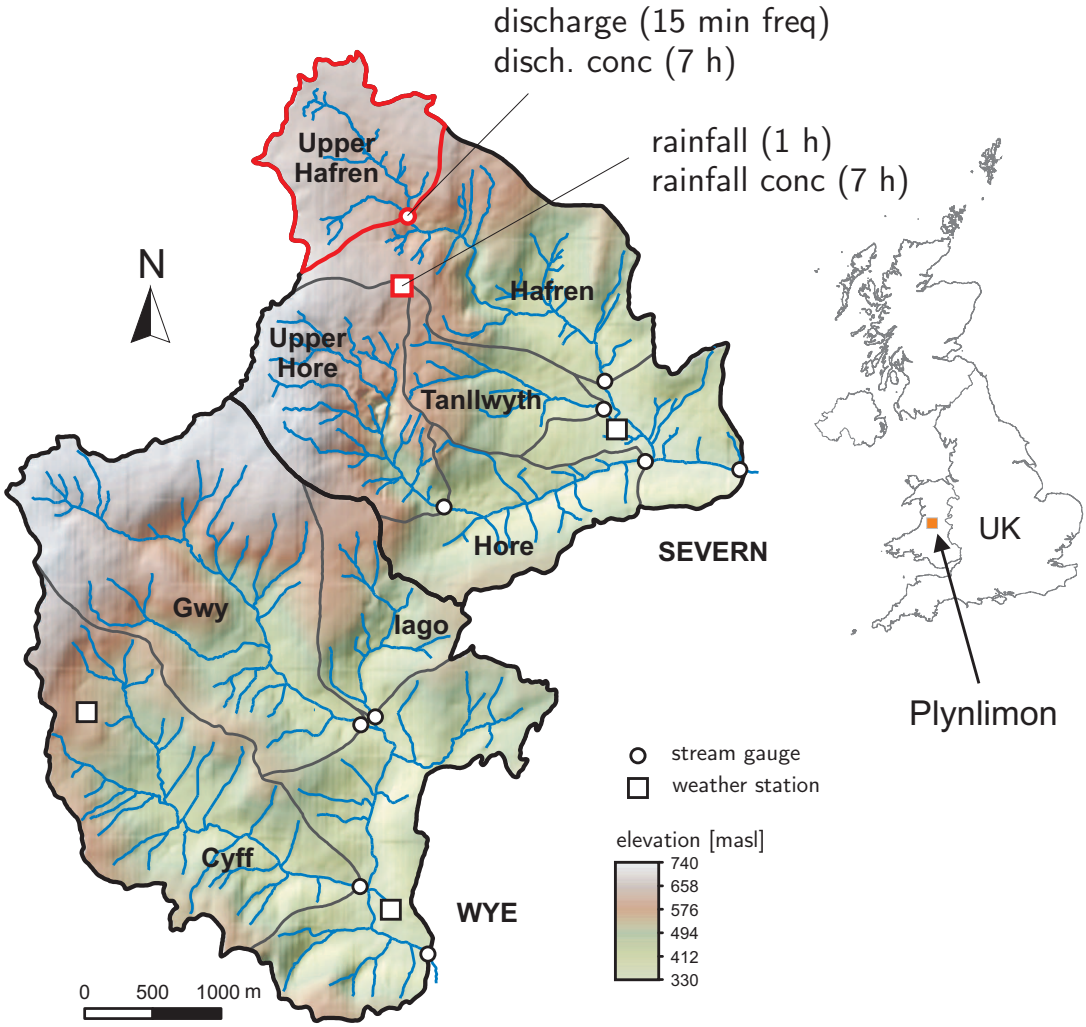

Figure 5.1: Map of the Plynlimon watersheds, obtained from a DTM.

campaign. Our analysis focuses on the UH because its high-frequency water quality record is longer. Further information describing the UH can be found in *Neal et al.* [2010, 2011]. The contributing catchment is small (1.2 km^2) with elevations ranging from 533 m at the gauging station to 738 m at the upper divides. A peat soil of about 40 cm overlies highly fractured mudstone and shale bedrock. The bedrock gets progressively less weathered with depth, but borehole investigations revealed volumetrically significant water at depths up to 35 meters and hydrologically active fracture flow at depths up to 95 meters [*Neal et al.*, 1997; *Haria and Shand*, 2004; *Shand et al.*, 2005].

The climate is generally wet, with annual average precipitation about 2650 mm. Although detailed evapotranspiration estimates are not available for UH, extrapolations from surrounding catchments [see *Marc and Robinson*, 2007] and a simple water balance based on precipitation and discharge measurements suggest that evapotranspiration may be 15% or less of precipitation. The hydrologic response is fast, with peak flows typically occurring within one hour of precipitation and with a marked non-linear relation between storage and discharge, as described by *Kirchner* [2009].

Chloride inputs are due to sea salt aerosols coming from the Atlantic Ocean, whose concentration can vary prominently from one storm to the next. The signal is much damped in discharge due to catchment transport processes that act as a fractal filter and convert white noise inputs into $1/f$ noise outputs [*Kirchner et al.*, 2000; *Kirchner and Neal*, 2013]. As shown by *Neal et al.* [2012], streamflow concentration displays time-varying correlations with discharge (Figure 5.2), with discharge peaks corresponding to both positive and negative fluctuations in chloride concentrations. This suggests the presence of a base-flow concentration that is temporarily increased/decreased when high-flow components are characterized by a higher/lower concentration [*Neal et al.*, 2012]. The rationale behind this idea will be further explored with the aid of the model results (Section 5.4).

To avoid some large gaps that occurred in the water quality measurements, the analysis spans the period from 22 December 2007 to 24 November 2008 (338 days) and comprises 1161 samples at 7-hour intervals, including a few minor gaps. Over the same period, hourly rainfall measurements from the Carreg Wen station and 15-minute discharges at the outlet are available. All water quality data are property of CEH and are freely available through their Information Gateway (https://gateway.ceh.ac.uk/).

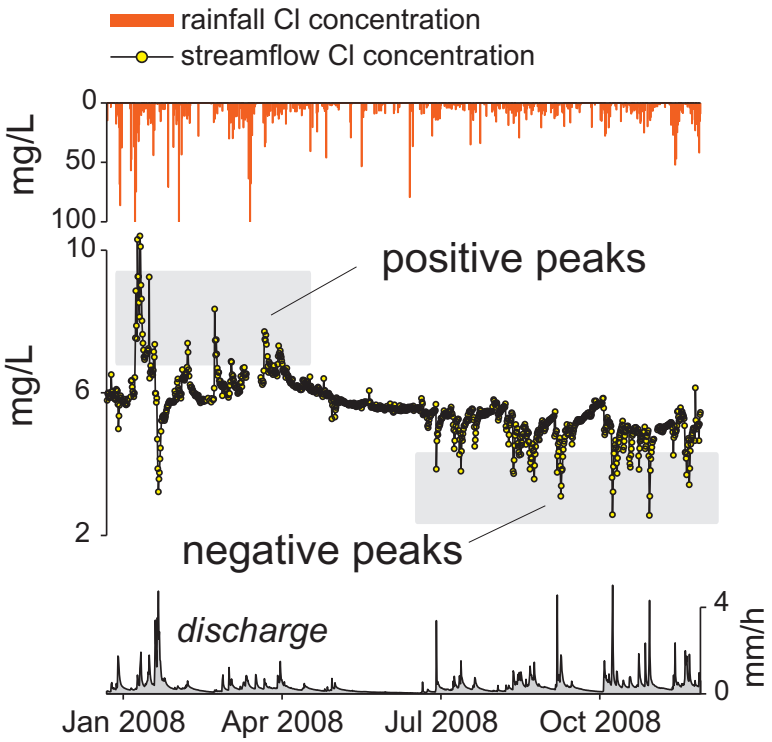

Figure 5.2: Chloride measurements over the considered period (22 December 2007 - 24 November 2008).

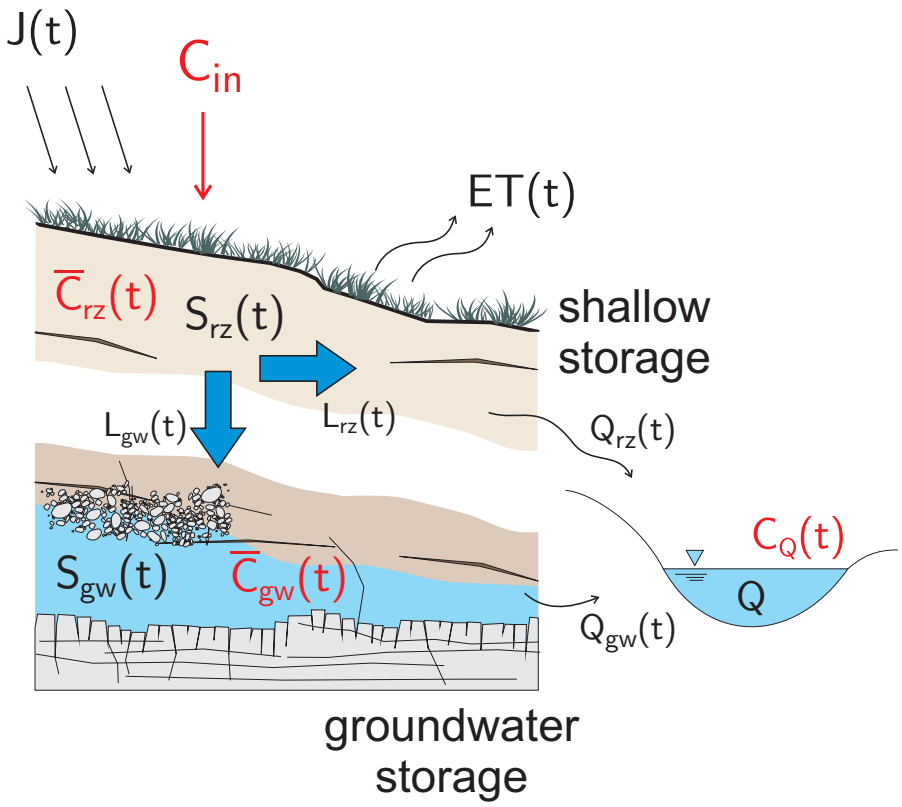

Figure 5.3: Conceptual catchment representation.

5.3 Hydrochemical model of Upper Hafren and its parameter calibration

A simple hydrochemical model was developed to simulate chloride transport at Upper Hafren. The model is similar to that used in *Benettin et al.* [2013b] and is made up of a hydrological and a chemical component: the hydrological model is needed to estimate water fluxes and storages over the simulation period, while the chemical model describes the evolution of chloride concentrations within the catchment and in the outflows.

5.3.1 Hydrologic Model

Previous studies of the Hafren catchment [e.g. *Shand et al.*, 2005; *Haria and Shand*, 2006] inspired the schematization of the catchment as a two-layers system, characterized by a shallow and a deep component (Figure 5.3).

The shallow layer includes both the upper portion of the fractured bedrock and the soil, where precipitation (J) infiltrates and water leaves as evapotranspiration (ET)

and leakage (L) (including both lateral and vertical flows, as explained below). All precipitation is assumed to infiltrate into the soil except when the system is fully saturated. Leakage production is modeled through a non linear storage-discharge relationship [*Brutsaert and Nieber*, 1977] of the kind $L = aS_{rz}^{b_{rz}}$, where S_{rz} represents the dynamic water storage of the shallow layer, i.e. the volume of water which is mobilized during the hydrologic response and can be computed through a hydrologic balance [*Birkel et al.*, 2011]. A fraction $\beta(t)$ of the leakage is assumed to flow laterally and discharge directly into the stream as shallow subsurface flow Q_{rz}, while the remaining fraction $(1 - \beta(t))$ recharges the deep groundwater system. Overland flow never occurs in the model simulation, hence subsurface flow results as the only shallow component. To ensure that during wet periods a higher fraction of the leakage drains directly into the stream, the partitioning term $\beta(t)$ is made storage-dependent and it is computed as the product between a coefficient β_0 and the dynamic storage normalized by the root zone pore volume $S_{rz}(t)/(nZ_r)$. Evapotranspiration has a minor role in the Upper Hafren catchment and was simply assumed equal to a reference value ET_{ref}, multiplied by a temperature-based term that accounts for daily and seasonal variations in vapor pressure deficit and net radiation. The main model equations are summarized in Figure 5.4.

The groundwater flow from the deep system is likewise modeled through a non-linear storage-discharge relationship $Q_{gw} = aS_{gw}^{b_{gw}}$, where in this case S_{gw} represents the dynamic groundwater storage. The use of four independent parameters to define the two storage discharge relations (for the shallow storage and the groundwater) leads to equifinality because different combinations of a and b provide very similar Q-S curves in the relevant range of discharges that pertain to each partition of the storage. Hence, to improve the identifiability of the parameters (and reduce their number), the coefficient a was assumed to be the same in the two storage-discharge relations, thereby removing one degree of freedom in the system characterization. The different behaviors of the two systems are then completely defined by the exponents b_{rz} and b_{gw}. This arbitrary choice has little impact on the overall model performance. The deep system is fed by vertical flow from the shallow storage, while the only output is groundwater discharge, because evapotranspiration from the deep storage is assumed to be negligible. Note that, even though for purely hydrologic purposes one non-linear storage would provide satisfying results, the second storage is crucial to reproducing the observed chemical transport dynamics [see *Benettin et al.*, 2013b, section 7]. For ease of computation, the shallow and deep dynamic storages were made dimensionless. The former was scaled to

	storage equation	inflows	discharge	evapotranspiration
shallow storage	$\frac{dS_{rz}}{dt} = J(t) - L(t) - ET(t)$	$J(t)$	$L(t) = a\left(\frac{S_{rz}(t)}{nZ_r}\right)^{b_{rz}}$	$ET(t) = ET_{ref}\frac{T(t)+30}{T(t)+30}$
groundwater storage	$\frac{dS_{gw}}{dt} = L_{gw}(t) - Q_{gw}(t)$	$L_{gw}(t) = [1-\beta(t)]\, L(t)$	$Q_{gw}(t) = a\left(\frac{S_{gw}(t)}{S_{max}}\right)^{b_{gw}}$	—

Figure 5.4: Hydrologic model equations.

the specific pore volume $n\,Z_r$, while the latter was scaled to a constant, S_{max}, explicitly designed to be larger than the maximum modeled S_{gw}. The normalization also allows the units of the a coefficient to be mm/h.

5.3.2 Chloride Circulation Model

The chemical component of the model aims at describing chloride concentration dynamics in storages and outflows.

The measured rainfall concentration C_J was used as model input after some adjustments to account for the adopted sampling arrangement, as described in Appendix A.6. A second chloride input to the Plynlimon catchments is dry deposition, which is enhanced by the higher surface area of vegetation [*Neal and Kirchner*, 2000]. However, dry deposition was not modeled explicitly because, due to the large size of the funnel, sampled precipitation is likely to include its contribution.

The measured rainfall concentration C_J was used as model input after some adjustments to account for the adopted sampling arrangement, as described in Appendix A.6. A second chloride input to the Plynlimon catchments is dry deposition, which is enhanced by the vegetation surface area [*Neal and Kirchner*, 2000]. However, dry deposition was not modeled explicitly because, due to the large size of the funnel, sampled precipitation is likely to include its contribution.

As water infiltrates into the soil, it mixes with water already contained in the shallow storage. The size of this storage has a huge influence on solute circulation, because it defines the storage capacity of the shallow system (and thus its chemical memory). The total storage size cannot be computed from hydrologic models, which are sensitive only to the dynamic storage that is mobilized during the hydrologic response. The remaining portion of storage, which is not hydrologically active, is usually referred to as residual storage [*Kirchner*, 2009] or passive storage [*Birkel et al.*, 2011] and plays a critical role in the chemical response of watersheds. Hence, in both the shallow and the deep system the actual storage $W(t)$ is modeled as the sum of a dynamic storage

$S(t)$ and a residual storage W_0, which is assumed to be constant for simplicity. The residual storage is assessed through calibration and, because it has no influence on the hydrologic response, it can be effectively considered as a chemical parameter.

The outflowing chloride concentration depends on how the outflows sample water parcels from the storage. This is simulated in the model by assigning the StorAge Selection function $\omega(T, t)$ to the relevant outflows from each compartment. The random sampling scheme involves a selection function constantly equal to unity (see section 2.3), implying that every age is sampled based on its relative abundance (the larger the volume of water in storage that shares a given age, the more that age is sampled). Under this assumption, and neglecting possible effects due to evapoconcentration (see later discussion on this issue), outflow concentrations can be expressed through Eq. (4.2), which can be conveniently computed by means of a mass balance [*Benettin et al.*, 2013b]. Each outflow was assumed to randomly sample water particles from the corresponding storage. Hence, leakage and groundwater flow concentrations are obtained from the average concentration in the shallow system $\bar{C}_{rz}(t) = M_{rz}(t)/(S_{rz}(t)+W_{0_{rz}})$ and in the groundwater $\bar{C}_{gw}(t) = M_{gw}(t)/(S_{gw}(t) + W_{0_{gw}})$, respectively.

Evapotranspiration was initially assumed to randomly sample water from the root-zone with a concentration that is a fraction $\alpha \leq 1$ of the average storage concentration. This coefficient is designed to include the possible effects of selective evapotranspiration in case of potentially toxic solutes, which would lead to an increased storage concentration during warmer periods. However, when chloride concentration in soil moisture is low it is not toxic for plants and it is instead useful for biochemical functioning [see *Xu et al.*, 1999]. Preliminary calibrations suggested optimal values of α in the range $0.9 - 1$ and in the measured time series there is no evidence of evapoconcentration in the warmer months (May to August 2008). Hence, to reduce the number of parameters, evapoconcentration was not modeled by keeping $\alpha = 1$ (thus implying that transpired water has the same chloride concentration as the average shallow storage), leaving the two residual storages $W_{0_{rz}}$ and $W_{0_{gw}}$ as the only chemical parameters that require calibration.

It is important to note that even though the two storages are individually randomly sampled, the overall catchment is not, because water is distributed differently between the upper and lower reservoirs. For example, younger ages can be a small fraction of the overall storage as they are mainly confined in a smaller shallow reservoir, yet they can dominate the catchment discharge if stormflow is mainly made of soil water. This key issue is described in detail in Section 5.5.

Table 5.1: Constant parameters

Parameter	Symbol	value
soil porosity [-]	n	0.35
root zone depth $[mm]$	Z_r	400
max gw storage $[mm\ H_2O]$	S_{max}	1000
initial gw conc. $[mg/l]$	$\bar{C}_{gw_0}$	5.4

5.3.3 Model calibration

The hydrochemical model was implemented using a forward semi-analytical approach. For both the storages (shallow and groundwater), the hydrologic balance is solved at any time step implementing the analytic solution of the mass balance equation based on the underlying storage-discharge relationship. In the shallow system, a little component of the storage is also removed by evapotranspiration. The mass balance is computed by multiplying each hydrologic flux by the corresponding chloride concentration at the considered time step. In doing so, measured chloride in precipitation is uniformly downscaled from 7 hours to 1 hour time step. All the outflows are assumed to be characterized by the mean storage concentration at the previous time step, which is a by-product of the RS assumption. The mass in storage is then updated according to the computed fluxes and then divided by the water storage (also including the constant residual component) to obtain the updates mean storage concentration. Chloride contained within the catchment storage before the start of the analyzed period is accounted for through the initial conditions of the system. A warm-up period is employed at the beginning of the simulations to reduce the influence of the initial conditions.

The estimate of internal fluxes and storages in the system requires the determination of the model parameters. Some of them were set a priori based on previous analyses and field surveys [e.g. *Neal et al.*, 2010] as summarized in Table 5.1. The remaining parameters were estimated through a Markov Chain Monte Carlo (MCMC) calibration procedure using $DREAM_{ZS}$ [*Vrugt et al.*, 2009; *ter Braak and Vrugt*, 2008]. The calibration parameters comprise 5 hydrologic parameters (3 for the storage-discharge relationships, 1 for the leakage partitioning and 1 for evapotranspiration) and 2 chemical parameters (the 2 residual storages), as summarized in Table 5.2. The hydrological and chemical parameters were calibrated separately, according to the procedure described in the following.

Hydrologic parameters were calibrated against hourly discharge data. The objective

Table 5.2: Calibration parameters. (SD=storage-discharge relationship)

Parameter	Symbol	Type	Low. bound	Upp. bound
reference ET $[mm/h]$	ET_c	hydrol.	0	0.15
leakage partitioning [-]	β_0	hydrol.	0	2.5
SD coeff. $[mm/h]$	a	hydrol.	10^{-1}	10^4
SD exponent rz [-]	b_{rz}	hydrol.	0	30
SD exponent gw [-]	b_{gw}	hydrol.	0	80
residual storage rz $[mm\ H_2O]$	W_{rz}	chemical	100	1000
residual storage gw $[mm\ H_2O]$	W_{gw}	chemical	100	5000

function that is implemented in the MCMC is the standard log-likelihood function:

$$logL = \frac{N}{2}\log(2\pi) - N\log(\sigma_e) - \sum_{i=1}^{N}\frac{\epsilon_i^2}{2\sigma_\epsilon^2} \tag{5.1}$$

where N is the number of measurements, ϵ_i is the model error at time i (calculated as the residual $Q(i) - Q_{obs}(i)$) and σ_e is the error standard deviation. The use of eq. (5.1) is based on the assumption of independent and identically distributed Gaussian errors. Even though these assumptions (especially the lack of error correlation) are unlikely when dealing with discharge or concentration time series, more sophisticated objective functions would require more parameters to be estimated, without completely avoiding the problem of introducing arbitrary assumptions at some point. To account for the loss of degrees of freedom induced by serial error correlation, an increased error standard deviation $\sigma_e = 1\ mm/h$ is employed. As 5 years of discharge measurements are available at the Upper Hafren, the parameters' posterior distributions resulting from the calibration of individual years could be compared. The obtained distributions mostly overlap (Figure 5.5a), indicating mutual consistency of our estimates across different years and serving as a verification tool to support the reliability of the model parameters. Consistently, a single calibration for the entire dataset of 5 years resulted in a narrower distribution, peaking where individual distributions overlap. Moreover, the optimal set obtained during the 5-year calibration performs well in each individual year (see Table 5.3), so it was selected and kept constant for chemical calibration and for the travel time analysis.

Chemical parameters were calibrated against chloride measurements using the likelihood function provided by eq. (5.1) with $\sigma_e = 1.5\ mg/l$. Again, the error standard deviation was adjusted to account for the observed serial correlation in the residuals. As

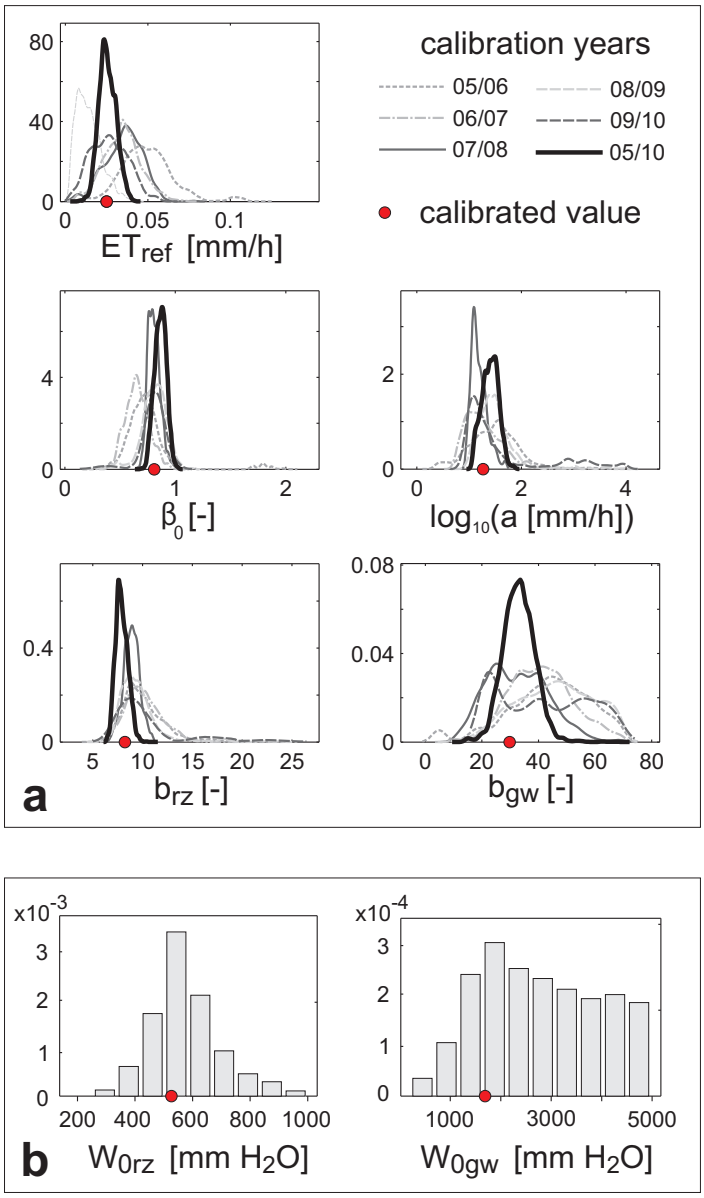

Figure 5.5: Posterior distributions of (a) hydrologic parameters, (b) chemical parameters. Red dots indicate calibrated values ($ET_{ref} = 0.025$, $\beta_0 = 0.85$, $\log_{10}(a) = 1.32$, $b_{rz} = 7.88$, $b_{gw} = 27.98$, $W_{0_{rz}} = 540$, $W_{0_{gw}} = 1700$). The units on the y-axes are relative number per x-axis unit.

Table 5.3: Nash-Sutcliffe efficiencies (for hourly discharge) of the calibrated hydrologic model.

year	E (1-year calib)	E (5-years calib.)
05/06	0.89	0.88
06/07	0.92	0.91
07/08	0.94	0.94
08/09	0.87	0.85
09/10	0.82	0.82
05/10	-	0.90

just one year of high-frequency chloride measurements is available, it has been entirely used for calibration. In the absence of validation periods, calibrated chemical parameters are less suitable for longer-term transport processes. The posterior distributions of the chemical parameters (Figure 5.5b) show that the residual component of the shallow storage is well identified ($W_{0rz} \approx 500 - 600\, mm\, H_2O$) and consistent with field observations of the fractured bedrock depth [*Shand et al.*, 2005]. In contrast, groundwater residual storage is much more uncertain ($W_{0gw} > 1500\, mm\, H_2O$), owing to the strong filtering of high-frequency information in the input signal by groundwater storage. The uncertainty in the size of the groundwater storage may be aggravated by the brevity of the simulation in our modeling exercise (approximately 1 year). Implications of the uncertainty in the deep residual storage are discussed in Sections 5.4 and 5.5.

5.4 Results

The calibrated hydrochemical model was run over the December 2007 - November 2008 period. Simulated discharge and its partition into root-zone and groundwater contributions are shown along with observed flows in Figure 5.6. Nash-Sutcliffe (NS) efficiencies are 0.94 for discharge and 0.91 for log-discharge, indicating that the model is able to capture both the peaks and the recessions of the observed hydrograph. The flow partitioning shows that hydrograph peaks are dominated by drainage from the rooting zone, while the groundwater, though quite reactive during wet periods, accounts for most of the recessions. The simulated chloride concentration is shown in Figure 5.7. Besides the first negative peak in the observed timeseries, which might be due to overland flow or other processes that could not be properly simulated by this simple model, all dilutions taking place in summer and fall are well reproduced by the model. Similarly, the positive concentration peaks around January 2008 are properly caught in the simula-

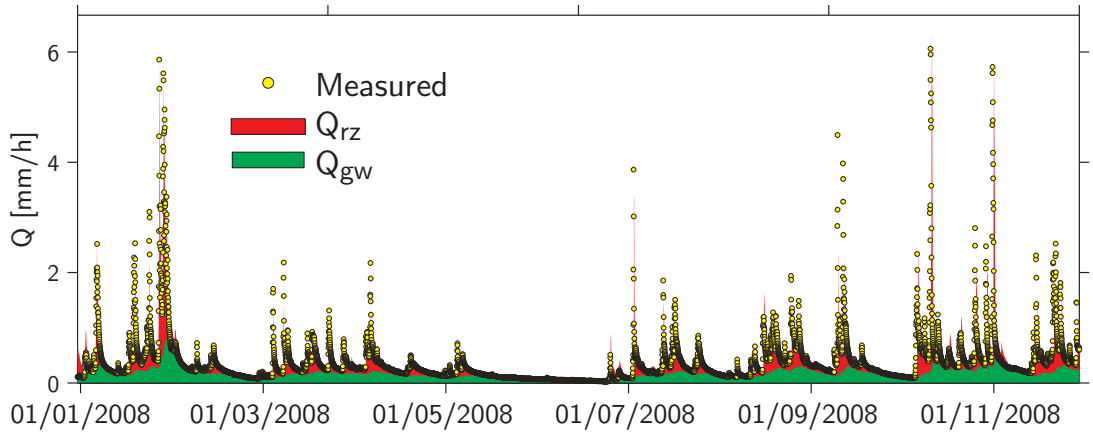

Figure 5.6: Measured and simulated discharge timeseries.

tion indicating that, in general, both behaviors (increased/decreased concentrations in response to floods) are reasonably represented by the model. NS efficiency of the best performance is 0.69.

The intuitive picture suggested by the model results is the following: during baseflow conditions, discharge and solute concentrations are mostly sustained by groundwater flow, whereas right after storm events, water from the soil and highly fractured bedrock is mainly responsible for runoff formation, so the concentration at the outlet promptly shifts towards the concentration in the shallow storage (which may be either higher or lower than groundwater's, depending on the season). Our analysis thus reinforces the conceptual hypothesis of *Neal et al.* [2012]. During recessions, streamflow concentration gradually shifts back to the groundwater concentration. Hence, high-frequency dynamics originate at the transition between shallow and deep water control on streamflow, induced by incoming storm events. Depending on whether shallow storage concentrations are higher or lower than that of groundwater, new storms may cause dilutions (e.g. August-November 2008 period) or positive concentration peaks (e.g. January-April 2008). This can be observed in Figure 5.7, where average storage concentration in the two compartments can be identified as the end-members of the observed chloride fluctuations. Figure 5.7 also explains the reason for groundwater size is highly uncertain: a bigger storage would result in nearly the same constant groundwater concentration, so the size of residual groundwater store is difficult to constrain by calibration. Nonetheless it is encouraging that the calibrated residual storage in the shallow and deep reservoirs implies a mean travel time of roughly 1.5 years, broadly consistent with the mean travel time of 0.9 years estimated independently for the Hafren catchment by *Kirchner et al.*

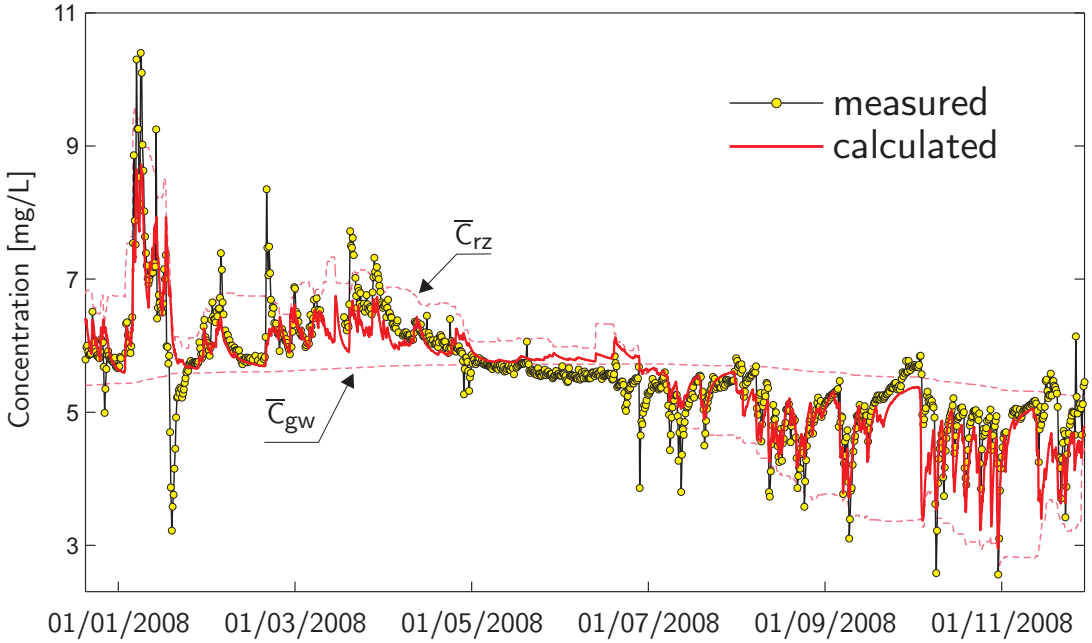

Figure 5.7: Measured and simulated chloride concentration timeseries. The dashed lines show the simulated mean concentrations of the shallow storage $\bar{C}_{rz}(t)$ and groundwater storage $\bar{C}_{gw}(t)$.

[2000] using spectral analysis of longer-term (but less detailed) chloride time series.

Though very simple, our model is able to reproduce the main chloride dynamics reasonably well, suggesting that the resulting flow partitioning is a reasonable representation of the catchment behaviors. Our results indicate that streamflow concentration dynamics can be inferred from spatially integrated storage concentrations within prescribed hydrologic compartments, even though these may not necessarily be mixed. From a physical viewpoint, this can be attributed to the pronounced heterogeneity of water velocities and flow paths that supply water to the stream network, resulting in enhanced mixing of waters originating from different source areas [*Kirchner et al.*, 2001].

Note that, as shown by *Neal et al.* [2012], the presence of both positive and negative peaks in the concentration is peculiar to chloride in this system because it is a conservative tracer whose input concentration fluctuates around a nearly constant long-term average. This implies that modeled shallow and deep storage concentrations cross each other during the year (see e.g. Figure 5.7 before and after day 190). For other solutes this might not be the case, because the concentration could be persistently lower in groundwater than in shallow storage (e.g. due to degradation processes, like for phosphorus), leading to positive concentration peaks in stormflow, or persistently higher in

groundwater than in shallow storage (because of e.g. rock weathering, like for silica), leading to negative peaks (i.e., dilution) in stormflow. Even for non-reactive tracers, one might observe persistent positive or negative concentration peaks if the input loads exhibit long-term non-stationarity. This was observed for chloride in the Hupsel Brook Catchment [*van der Velde et al.*, 2010a], where soil water is systematically less concentrated than groundwater because of the reduction of fertilization loads during the last decades, induced by environmental policies.

5.5 Travel time Analysis

Backward travel time distributions over the simulation period 2007-2008 were reconstructed based on the equations (A.14), (A.15), (A.17), using the total storage $W = S + W_0$ as the storage term. Because backward distributions are based on precipitation events that happened up to many years before the considered period, the hydrochemical model was run from 1985 to 2008, to provide an estimate of all the hydrologic fluxes required for TTD computation. In order to balance between numerical efforts and accuracy in calculating TTDs, distributions were computed at 6-hours time step.

For each individual storage (shallow and deep), the age distributions in the storage and in the outflows coincide, as prescribed by the adopted RS mixing scheme. In the root zone, TTDs (and hence RTDs) show enhanced time-variance due to the high variability in flows and storages. Groundwater TTDs are, by contrast, relatively constant because flow variability is damped owing to the large storage size. This can be seen in Figure 5.8, where a few TTDs are reported for individual points in the time series and compared to the stationary marginal distributions. While root zone individual distributions show large departures from the corresponding marginal distribution, groundwater distributions are almost indistinguishable.

It is worth highlighting that when one considers the catchment as a whole, the overall system is far from being randomly sampled. This is because the shallow storage makes only a small contribution to total storage, but it is preferentially sampled by discharge, especially during high flows. The difference between the age distributions of the overall storage and discharge can be seen in Figure 5.9, where all cumulative distributions obtained during the simulation period are plotted. Two main features clearly emerge: i) cumulative TTDs are generally shifted upward with respect to their corresponding RTDs, meaning that discharge is mostly made up of younger water than storage; ii)

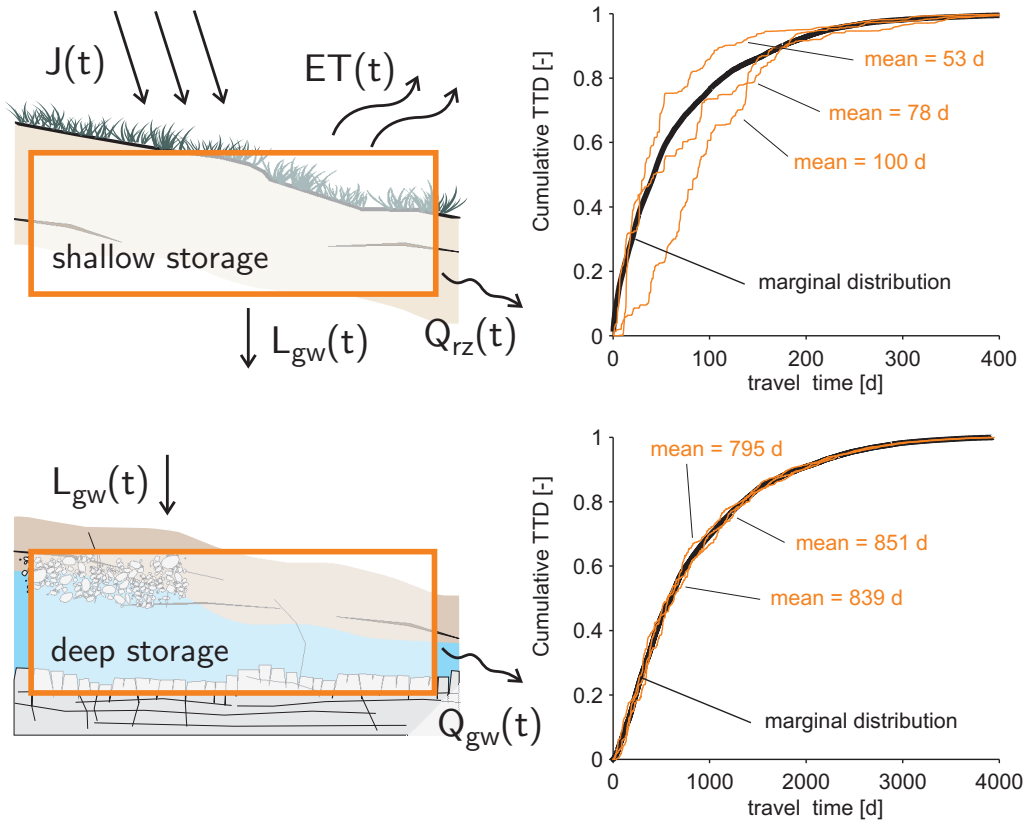

Figure 5.8: Example of three individual cumulative TTDs drawn from the shallow and deep storages, compared to the corresponding marginal distribution $p_m(T)$. The distributions are taken on 14/06/2008 (mean values 100 and 839 days), 16/09/2008 (mean values 78 and 851 days) and 20/11/2008 (mean values 53 and 795 days)

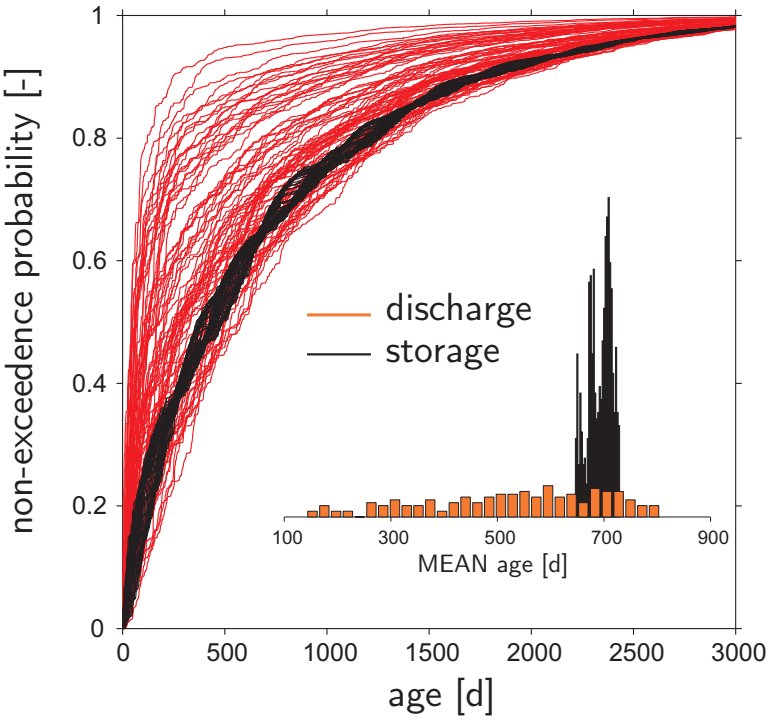

Figure 5.9: Cumulative age distributions in the overall water storage and discharge (i.e. considering the combined effect of the shallow and deep systems). The distributions are computed over the whole simulation period. The inset reports the pdf of mean values.

TTDs are much more variable over time, as shown by the larger range spanned by their mean values (inset). Discharge can release both very young waters (during storm events) and old waters (during dry periods), while total storage is always dominated by old waters contained in the deep storage.

The difference between discharge and storage age dynamics is best explained by looking at the corresponding SAS functions ω (eq.(5.10)). The functions were computed as the TTD/RTD ratio and then rescaled over the transformed residence time domain proposed by *van der Velde et al.* [2012] and shown in Appendix. Such a change of variables conveys notable advantages because, in the new transformed domain, the StorAge Selection functions turn into probability density functions and display a more regular and smooth shape. The functions are reported in Figure 5.10, where different colors are used for different shapes. The same color is used to identify the corresponding shallow storage level (inset). The plot suggests that during wet conditions outflows have a preference for younger waters and that this tendency is enhanced with catchment wetness. Conversely, when the catchment becomes dry, older water parcels tend to be preferentially sampled because the shallow system becomes almost inactive. The link

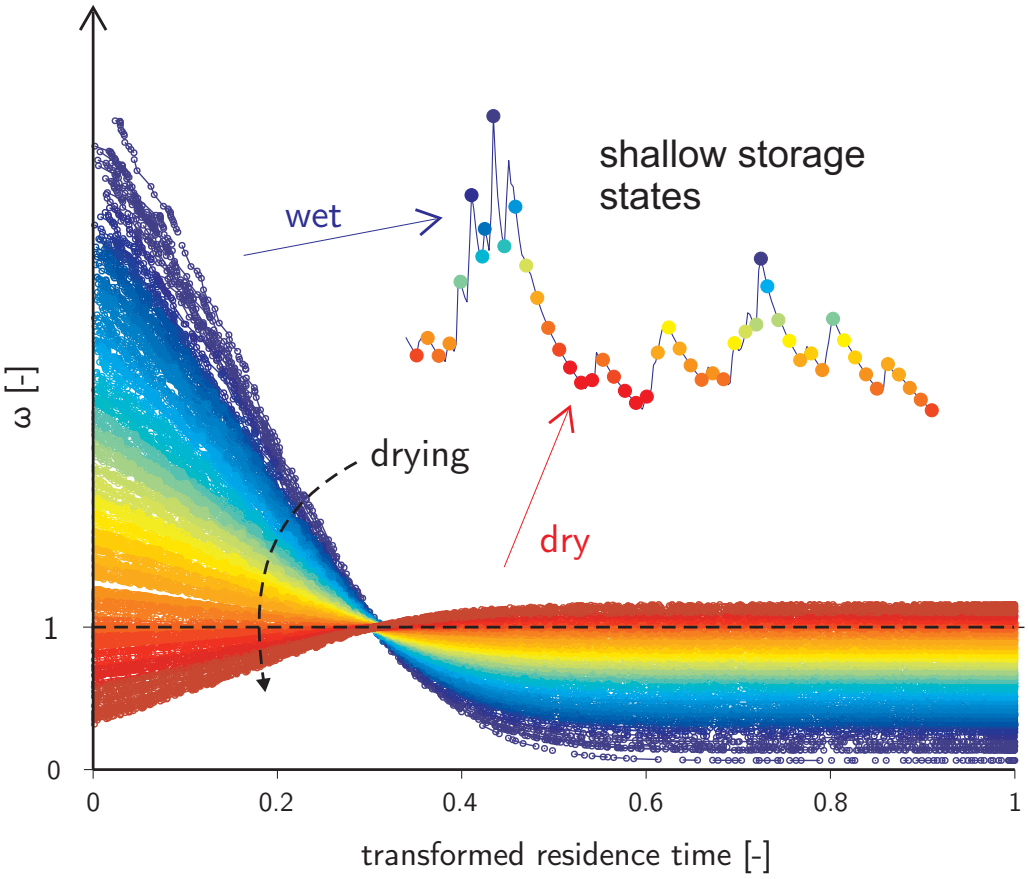

Figure 5.10: SAS functions computed over the whole simulation period. The color scheme links the functions with their corresponding (shallow) storage state.

between age-selection and storage, however, is not one-to-one because the system is characterized by some degree of hysteresis. The same storage can correspond to different catchment conditions, depending on whether the catchment is wetting or drying. This is visible in Figure 5.10 where similar age-selection functions (i.e., similar colors of curves) correspond to different shallow storage states (e.g. during peaks or recessions). Therefore, SAS functions can provide useful insights for the characterization of the catchment state.

So far each TTD is representative of one simulation time step, regardless of the amount of discharge water it refers to, but one may want to get flow-weighted distributions that are more representative of the masses of water that leave the catchment. As higher discharges are characterized by younger water, flow-weighted average travel times are younger than time-weighted averages [*Peters et al.*, 2013]. Marginal travel time distributions are intrinsically flow-weighted functions because individual TTDs are aver-

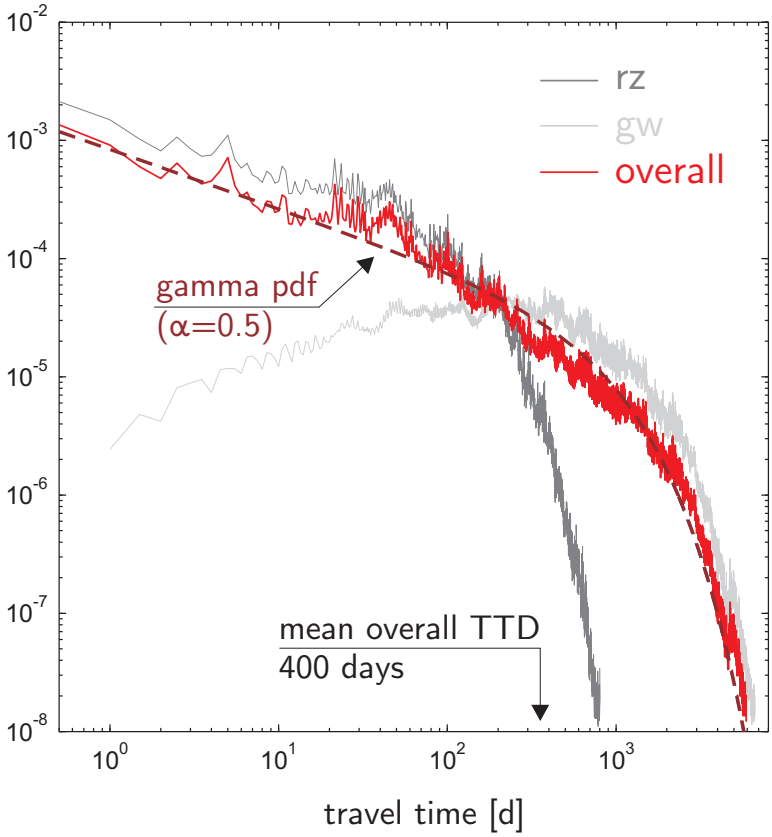

Figure 5.11: Marginal travel time distributions for the root zone, groundwater and overall discharge. The overall marginal distribution is also compared to a gamma pdf with shape parameter *alpha* = 0.5 and mean value 400 days (which is the same as the overall distribution).

aged out by weighting them by the corresponding discharge value. The marginal distributions were calculated using eq. (A.18) over the whole simulation period to explore the time-integrated behavior of the TTDs. Distributions computed for the shallow storage, groundwater and overall discharge are compared in Figure 5.11. The plot shows that shallow-storage and groundwater distributions are characterized by different time scales (a few months and a few years respectively), while the overall marginal distribution displays a smooth transition between shallow-storage and groundwater distributions, and hence spans a wide range of time scales. Interestingly, the overall marginal TTD closely resembles a Gamma pdf with shape parameter $\alpha = 0.5$, which has often emerged from analyses of tracer time series using spectral methods to estimate stationary travel time distributions [*Kirchner et al.*, 2000, 2001; *Godsey et al.*, 2010; *Kirchner and Neal*, 2013].

Notwithstanding uncertainties involved in the spatial variability of chloride deposition, the travel time analysis allows for preliminary inferences about the catchment mass

balance. The measurements suggest that during the study period a total of $15.7\,g/m^2$ enter the catchment through atmospheric deposition and $16.0\,g/m^2$ leave the catchment as discharge (very close to the value of $16.5\,g/m^2$ predicted by the calibrated model). However, the close match between input and output mass only reflects the equilibrium between deposition and mass displaced from the catchment during the considered 11 months, without implying any balance closure in a kinematic sense. Indeed, the kinematic picture provided by the travel time analysis suggests that 55% of the total mass removed by discharge during the simulation period was already stored within the catchment before the start of that period.

A word of caution is needed at this point. The travel time analysis is based on the underlying hydrochemical model, so one may want to assess the impact of model parameters and the related uncertainty on estimated travel times. While a complete sensitivity analysis would be a time-consuming task left for future work, informal analyses showed general stability of travel time distributions under different parameter combinations. The only parameter which could have a substantial impact on travel times is the groundwater residual storage $W_{0_{gw}}$, because it does not have a clearly definable upper bound (see Section 5.3.3). However, larger $W_{0_{gw}}$ values would leave the fundamental interaction between shallow and deep system (hence the age-selection) unchanged and its effect would be limited to increased groundwater ages, without affecting the overall patterns of behavior outlined by our results.

5.6 Final remarks

The hydrochemical model, based on a reasonable conceptualization of the Upper Hafren catchment, could accurately reproduce its hydrologic and chemical response. This allowed for the estimation of the storages involved in solute mixing, and enabled to infer dynamic travel time distributions.

Most of the high-frequency fluctuations in the measured chloride concentration can be explained by the sharp transition between groundwaters (with an almost constant Cl concentration) and faster flows originating from shallower storage layers (with higher or lower concentration, as driven by the inter-seasonal variability of atmospheric inputs). The same transition in dominance between deep and shallow storage also drives large fluctuations in the mean age of stream water.

Emerging age-selection patterns indicate a clear preference of discharge for the youngest ages in storage. Such a preference is enhanced when the catchment is wet

and faster flows dominate the hydrologic response, thereby implying that discharge is always younger than storage.

Chapter 6

Modeling the Hubbard Brook Watershed 3 (USA)

6.1 Introduction

The Hubbard Brook Experimental Forest (HBEF) is a research area established in New Hampshire (USA) that has pioneered ecosystem studies since the 1960s. Research based on the extensive available datasets has led to the publication of more than 1000 journal papers on topics that span from biology to forest chemistry and hydrology [*Likens*, 2013].

As in the previous applications (Chapters 4 and 5), this study is based on the use of backward travel time distributions obtained from different compartments of the catchment, where the random-sampling (RS) scheme can be reasonably assumed. The water fluxes needed to compute the TTDs were calculated by means of a hydrochemical model that was calibrated against discharge and isotopic data. The innovative contribution of this application is the use of TTDs to simulate, in a first-order kinetic framework, the export of geogenic solutes produced by mineral weathering. This is complementary to several papers that related silica dynamics to catchment hydrologic conditions and travel times [e.g. *Hornberger et al.*, 2001; *Scanlon et al.*, 2001; *Asano et al.*, 2003; *Stelzer and Likens*, 2006; *Maher*, 2011; *Clymans et al.*, 2013]. The results suggest that sodium and silica stream concentrations at HBEF result as being driven by the contact time between the water and mineral interfaces.

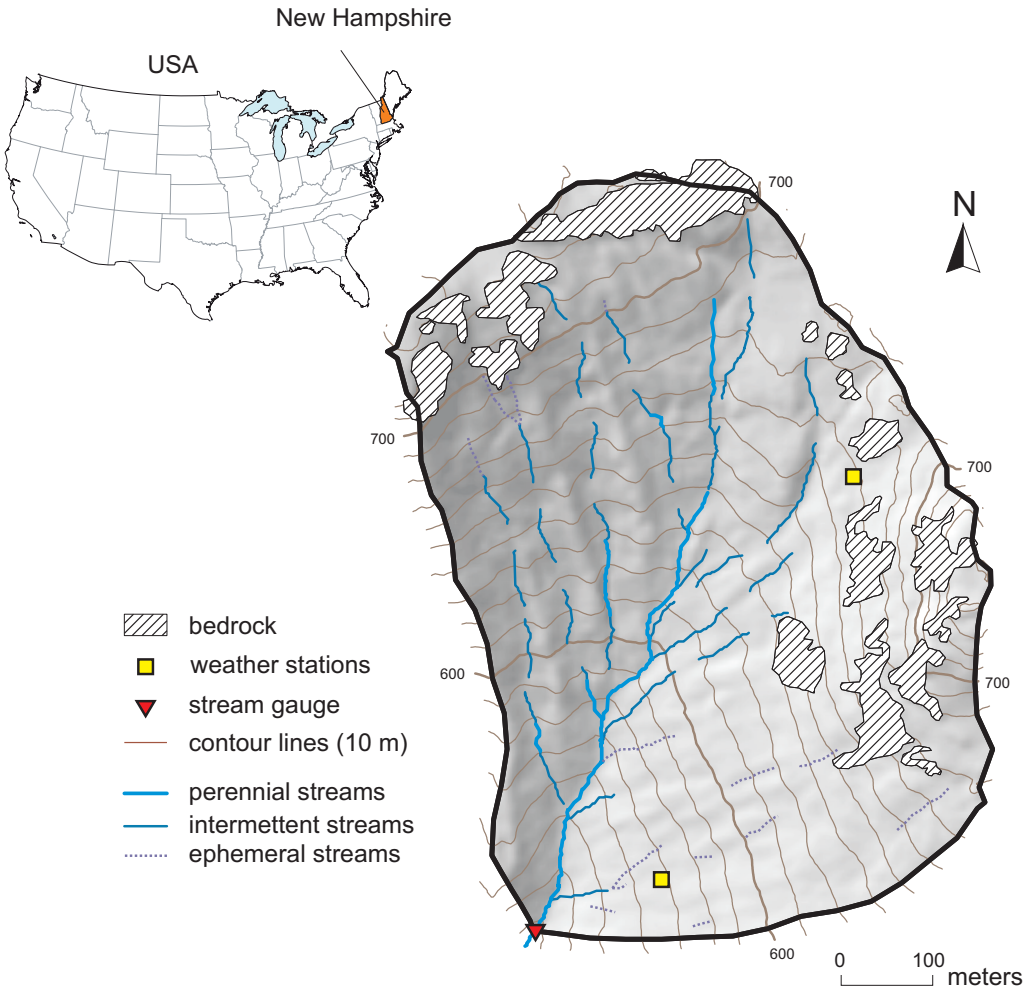

Figure 6.1: Map of WS3 (0.42 km^2). Elevation is expressed in m.a.s.l.

6.2 Data and study area

The study site is Watershed 3 (WS3, 0.42 km^2) of the Hubbard Brook Experimental Forest (HBEF), which is located within the southern White Mountains of central New Hampshire, USA (43°56′N, 71°45′W, Figure 6.1). WS3 is the hydrologic reference catchment for a series of long-term paired catchment studies [*McGuire and Likens*, 2011; *Likens*, 2013] and has been a center for hillslope hydrology studies [*Hooper and Shoemaker*, 1986; *Cedarholm*, 1994; *Detty and McGuire*, 2010a,b; *Gannon et al.*, 2014] at HBEF. Aerially-averaged daily precipitation and continuous stream discharge records for WS3 date back to 1957. The climate is humid continental with mean monthly temperatures ranging from -9 to 18°C and annual precipitation of about1400 mm of which a quarter to a third falls as snow [*Bailey et al.*, 2003a]. Bedrock of the catchment is sillimanite-grade pelitic schist and calc-silicate granulite of the Silurian Rangeley Formation. The catchment was glaciated by the sequence of Pleistocene glaciations, with the latest Wisconsinan glacial period leaving basal tills and water worked glacial drift of granitic composition and varying thickness, texture, and hydraulic conductivity [*Bailey et al.*, 2003a, 2014]. Plagioclase feldspar of oligoclase composition is present in both the bedrock and glacial deposits, and is likely the major source of Na^+ and H_2SiO_4 and released by primary mineral weathering reactions [*Bailey et al.*, 2003b]. *Bailey et al.* [2014] and *Gannon et al.* [2014] describe the soils as podzols with distinct variations in horizonation supporting a hydropedological functional classification with a broad range of drainage classes, soil morphology, and soil development history. Slopes in WS3 are about 20-30% and the aspect is dominantly southern with elevation ranging from 527-732 m. The site is northern hardwood forest dominated by *Fagus grandifolia Ehrh.* (American beech), *Acer saccharum Marsh.* (sugar maple), *Betula alleghaniensis Britt.* (yellow birch) and with *Picea rubens Sarg.* (red spruce), *Abies balsamea (L.) Mill.* (balsam fir), and *Betula cordifolia Regel* (mountain white birch) in upper elevations and shallow-to-bedrock areas.

Streamflow has a marked seasonality due to the snow accumulation and snowmelt cycles (Figure 6.2). During dry summer periods, most of the first and second order streams get dry and streamflow is mostly sustained by a number of perennial seeps that are characterized by a different chemical composition [*Zimmer et al.*, 2013].

Water sampling for isotopic analysis occurred in W3 from November 2006 to November 2010 (4 years total). Precipitation and snowmelt samples were collected biweekly and stream samples were collected at least weekly. Isotopic data are shown in Figure 6.3. Deuterium in precipitation varied seasonally, with lower values in winter and higher

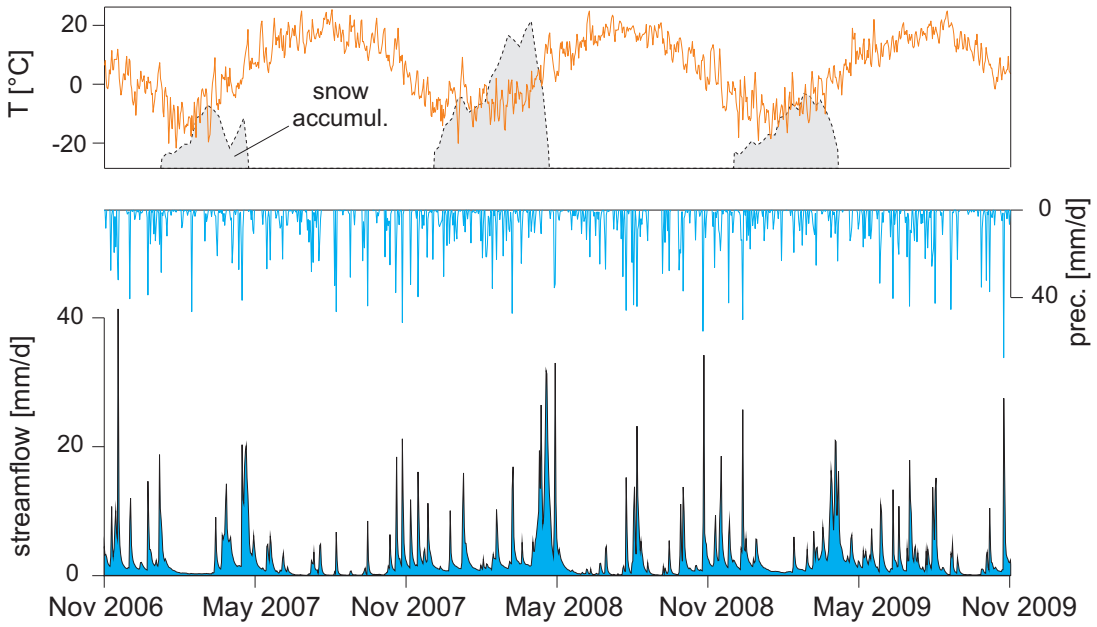

Figure 6.2: Measured hydrologic flows from November 2006 to November 2009.

values in summer. This temporal pattern reflects the isotopic composition of the source water and factors that influence moisture in the air mass during transport, such as temperature, the amount of rainout, and prevailing weather patterns [*Dansgaard*, 1964; *Gat*, 1996]. The seasonal increases in deuterium in precipitation that were observed during summer are typical of the northeastern U.S. and in part reflect atmospheric water that has been recycled/recondensed and evaporated at warm temperatures during summer [see *Ingraham*, 1998]. The amplitude of the deuterium signal tends to be relatively large at Hubbard Brook because of the greater climatic variability associated with the higher latitude and elevation of the site.

6.3 Hydrochemical model

6.3.1 Model description

The conceptual representation of an idealized hillslope soil catena presented by *Bailey et al.* [2014] provides a framework to conceptualize the catchment as a composition of a soil storage and a groundwater storage, plus a "buffer zone" where waters from the two storages are likely to come together upon entering the stream (Figure 6.4). The model is similar to that employed in [*Benettin et al.*, 2013b] but differs in the presence of a snowmelt component and the buffering zone. The model is briefly described below.

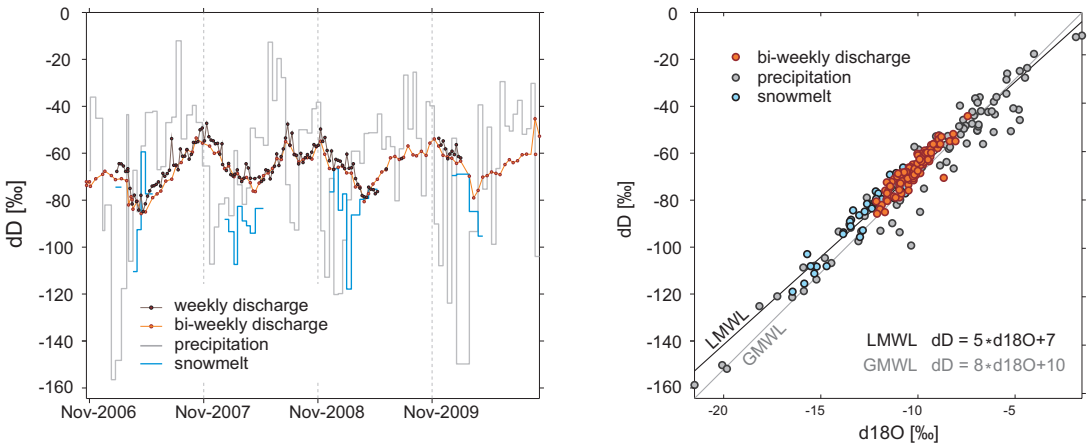

Figure 6.3: Timeseries of measured isotopic content in precipitation, snowmelt and streamflow.

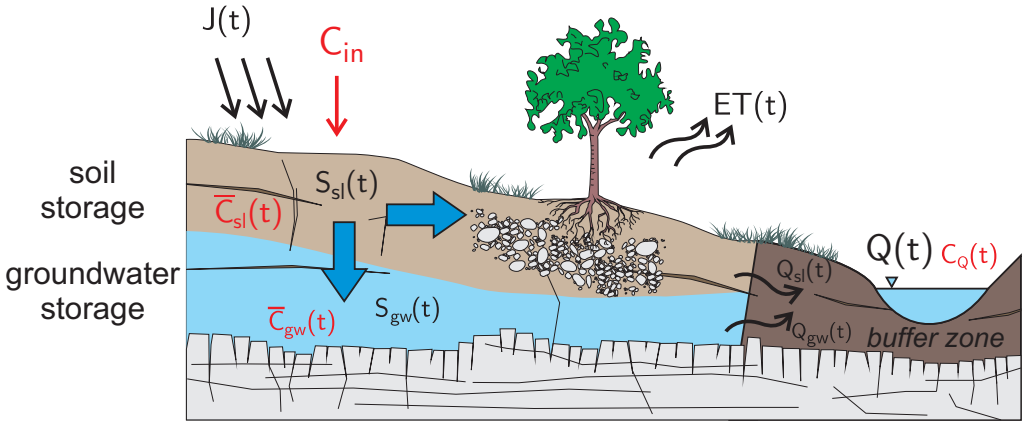

Figure 6.4: Illustration of the conceptual hydrochemical model.

The soil compartment is meant to include O to upper C soil horizons. Main hydrologic processes describing the soil compartment of the model are: infiltration from precipitation and snowmelt, evapotranspiration and lateral and vertical flow generation. A threshold T_{th} on daily-mean temperature T was used to distinguish between snowfall and rainfall. $T \leq T_{th}$ resulted in water infiltration I_R into the soil, while $T < T_{th}$ resulted in snow accumulation. Snowmelt infiltration I_S was determined using a Degree-Day approach [see *Rango and Martinec*, 1995], which computes snowmelt flux as the product between a Degree-Day factor D_f and the temperature difference $T - T_{th}$. Potential evapotranspiration was computed as the product between a reference value ET_{ref} and a temperature-based term that could account for daily and seasonal evapotranspiration patterns. Actual evapotranspiration ET was limited by the available water in the normalized root-zone storage $S_{sl}(t)/(nZ_r)$ [see *Laio et al.*, 2001] assuming an average root zone depth Z_r of 500 mm. Leakage L production was modeled through a non linear storage-discharge relationship of the kind $L = aS_{sl}^b$. A fraction $\beta(t)$ of the leakage is responsible for lateral flow and discharges directly into the stream as soil discharge Q_{sl}, while the remaining $(1-\beta(t))$ fraction recharges the deeper groundwater system. The partitioning term $\beta(t)$ is computed as the product between a coefficient β_0 and the normalized root-zone storage $S_{sl}(t)/(nZ_r)$. δD isotopic composition measured in precipitation and snowmelt was used to characterize infiltrating water. Fractionation in the subsurface flow and evaporation was assumed to be negligible, so the isotopic compositions were kept as conservative. The storage could thus be characterized at any time by its average Deuterium content δD as:

$$\overline{\delta D}(t) = \int_0^\infty \delta D_{in}(t-T)\, p_S(T,t)\, dT\,, \tag{6.1}$$

where $p_S(T,t)$ is the soil storage age distribution at time t [*Botter et al.*, 2011].

All water fluxes leaving the soil were assumed to randomly sample water particles from the storage, hence their isotopic composition is the same as the storage composition [*Botter et al.*, 2010; *Hrachowitz et al.*, 2013] $\delta D_L(t) = \delta D_{ET}(t) = \overline{\delta D}(t)$.

To account for water flowing in the deep C horizon down to the bedrock, a deeper groundwater storage was modeled. The input flux to the deep system is the vertical flow from the shallow storage, characterized by its modeled isotopic composition. The only output of the system is groundwater flow, which was modeled through the linear relationship $Q_{gw} = c\, S_{gw}$, where S_{gw} represents the dynamic component of the groundwater storage. Evapotranspiration has been neglected as it is unlikely to occurr at such depths. The random-sampling scheme in the groundwater storage implies that deep

Table 6.1: Constant parameters

Parameter	Symbol	value
soil porosity [-]	n	0.35
root zone depth $[mm]$	Z_r	500
max gw storage $[mm\ H_2O]$	S_{max}	200
buffer area fraction [%]	f_{buf}	5
buffer storage $[mm\ H_2O]$	W_{buf}	100
initial sl δD [‰]	–	-65
initial gw δD [‰]	–	-75

discharge has the same isotopic composition as the average groundwater composition.

Soil- and ground-water eventually mix in the riparian area and in the stream. This effect was reproduced in the model by introducing a 'buffering zone' f_{buf} (5% of the total catchment area), roughly corresponding to the stream network and part of the riparian Bh podzol area. For the sake of simplicity, the buffering zone does not induce any storage effect and at any time water entering the buffer Q_{pb} is equal to water displaced from the buffer $Q + f_{buf}\, ET$, implying that the storage W_{buf} remains constant in time.

6.3.2 Model calibration

Model parameters were set a priori when previous work and field surveys [e.g. *Bailey et al.*, 2014] were available (Table 6.1). The remaining parameters were estimated through a Markov Chain Monte Carlo (MCMC) calibration procedure using $DREAM_{ZS}$ [*Vrugt et al.*, 2009; *ter Braak and Vrugt*, 2008].

The calibration parameters comprise 7 hydrologic parameters (2 for the Degree-Day model, 3 for the storage-discharge relationships, 1 for the leakage partitioning and 1 for evapotranspiration) and 2 transport parameters (the 2 residual storages), as summarized in Table 6.2. Following the procedure used in Sectionn 5.3.3, the hydrological and chemical parameters were calibrated separately (see below).

An intermediate approach was used to calibrate the buffer zone storage parameter W_{buf}. The parameter only affects the chemical component of the model and basically controls the smoothness of the modeled signal. Weekly data contain little information on the higher-frequency component of the signal, hence optimization procedures tend to favor very smooth modeled signals, featured by higher values of the storage. After preliminary runs, the value was forced to be 100 mmH_2O, which is lower than the opti-

Table 6.2: Summary of the calibration parameters. DD=degree-day, SD=storage-discharge relationship, sl and gw refer to the soil layer and groundwater, respectively.

Parameter	Symbol	Type	min	max	Calib.
DD threshold temp. [°C]	T_{th}	hydrol.	-3	1	-1
DD factor [mm/d °C]	D_f	hydrol.	0.5	5	2.2
reference ET [mm/d]	ET_{ref}	hydrol.	0.5	3	2.2
leakage partitioning [-]	β_0	hydrol.	0.5	1.5	1.1
SD coeff. sl [mm/d]	a	hydrol.	10^0	10^5	$10^{2.05}$
SD exponent sl [-]	b	hydrol.	0	30	12.5
SD coefficient gw [-]	c	hydrol.	10^{-2}	10^2	$10^{-0.51}$
resid. storage sl [$mm\ H_2O$]	W_{sl}	chem.	100	1000	250
resid. storage gw [$mm\ H_2O$]	W_{gw}	chem.	100	5000	750

mum, to preserve higher frequencies. In the presence of higher-frequency measurements the parameter could be better characterized.

Hydrologic parameters were calibrated against daily log-discharge data over the four years period November 2006 - October 2010. Log-discharge measurements were chosen for calibration to favor the reproduction of very low flows, which otherwise would be completely disregarded by the calibration as runoff varies over three orders of magnitude. The model was run at hourly time-steps and then aggregated to provide daily average values. MCMCs were implementd with a standard log-likelihood function, with increased residuals standard deviation $log(\sigma_e) = 1.2$, to account for serial residuals correlation. Residual storage parameters were calibrated against weekly Deuterium measurements over the period November 2006 - May 2009. Again, a standard log-likelihood function was used for calibration, with $\sigma_e = 9.1‰$ (that accounts for observed residuals correlation).

6.4 Results

6.4.1 Discharge, Deuterium content and storage size

The calibration procedure resulted in relatively narrow posterior distributions of the model parameters (Figure 6.5)). Modeled discharge is reported in Figure 6.6a,b, where 95% parameters bounds are plotted against measurements. A simple sensitivity analysis showed that the model is most sensitive to the snow model parameters. This is

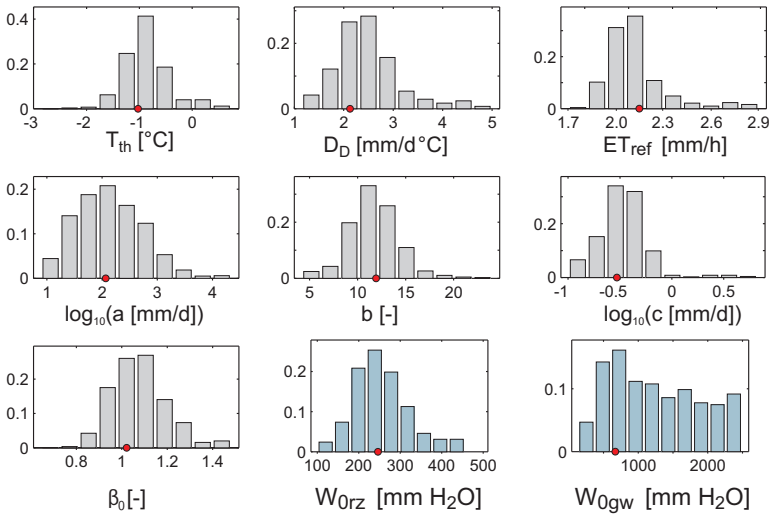

Figure 6.5: Posterior distributions of hydrologic (grey bars) and transport (blue bars) parameters.

not surprising as occasionally discharge peaks are completely missed because the precipitation event was interpreted by the model as snowfall accumulation. In any case, these events are quite in a small number and overall the model is able to reproduce the observed discharge signal. The calibrated model has Nash-Sutcliffe efficiency NS=0.78 for log-discharge and NS=0.75 for discharge. Validation over the period January 2000 - May 2006 resulted in NS=0.78 for log-discharge and NS=0.73 for discharge, indicating robust calibrated values. The partitioning of streamflow into soil and groundwater components (not shown) reveals that, on yearly average, only 25% of the discharge is made of groundwater, but it accounts for more than 95% of the flow during dry summer periods. Modeled snowfall accumulation is visually compared to measurements in Figure 6.6c, and displays a correct timing and the right pattern in snow accumulation.

Calibrated Deuterium signal is compared to measurements in Figure (6.6d). Both weekly and biweekly measurements were reported in the plot to provide an idea of measurement uncertainty. Moreover, as biweekly data are available over a longer period, they can serve as a sort of visual validation over the period May 2009 - October 2010. The modeled signal features both the seasonal and higher-frequency observed fluctuations, and has NS=0.62. Given the simple tools used to model rather complex processes like snowmelt and forest transpiration, the model results are considered as satisfactory.

Model calibration allows for the estimate of the catchment storages. Modeled soil storage is $380\,mmH_2O$ on average. Depending on porosity n, this requires a depth of about 1200-1400 mm ($n = 0.4 - 0.3$), which roughly corresponds to 20-30 cm into the

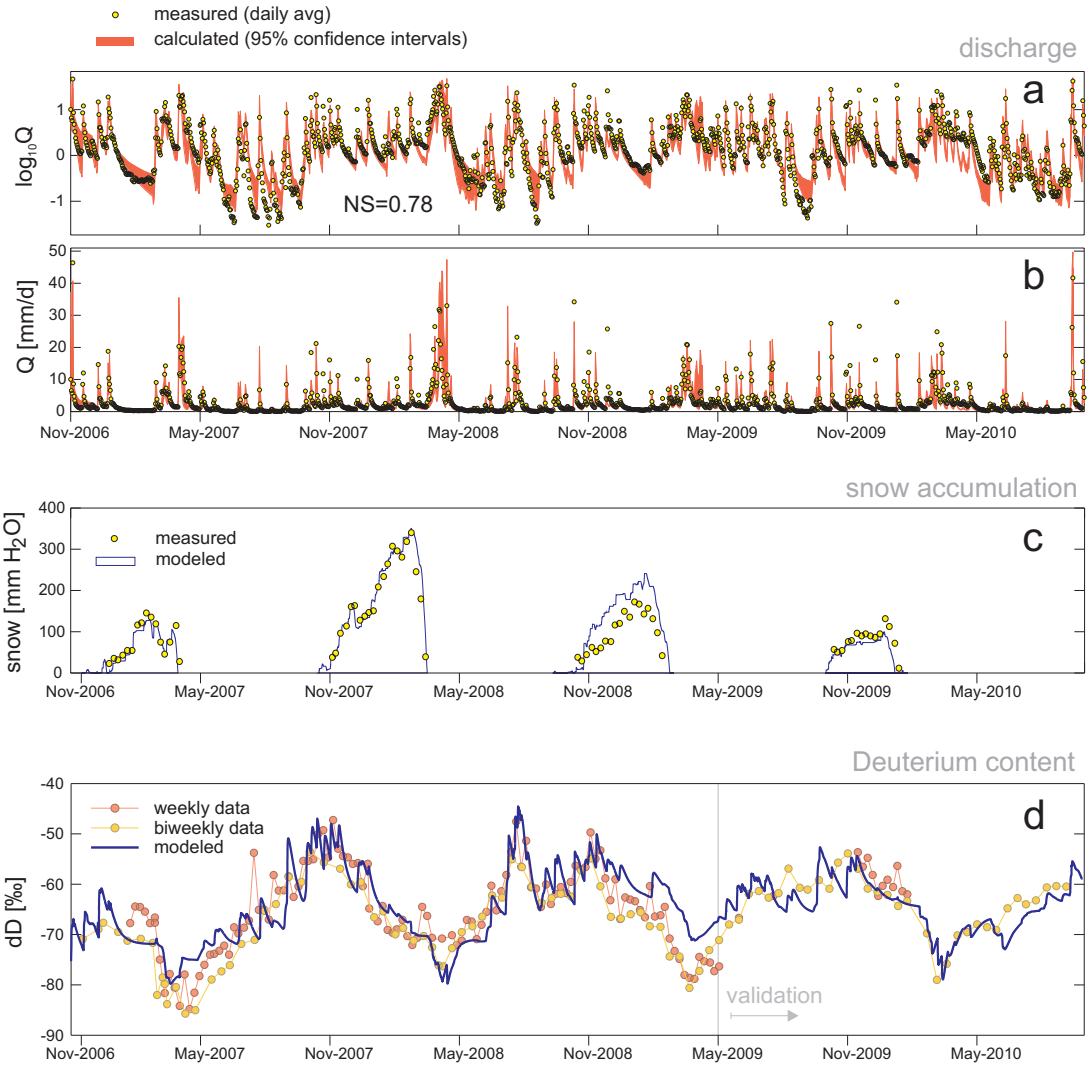

Figure 6.6: Model performances for (a) discharge, (b) log-discharge, (c) snow accumulation, (d) streamflow isotopic composition.

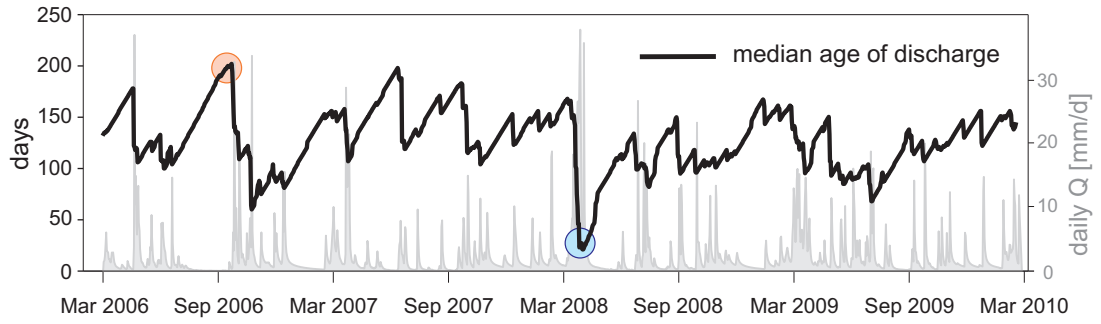

Figure 6.7: Evolution of the simulated median age of discharge during a 4 years period. The red and blue circles denote the dry and wet periods explored in Figure 6.8.

C horizon. Deep groundwater storage estimates indicate a larger storage size (about $760\,mmH_2O$), but the value is less identified because higher values would provide a similar (almost flat) contribution to the stream in terms of deuterium content. This is a rather typical problem (see Section 5.3.3) that deals with the very long time scales of groundwater compared to the input variability. This induces some degree of uncertainty in the longer travel times, but leaves the younger part of the distributions, which is mostly responsible for water-quality variations, almost unchanged.

6.4.2 Travel Time Analysis

The travel time distributions that underly model results were computed by aggregating fluxes to daily averages and using the analytical formulas for the random sampling age-selection scheme properly arranged in series and in parallel (Eq. A.17).

The uncertainty in the groundwater residual storage size induces some uncertainty in the longer travel times, which in turn affect the mean of the distributions. The use of percentiles, that depend on the more determined part of the distributions, is hence more desirable. Median travel time (i.e. the age that is not exceeded by 50% of the discharge) shows quite some variability during the year which is linked to the catchment hydrologic conditions (Figure 6.7), ranging from 40-60 days during wet periods (e.g. after intense storms, or during spring snowmelt) to 180-200 days during dry summers and winter snow accumulations. Figure 6.7 also shows that every storm event causes a drop in the median travel time, because discharge peaks tipically mobilize younger water particles.

The different features displayed by the TTDs during different periods are visible in Figure 6.8, where some travel time pdf and CDF are reported. The wet period corresponds to an intense storm event taking place during snowmelt in April 2008. The corresponding modeled TTDs are largely composed of younger waters, even though half

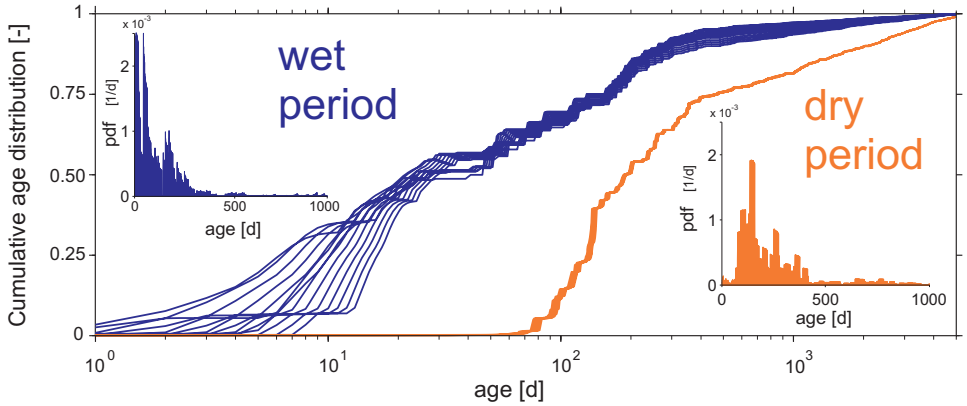

Figure 6.8: Cumulative TTD of discharge, during the wet and dry periods indicated in Figure 6.7. The insets also report the corresponding TTD.

of the released particles are still non-event as they are older than 20 days. The dry period corresponds to the end of a recession in September 2006 and its dynamics are similar to those of other long recessions. Young water particles are almost absent due to the dry antecedent weeks and youngest significant contributions are from storm events from 80-100 days before.

6.5 Silica and sodium transport

The TTDs obtained from the hydrochemical model were used to compute the stream-flow concentration of solutes produced by mineral weathering, following the approach proposed by *Maher* [2011].

Due to primary mineral weathering processes, the immobile water in contact with the soil matrix is enriched in mineral solutes. When a water parcel travels within subsurface environments and interacts with the minerals and/or immobile water (Figure 6.9), the underlying solute concentration gradients trigger mass transfer processes through which minerals are transferred to the mobile phase of water. The travel time T represents the time available for solute transfer and thus is assumed as the main driver of the process. The solution concentration c_i of the traveling particles changes through time according to a first order kinetics towards the immobile-phase equilibrium concentration C_{eq} [*Maher*, 2011]:

$$c_i(T) = C_{eq}\left(1 - \exp^{-kT}\right), \tag{6.2}$$

where k is a kinetic constant [1/T]. Equation (6.2) implies that when the transfer time T is short compared to $1/k$ (e.g. in the case of a short hydrologic flowpath), the parcel

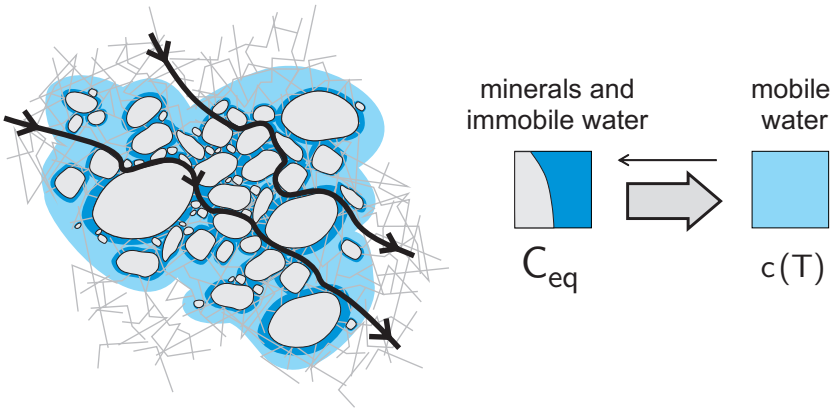

Figure 6.9: Graphical representation of the solute exchange between the mobile water and the minerals.

concentration is much lower than C_{eq}. Conversely, for travel times that are significantly longer than $1/k$, the parcel concentration reaches the equilibrium value ($C \approx C_{eq}$). The dissolution process is influenced by a number of relevant local factors, such as pH and temperature [see *Maher*, 2011], but, in large and complex domains like subsurface environments, flowpaths heterogeneity reduces the effect of spatial gradients in local factors [*Botter et al.*, 2005] thereby allowing the description of transport processes through spatially uniform parameters (k and C_{eq}). When considering the whole distribution of pathways that contribute to discharge at any time, the ages T of the parcels that leave the catchment can be quantified through the (backward) travel time distribution $p_Q(T,t)$. The resulting streamflow concentration can be expressed as:

$$C(t) = \int_0^\infty C_{eq}\,(1 - \exp^{-kT})\,p_Q(T,t)\,dT\,. \tag{6.3}$$

Eq. (6.3) can be directly used to compute silicon and sodium concentration at the catchment outlet. Though, a better representation of the observed concentration signal can be achieved when accounting for the presence of the seeps. Seep flow at WS3 is persistently characterized by higher concentrations of solutes such as Na^+, Ca^{2+} and H_2SiO_4, liberated during mineral weathering reactions. Some seeps are high in other metals of weathering origin such as Mn^{2+}. These patterns may reflect particular pathways that bring water in contact with fresh mineral surfaces or particular pathways with different mineral compositions. This pattern is not observed in the isotope data, suggesting that the higher concentrations of Si and Ca in some seeps are likely due to the nature of the hydrologic pathways rather than to the age of the particles. Note that seep flow contribution to discharge is negligible in the majority of the cases, but it dominates

Table 6.3: Kinetic parameters

Parameter	Symbol	value (Si)	value (Na)
kinetic. const. [1/d]	k	0.13	0.10
Equil. conc. [mg/l]	C_{eq}	2.5	0.95
Seep conc. [mg/l]	C_{seep}	3.4	1.5

the chemistry at the catchment outlet during extremely low flows (few weeks per year). Hence, seep influence has minor importance for solute mass balance, but it is highly visible in the concentration timeseries. The effect of the seeps is simulated by assuming a stationary seep flow of 0.15 mm/d (about 1 l/s). The related seep concentration is computed through Eq. (6.3) using a different value of the equilibrium concentration (C_{seep}). The chemograph is thus simulated using three parameters (C_{eq}, C_{seep} and k).

The kinetic constant k needs calibration, while C_{eq} and C_{seep} can be derived from available observations during low flow conditions at seeps and at the catchment outlet, where it can be reasonably assumed that solute concentration has reached the equilibrium. However, all the three model parameters were calibrated in the simulation to check if optimal C_{eq} and C_{seep} values are consistent with those suggested by the measurements. Calibration was run over the period March 2008 - March 2010 and calibrated values (table 6.3) were used to calculate the solute concentration over the 14-years period 1998-2012 (Figure Figure 6.10).

The simulated timeseries is generally able to reproduce the main features of the measured signal, including the dilution during stormflow, the increase in concentration during recession and the positive peaks during the periods dominated by the seep flow. Calibrated equilibrium and seep concentrations for both solutes are consistent with the value of measured concentration during late recessions, suggesting that calibration may not be needed for those parameters.

The kinetic constant k provides an estimate of mass transfer time-scales. For both the solutes, the kinetic constant is about 0.1 d^{-1}, which suggests that the driver of the streamflow concentration dynamics is the relative abundance of particles younger than 30 days. When a notable fraction of particles have a short contact time with the immobile phase (e.g. right after a storm), the overall streamflow concentration decreases. The opposite holds during dry periods, when most of the particles have traveled much longer than 30 days and exit the catchment at the equilibrium concentration. When flows are extremely low, the influence of the seeps further increases the streamflow concentration.

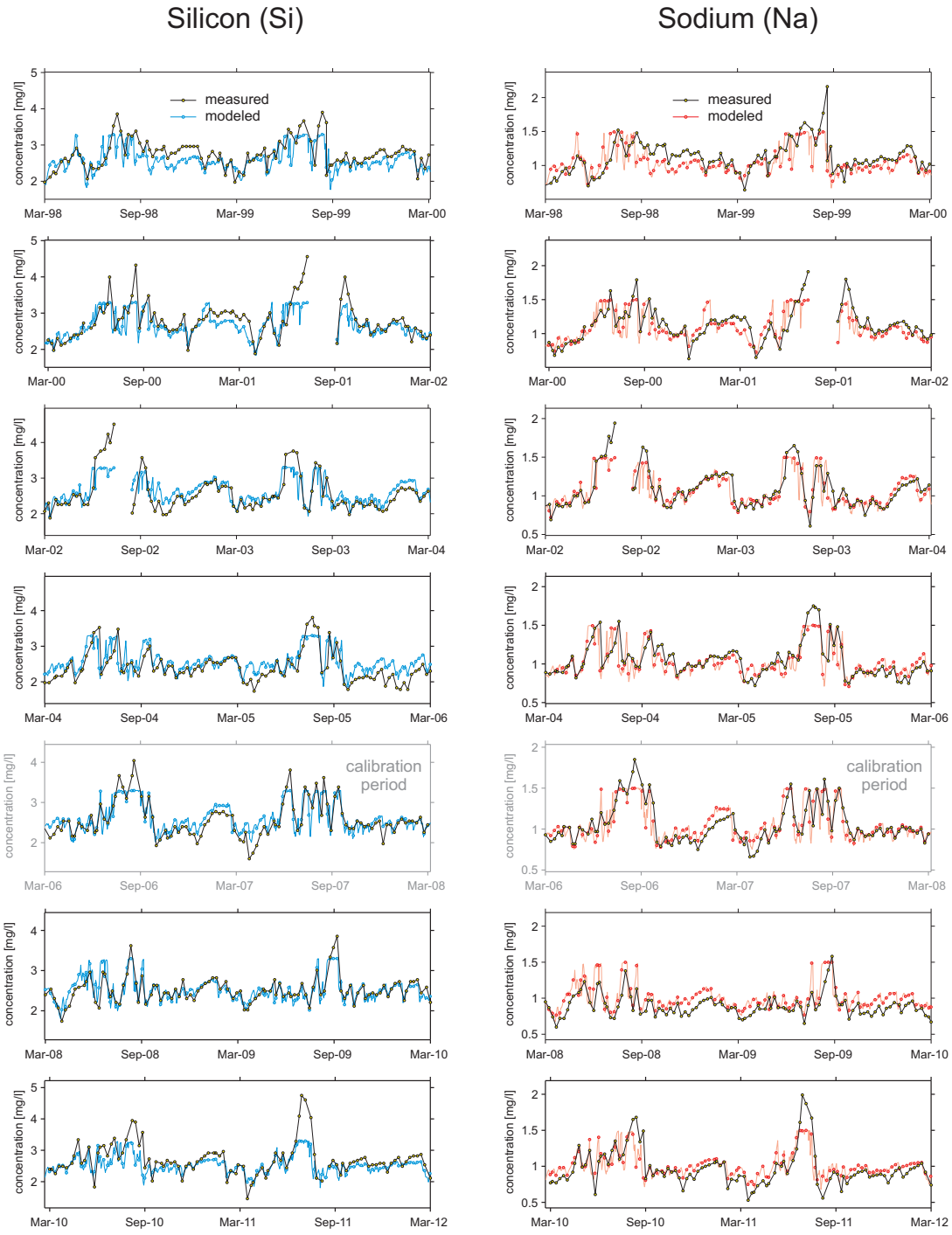

Figure 6.10: 14-years simulation of silicon and sodium concentration using the TTD-based approach.

The results suggest that silicon and sodium concentration dynamics at the catchment scale are mostly driven by hydrological factors. The outlined approach provides a meaningful and consistent representation of the observed concentration dynamics for multiple solutes. The main advantage of the method relies on the flexibility to the hydrologic variations of the system, which is allowed by the use of time-variable TTDs.

6.6 Final remarks

Despite the challenge of modeling a small catchment with intense evapotranspiration and snowmelt, the hydrochemical model was able to reproduce a number of catchment dynamics including runoff, snow accumulation and discharge isotopic content. The accuracy in reproducing the observed signals is a necessary condition to estimate catchment TTDs. Even though longer travel times are typically difficult to constrain, shorter travel times are better identifiable and are mostly responsible for the variations in stream hydrochemistry.

The travel time analysis not only allowed for an estimate of the relevant transport time-scales, but was also used to simulate the fate of geogenic solutes in surface waters. The results support the coupled use of solute measurements and transport models to quantify catchment-scale mixing processes and interpret hydrochemical datasets. The dynamic TTD analysis, which is the essence of this approach, represents a fruitful way forward for catchment-scale transport studies.

Conclusions

A comprehensive description of catchment-scale transport processes has been provided, including theoretical advances and applications to real-world catchments. The main conclusions of this contribution can be summarized as follows:

- transport processes can be described through a backward or a forward point of view, which requires the use of different variables (age or life expectancy) and equations. The two approaches are fully equivalent and can be derived from a single governing equation;
- the kinematic origin of age mixing can be formally related to advection-dispersion processes. This is shown to cause major differences between the age distribution of the water storage and that of the hydrologic fluxes crossing the system's borders.
- the coupled use of hydrochemical datasets and transport models allows for insightful inferences on catchment functioning. The use of a travel time approach can explain the long term export of solutes and their strong persistency in rivers, as well as short term dynamics induced by the sharp transitions between distinct water sources (e.g. soil waters and groundwater flow);
- overall, mean travel times are in the range of months to few years. However, the younger part of the distributions is usually better constrained, while the older fraction is more difficult to characterize. This affects the mean values of the distributions, that do not have a well-identified upper bound. Modeling results also show that discharge mostly removes, time by time, the younger fraction of particles contained in the catchment storage;
- TTDs can be sucesfully used to model the fate or reactive solutes that can be described through a first-order kinetic reaction. The applications show that the concentrations of silica and sodium produced by mineral weathering are mostly driven by the contact time between the water and mineral interfaces;

- the use of StorAge-Selection functions to solve transport problems has been proved to be a powerful and promising tool for further hydrochemical applications at catchment-scales.

Appendix

A.1 Derivation of Equation 3.5

Starting from equation (3.4) let us first take the derivatives of ρ with respect to t and T_R. By recalling that $t_0 = t - T_R$, one gets:

$$\begin{aligned}\frac{\partial \rho(\mathbf{x}, T_R, t)}{\partial t} &= \frac{\phi_{in}(t-T_R)}{\partial t} g(\mathbf{x}, t|t-T_R) - \phi_{in}(t-T_R)\frac{\partial g(\mathbf{x}, t|t-T_R)}{\partial T_R} \\ &+ \phi_{in}(t-T_R)\left.\frac{\partial g(\mathbf{x}, t|t-T_R)}{\partial t}\right|_{t-T_R=const} \qquad \text{(A.1)} \\ \frac{\partial \rho(\mathbf{x}, T_R, t)}{\partial T_R} &= -\frac{\phi_{in}(t-T_R)}{\partial t} g(\mathbf{x}, t|t-T_R) + \phi_{in}(t-T_R)\frac{\partial g(\mathbf{x}, t|t-T_R)}{\partial T_R} \qquad \text{(A.2)}\end{aligned}$$

and by combining equations (A.1) and (A.2) the following result is obtained:

$$\frac{\partial \rho(\mathbf{x}, T_R, t)}{\partial t} + \frac{\partial \rho(\mathbf{x}, T_R, t)}{\partial T_R} = \phi_{in}(t-T_R)\left.\frac{\partial g(\mathbf{x}, t|t-T_R)}{\partial t}\right|_{t-T_R=const}. \qquad \text{(A.3)}$$

Eq. (A.3) states that, at any position $\mathbf{x}$, the amount of particles with age T_R (quantified by $\rho(\mathbf{x}, T_R, t)$) changes in time because particles get older (second term at left hand side of the equation) and because they move, as quantified by the change in the displacement distribution g over time. Finally, substitution of eq. (3.1) into eq. (A.3) readily returns equation (3.5).

A.2 TTD formulas in advection-dispersion models

Travel and residence time distribution formulas can be equivalently obtained by integration over the control volume of the age mass function $\rho(\mathbf{x}, t, T_R)$ or by integration of the displacement pdf $g(\mathbf{x}, t|t_0)$. By inserting equation (3.4) into eq. (3.6) and (3.7), travel and residence time distributions are derived with explicit dependence on g. In the following, notation is simplified by calling $G = \int_V g d\mathbf{x}$ and $\dot{G}$ its derivative over

time. Equations read:

$$\begin{aligned} p_S(T_R,t) &= \frac{\phi_{in}(t-T_R)}{M(t)} \int_V g(\mathbf{x},t|t-T_R)d\mathbf{x} \\ &= \frac{\phi_{in}(t-T_R)}{M(t)} G(t|t-T_R)\,. \end{aligned} \tag{A.4}$$

$$\begin{aligned} p_Q(T_T,t) &= -\frac{\phi_{in}(t-T_T)}{\phi_{out}(t)} \frac{d}{dt} \int_V g(\mathbf{x},t|t-T_T)d\mathbf{x} \\ &= -\frac{\phi_{in}(t-T_T)}{\phi_{out}(t)} \dot{G}(t|t-T_T)\,. \end{aligned} \tag{A.5}$$

$$\omega(T_R,t) = \frac{p_Q}{p_S} = -\frac{M(t)}{\phi_{out}(t)} \frac{\dot{G}(t|t-T_R)}{G(t|t-T_R)}\,. \tag{A.6}$$

Formulas based on the integration of g can be readily used after an explicit solution to the Fokker-Plank equation is provided. This approach is the one used in section 3.5.

A.3 Solutions to the 1D advection-dispersion problem with absorbing and reflecting barriers

This appendix is devoted to the solution of the advection-dispersion equation for the particular boundary conditions described in equations (3.13). The solution makes use of the method of images, according to which additional terms (image terms) are superimposed to the fundamental solution g_0 (eq. (3.12)) in order to verify both the differential equation and the boundary conditions. This Appendix mainly follows *Cox and Miller* [1978] in the separate development of the reflecting/absorbing barriers and then introduces to the simultaneous use of both conditions.

The zero-flux boundary condition (BC1) can be obtained by adding an image term (from hereon reflecting term) to g_0 . If we call d_r the distance of g_0 from the reflecting barrier, the image is to be applied at the same distance d_r, in opposite direction. The application point of the reflecting terms is called x_{0r} (in this particular case the barrier is in $x = 0$, so $x_{0r} = -d_r$). The reflecting term has the following form [*Cox and Miller*, 1978]:

$$\begin{aligned} g_r(x,t) &= \frac{1}{\sqrt{4\pi Dt}} \left\{ A \ \exp\left[-\frac{(x-x_{0r}-ut)^2}{4Dt} \right] \right\} \\ &+ \frac{1}{\sqrt{4\pi Dt}} \left\{ \int_{-\infty}^{x_{0r}} \exp\left[-\frac{(x-\xi-ut)^2}{4Dt} \right] k(\xi)d\xi \ \right\} \end{aligned} \tag{A.7}$$

The constant A and the function $k(\xi)$ are determined by imposing BC1 yielding:

$$A = \exp\left(-\frac{d_r u}{D}\right), \quad k(\xi) = -\frac{u}{D}\exp\left(\frac{u\xi}{D}\right) \tag{A.8}$$

The term A rapidly decays with increasing distance from the barrier, meaning that the effect of the barrier is negligible when the barrier is far from the injection point. This becomes particularly important when series of reflecting terms with increasing distance from the barrier are considered, because it allows for a reduction in the number of terms that need to be considered. By inserting eq. (A.8) into (A.8) and rearranging terms in the equation, one obtains the solution to the problem for a purely reflecting barrier condition at the origin as:

$$\begin{aligned} g(x,t) &= g_0(x,t) \\ &+ \frac{1}{\sqrt{4\pi D t}}\left\{\exp\left[-\frac{u x_0}{D} - \frac{(x+x_0-ut)^2}{4Dt}\right]\right\} \\ &- \frac{u}{D}\exp\left(\frac{xu}{D}\right) erfc\left(\frac{x+x_0+ut}{\sqrt{4Dt}}\right) \end{aligned} \tag{A.9}$$

Note that this solution holds on a reduced domain $[0, +\infty)$, but still implies the second boundary condition to be set at infinity.

In a similar manner, the absorbing barrier (BC2) in $x = L$ is obtained by adding an image term (from hereon absorbing term) to g_0, and imposing $g(L,t) = 0$ (eq. (3.13)). In analogy with the reflecting barrier, the distance between g_0 and the absorbing barrier is termed d_a. The absorbing term must be applied at the same distance d_a, on the opposite side of the barrier, at a location x_{0a} (in this particular case $x_{0a} = L + d_a$) and has the following form [*Cox and Miller*, 1978]:

$$g_a(x,t) = -\frac{1}{\sqrt{4\pi D t}}\left\{B\ \exp\left[-\frac{(x+x_{0a}-ut)^2}{4Dt}\right]\right\} \tag{A.10}$$

By imposing $g(L,t) = g_0(L,t) + g_a(L,t) = 0$, the resulting constant B becomes:

$$B = \exp\left(\frac{d_a u}{D}\right) \tag{A.11}$$

The solution is valid for $x \in [-\infty, L)$.

The simultaneous use of both barriers requires, to satisfy BC2, the application of the absorbing term not just to g_0 but also to g_r. However, as already mentioned in section 3.4, the new absorbing terms induce an additional mass flux into the control volume which is in general different from zero at the origin and hence violates BC1. The influence of the absorbing terms on BC1 depends on the ability for particles to move

against flow direction so it depends on the relative strength of dispersion. To ensure BC1 to be satisfied, the new absorbing terms need to be matched by a second layer of reflecting terms. In turn, these additional terms need to be absorbed by a second generation of absorbing terms to respect BC2 and so on, making up an infinite series of subsequent generations. However, the relative importance of additional generations decreases relatively fast (depending on dispersion, recall (eq.(A.8)), so one can expand the series up to the desired precision. The final solution is given by the summation of many reflecting and absorbing generations:

$$g(x,t) = g_0(x,t) + \sum g_r(x,t) + \sum g_a(x,t) \tag{A.12}$$

where reflecting/absorbing terms are derived by subsequently imposing BC1/BC2 to the new generations and the position of the barriers is obtained by calculating new distances d_r and d_a from the barriers.

An example of the solution limited to the first generation of absorbing and reflecting terms, valid for $Pe \geq 10$, is:

$$\begin{aligned}
g(x,t) &= \frac{1}{\sqrt{4\pi Dt}} \exp\left[-\frac{(x-x_0-ut)^2}{4Dt}\right] \\
&+ \frac{1}{\sqrt{4\pi Dt}} \left\{\exp\left[-\frac{ux_0}{D} - \frac{(x+x_0-ut)^2}{4Dt}\right]\right\} \\
&- \frac{u}{2D}\exp\left(\frac{xu}{D}\right) erfc\left(\frac{x+x_0+ut}{\sqrt{4Dt}}\right) \\
&- \frac{1}{\sqrt{4\pi Dt}} \left\{\exp\left[\frac{(L-x_0)u}{D} - \frac{(x-(2L-x_0)-ut)^2}{4Dt}\right]\right\} \\
&- \frac{1}{\sqrt{4\pi Dt}} \left\{\exp\left[\frac{Lu}{D} - \frac{(x-(2L+x_0)-ut)^2}{4Dt}\right]\right\} \\
&+ \frac{u}{2D}\exp\left(\frac{Lu}{D}\right) erfc\left[\frac{-x+(2L+x_0)+ut}{\sqrt{4Dt}}\right]
\end{aligned} \tag{A.13}$$

The implementation of a multi-barrier system for $Pe = 1$ is shown in figure A.1a, where eq. (A.12) is developed up to the second generation of reflecting and absorbing terms. Figure A.1b shows the evolution of g over time, to enhance the effect of both the barriers. This is further shown for a fixed time t^* in Figure A.1c, where reflecting and absorbing terms are separately displayed and the clear difference between complete solution g and unconfined solution g_0 is made evident.

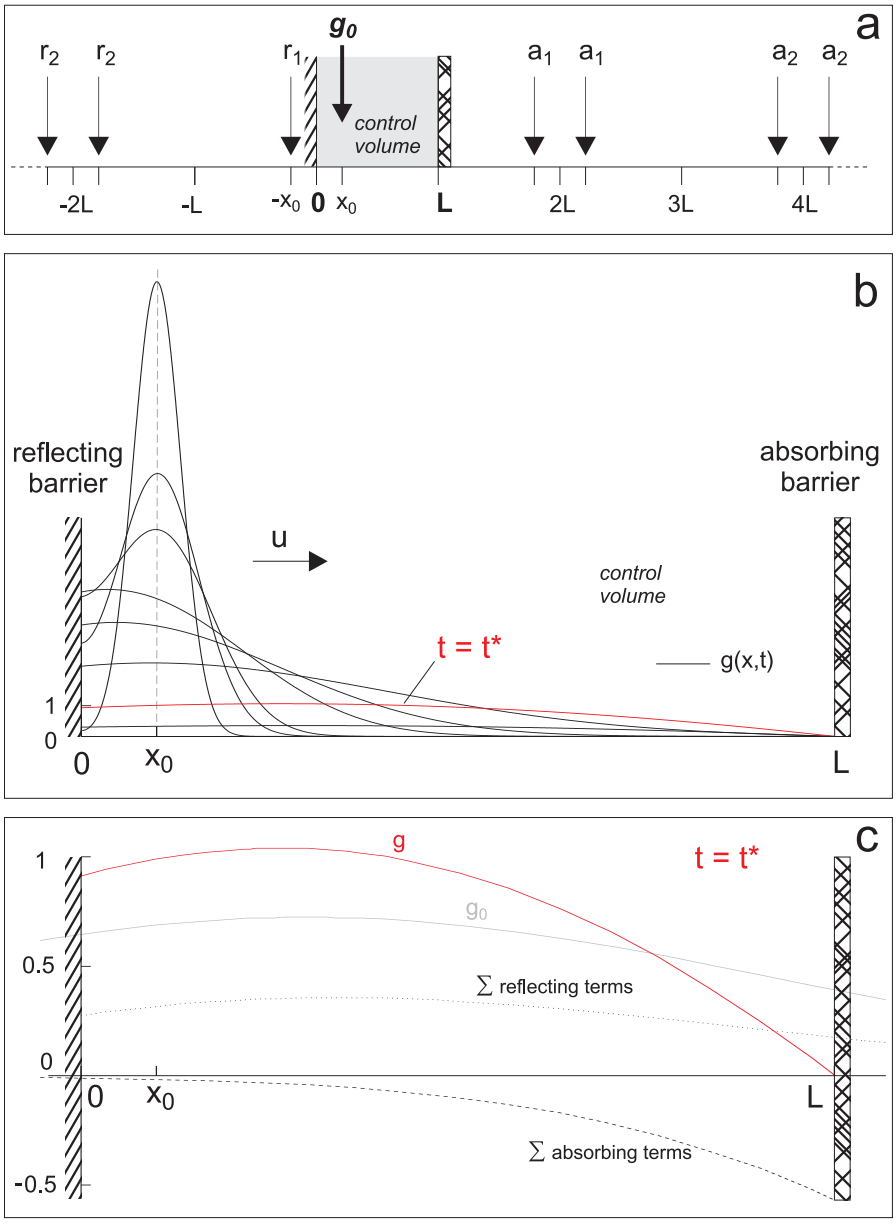

Figure A.1: Example of solution $g(x,t)$ for $Pe = 1$ obtained by using two generations of reflecting and absorbing terms. (a) shows the application of reflecting/absorbing terms. (b) shows the solution $g(x,t)$ at different times. (c) shows g at the particular time $t = t^*$ and its separate components (basic solution g_0, reflecting terms $\sum g_r$ and absorbing terms $\sum g_a$).

A.4 TTDs for multi-RS systems

In Section 4.2 it was shown that, under the hypothesis of randomly-sampled storage, travel time distributions p_Q and p_{ET} are equal to residence time distributions p_S.

In case the catchment is made up of two storages (e.g. one for the root zone and one for the groundwater, Figure 4.3 b, c, d), each storage is characterized by its associated TTDs. Note that for particles that reach the groundwater storage, the travel time must be computed starting with entrance into the catchment (i.e. entrance into the root zone), so the travel time distributions are obtained as the convolution between the pdf's in the root zone and the pdf's in the purely-groundwater storage. Finally, the overall p_Q (that accounts for the contribution of the two storages to discharge Q) is computed by means of weighted averages between the distributions of the two storages.

In order to simplify the notation, the following simbology is used:
$rz \rightarrow 1$,
$gw \rightarrow 2$,
$rz + gw \rightarrow 1 + 2$
(e.g. the function p_Q referred to the root zone is named p_1 and so on). So the TTD equations for the root zone in the simplified notation are:

$$p_1(T,t) = p_S(T,t) = \frac{J(t-T)}{S_{rz}(t-T)}\, exp\left(-\int_{t-T}^{t} \frac{J(\tau)}{S_{rz}(\tau)} d\tau\right) \tag{A.14}$$

where J is the input rainfall and S_{rz} is the root zone storage. The equation for the purely-groundwater storage has the same form, but in this case the input is given by the leakage to the groundwater L_{gw} and the storage is the deep S_{gw}.

$$p_2(T,t) = p_S(T,t) = \frac{L_{gw}(t-T)}{S_{gw}(t-T)}\, exp\left(-\int_{t-T}^{t} \frac{L_{gw}(\tau)}{S_{gw}(\tau)} d\tau\right) \tag{A.15}$$

To obtain the overall groundwater storage TTD's, the convolution between p_1 and p_2 is performed:

$$p_{1+2}(T,t) = p_2 * p_1(T,t) \tag{A.16}$$

Finally the global TTD's are:

$$p_T(T,t) = \frac{Q_1(t)}{Q_1(t)+Q_2(t)} p_1(T,t) + \frac{Q_2(t)}{Q_1(t)+Q_2(t)} p_{1+2}(T,t) \tag{A.17}$$

A.5 The marginal TTD

The marginal TTD represents the probability of observing a particular travel time during the considered observation period, and can be computed as:

$$p_m(T) = \int_{\Gamma} p_Q(T/t) f(t)\ dt \tag{A.18}$$

where Γ is the observation period for the averaging and $f(t)$ is a weighting function, in this case representing the probability of observing a particular exit time (t). In fact, $f(t)$ is proportional to $Q(t)$, because the higher the discharge at time t, the higher the probability of having many particles leaving the catchment at that time. Hence, the normalized discharge time series over Γ can be used in $f(t)$ and the marginal pdf basically serves as a flow-weighted average TTD.

A.6 Chloride input adjustments

In order to capture even small rainfall events, the autosampler was designed to have a large (57.5 cm) funnel which drained into a small (308 ml) bottle [*Neal et al.*, 2012], approximately corresponding to 1.2 mm of precipitation during the 7-hour sampling interval. Hence, all rainfall events larger than 1.2 mm per 7 hours produced some overflow. Because the initial part of the precipitation is usually higher in chloride due to the atmospheric (and funnel) washout, and given that the degree of mixing in such conditions is not well defined, samples taken during such events might not be very representative of the average 7-hour precipitation. During the modeled period (December 2007 - November 2008), 37% of the rainfall events exceeded 1.2 mm per 7 hours (9% exceeded 10 mm), requiring the determination of the corresponding overflow concentration. A simple estimation method is to assign a virtual concentration that matches the mass balance with weekly chloride measurements taken at the same location with a different instrument [see *Neal et al.*, 2011]. This procedure is consistent with mass balance, but tends to flatten concentration values towards the corresponding weekly average. For this reason, we decided to adjust precipitation volumes only exceeding a suitable threshold value larger than 1.2 mm. After some preliminary tests using different thresholds, the final value was 5 mm, that required the adjustment of 16% of the sampled concentrations.

Bibliography

Allen, M. B., I. Herrera, and G. F. Pinder (1988), *Numerical modeling in science and engineering*, Wiley-Interscience, New York.

Aquilina, L., V. Vergnaud-Ayraud, T. Labasque, O. Bour, J. Molenat, L. Ruiz, V. de Montety, J. De Ridder, C. Roques, and L. Longuevergne (2012), Nitrate dynamics in agricultural catchments deduced from groundwater dating and long-term nitrate monitoring in surface- and groundwaters, *Science of the Total Environment*, *435*, 167–178, doi:{10.1016/j.scitotenv.2012.06.028}.

Asano, Y., T. Uchida, and N. Ohte (2003), Hydrologic and geochemical influences on the dissolved silica concentration in natural water in a steep headwater catchment, *Geochimica et Cosmochimica Acta*, *67*(11), 1973–1989, doi:{10.1016/S0016-7037(02)01342-X}.

Aubert, A., C. Gascuel-Odoux, G. Gruau, N. Akkal, M. Faucheux, Y. Fauvel, C. Grimaldi, Y. Hamon, A. Jaffrezic, M. Le Coz-Bouhnik, J. Molénat, P. Petitjean, L. Ruiz, and P. Mérot (2013), Solute transport dynamics in small, shallow groundwater-dominated agricultural catchments: insights from a high-frequency, multisolute 10 yr-long monitoring study, *Hydrology and Earth System*, *17*(4), 1379–1391, doi:10.5194/hess-17-1379-2013.

Bailey, A. S., J. W. Hornbeck, J. L. Campbell, and E. C. (2003a), Hydrometeorological database for hubbard brook experimental forest: 1955-2000, *Tech. rep.*, U.S. Dept. of Agriculture, Forest Service, Northeastern Research Station.

Bailey, S., D. Buso, and G. Likens (2003b), Implications of sodium mass balance for interpreting the calcium cycle of a forested ecosystem, *Ecology*, *84*(2), 471–484, doi:{10.1890/0012-9658(2003)084[0471:IOSMBF]2.0.CO;2}.

Bailey, S., P. Brousseau, K. McGuire, and D. Ross (2014), Influence of landscape posi-

tion and transient water table on soil development and carbon distribution in a steep, headwater catchment, *Geoderma*, *227*, 279–289.

Basu, N. B., G. Destouni, J. W. Jawitz, S. E. Thompson, N. V. Loukinova, A. Darracq, S. Zanardo, M. Yaeger, M. Sivapalan, A. Rinaldo, and P. S. C. Rao (2010), Nutrient loads exported from managed catchments reveal emergent biogeochemical stationarity, *Geophysical Research Letters*, *37*, doi:{10.1029/2010GL045168}.

Benettin, P., A. Rinaldo, and G. Botter (2013a), Kinematics of age mixing in advection-dispersion models, *Water Resources Research*, *49*(12), 8539–8551, doi:10.1002/2013WR014708.

Benettin, P., Y. van der Velde, S. E. A. T. M. van der Zee, A. Rinaldo, and G. Botter (2013b), Chloride circulation in a lowland catchment and the formulation of transport by travel time distributions, *Water Resources Research*, *49*(8), 4619–4632, doi:10.1002/wrcr.20309.

Bertuzzo, E., M. Thomet, G. Botter, and A. Rinaldo (2013), Catchment-scale herbicides transport: Theory and application, *Advances in Water Resources*, *52*(0), 232 – 242, doi:10.1016/j.advwatres.2012.11.007.

Beven, K. (2012), *Predicting Hydrographs Using Distributed Models Based on Process Descriptions*, pp. 119–183, John Wiley & Sons, Ltd, doi:10.1002/9781119951001.ch5.

Beven, K., and J. Freer (2001), Equifinality, data assimilation, and uncertainty estimation in mechanistic modelling of complex environmental systems using the GLUE methodology, *Journal of Hydrology*, *249*(1-4), 11–29, doi:{10.1016/S0022-1694(01)00421-8}.

Beven, K. J. (2010), Preferential flows and travel time distributions: defining adequate hypothesis tests for hydrological process models Preface, *Hydrological Processes*, *24*(12, SI), 1537–1547, doi:{10.1002/hyp.7718}.

Beven, K. J., D. E. Henderson, and A. D. Reeves (1993), Dispersion parameters for undisturbed partially saturated soil, *Journal of Hydrology*, *143*, 19 – 43, doi:http://dx.doi.org/10.1016/0022-1694(93)90087-P, xVI General Assembly of the European Geophysical Society.

Birkel, C., C. Soulsby, and D. Tetzlaff (2011), Modelling catchment-scale water storage dynamics: reconciling dynamic storage with tracer-inferred passive storage, *Hydrological Processes*, *25*(25), 3924–3936, doi:10.1002/hyp.8201.

Birkel, C., C. Soulsby, D. Tetzlaff, S. Dunn, and L. Spezia (2012), High-frequency storm event isotope sampling reveals time-variant transit time distributions and influence of diurnal cycles, *Hydrological Processes*, *26*(2), 308–316, doi:10.1002/hyp.8210.

Botter, G. (2012), Catchment mixing processes and travel time distributions, *Water Resources Research*, *48*, doi:{10.1029/2011WR011160}.

Botter, G., and A. Rinaldo (2003), Scale effect on geomorphologic and kinematic dispersion, *Water Resources Research*, *39*(10), n/a–n/a, doi:10.1029/2003WR002154.

Botter, G., A. Porporato, I. Rodriguez-Iturbe, and A. Rinaldo (2009), Nonlinear storage-discharge relations and catchment streamflow regimes, *Water Resources Research*, *45*(10), doi:10.1029/2008WR007658.

Botter, G., E. Bertuzzo, A. Bellin, and A. Rinaldo (2005), On the Lagrangian formulations of reactive solute transport in the hydrologic response, *Water Resources Research*, *41*(4), doi:{10.1029/2004WR003544}.

Botter, G., E. Bertuzzo, and A. Rinaldo (2010), Transport in the hydrologic response: Travel time distributions, soil moisture dynamics, and the old water paradox, *Water Resources Research*, *46*, doi:{10.1029/2009WR008371}.

Botter, G., E. Bertuzzo, and A. Rinaldo (2011), Catchment residence and travel time distributions: The master equation, *Geophysical Research Letters*, *38*, doi:{10.1029/2011GL047666}.

Brandt, C., M. Robinson, and J. W. Finch (2004), Anatomy of a catchment: the relation of physical attributes of the Plynlimon catchments to variations in hydrology and water status, *Hydrology and Earth System Sciences*, *8*(3), 345–354, doi:10.5194/hess-8-345-2004.

Brauer, C. C., A. J. Teuling, A. Overeem, Y. van der Velde, P. Hazenberg, P. M. M. Warmerdam, and R. Uijlenhoet (2011), Anatomy of extraordinary rainfall and flash flood in a Dutch lowland catchment, *Hydrology and Earth System Sciences*, *15*(6), 1991–2005, doi:{10.5194/hess-15-1991-2011}.

Brooks, J. R., H. R. Barnard, R. Coulombe, and J. J. McDonnell (2010), Ecohydrologic separation of water between trees and streams in a Mediterranean climate, *Nature Geoscience*, *3*(2), 100–104, doi:{10.1038/NGEO722}.

Brutsaert, W., and J. L. Nieber (1977), Regionalized drought flow hydrographs from a mature glaciated plateau, *Water Resources Research*, *13*(3), 637–643, doi:10.1029/WR013i003p00637.

Cedarholm, D. (1994), Dominant soil water pathways on a northern new england forested hillslope, M.s. thesis, University of New Hampshire, Durham, NH.

Charbeneau, R. J. (2006), *Groundwater hydraulics and pollutant transport*, Waveland Press, Long Grove, IL.

Chen, M. (1971), The theory of micromixing for unsteady state flow reactors, *Chemical Engineering Science*, *26*, 17–28.

Clapp, R. B., and G. M. Hornberger (1978), Empirical equations for some soil hydraulic properties, *Water Resources Research*, *14*(4), 601–604, doi:10.1029/WR014i004p00601.

Clymans, W., G. Govers, E. Frot, B. Ronchi, B. Van Wesemael, and E. Struyf (2013), Temporal dynamics of bio-available Si fluxes in a temperate forested catchment (Meerdaal forest, Belgium), *Biogeochemistry*, *116*(1-3), 275–291, doi:10.1007/s10533-013-9858-9.

Cornaton, F., and P. Perrochet (2006), Groundwater age, life expectancy and transit time distributions in advective-dispersive systems: 1. Generalized reservoir theory, *Advances in Water Resources*, *29*(9), 1267–1291, doi:10.1016/j.advwatres.2005.10.009.

Cornaton, F. J. (2012), Transient water age distributions in environmental flow systems: The time-marching Laplace transform solution technique, *Water Resources Research*, *48*(3), n/a–n/a, doi:10.1029/2011WR010606.

Cox, D. R., and H. D. Miller (1978), *The theory of stochastic processes*, Chapman & Hall, London.

Cvetkovic, V., and G. Dagan (1994), Transport of kinetically sorbing solute by steady random velocity in heterogeneous porous formations, *Journal of Fluid Mechanics*, *265*, 189–215, doi:{10.1017/S0022112094000807}.

Cvetkovic, V., C. Carstens, J.-O. Selroos, and G. Destouni (2012), Water and solute transport along hydrological pathways, *Water Resources Research*, *48*(6), W06,537, doi:10.1029/2011WR011367.

Dagan, G. (1989), *Flow and transport in porous formations*, Springer-Verlag, New York.

Dagan, G., and V. Nguyen (1989), A comparison of travel time and concentration approaches to modeling transport by groundwater, *Journal of contaminant hydrology*, *4*, 79–91.

Danckwerts, P. (1953), Continuous flow systems: distribution of residence times, *Chemical Engineering Science*, *2*(8).

Dansgaard, W. (1964), Stable isotopes in precipitation, *Tellus*, *16*(4), 436–468, doi: 10.1111/j.2153-3490.1964.tb00181.x.

Davies, J., K. Beven, A. Rodhe, L. Nyberg, and K. Bishop (2013), Integrated modeling of flow and residence times at the catchment scale with multiple interacting pathways, *Water Resources Research*, *49*(August), 4738–4750, doi:10.1002/wrcr.20377.

Deleersnijder, E., J.-m. Campin, and E. J. M. Delhez (2001), The concept of age in marine modelling I . Theory and preliminary model results, *Journal of Marine Systems*.

Delhez, E. J., J.-M. Campin, A. C. Hirst, and E. Deleersnijder (1999), Toward a general theory of the age in ocean modelling, *Ocean Modelling*, *1*(1), 17–27, doi:10.1016/S1463-5003(99)00003-7.

Delhez, E. J., A. W. Heemink, and E. Deleersnijder (2004), Residence time in a semi-enclosed domain from the solution of an adjoint problem, *Estuarine, Coastal and Shelf Science*, *61*(4), 691–702, doi:10.1016/j.ecss.2004.07.013.

Detty, J. M., and K. J. McGuire (2010a), Threshold changes in storm runoff generation at a till-mantled headwater catchment, *Water Resources Research*, *46*(7), doi:10.1029/2009WR008102.

Detty, J. M., and K. J. McGuire (2010b), Topographic controls on shallow groundwater dynamics: implications of hydrologic connectivity between hillslopes and riparian zones in a till mantled catchment, *Hydrological Processes*, *24*(16), 2222–2236, doi: 10.1002/hyp.7656.

Engdahl, N. B., T. R. Ginn, and G. E. Fogg (2012), Non-Fickian dispersion of groundwater age, *Water Resources Research*, *48*(7), n/a–n/a, doi:10.1029/2012WR012251.

Engdahl, N. B., T. R. Ginn, and G. E. Fogg (2013), Advances in Water Resources Using groundwater age distributions to estimate the effective parameters of Fickian

and non-Fickian models of solute transport, *Advances in Water Resources*, *54*, 11–21, doi:10.1016/j.advwatres.2012.12.008.

Fiori, A. (1996), Finite Peclet extensions of Dagan's solutions to transport in anisotropic heterogeneous formations, *Water Resources Research*, *32*(1), 193–198, doi:{10.1029/95WR02768}.

Fiori, A., and D. Russo (2008), Travel time distribution in a hillslope: Insight from numerical simulations, *Water Resources Research*, *44*(12), doi:{10.1029/2008WR007135}.

Gannon, J. P., S. W. Bailey, and K. J. McGuire (2014), Organizing groundwater regimes and response thresholds by soils: A framework for understanding runoff generation in a headwater catchment, *Water Resources Research*, doi:10.1002/2014WR015498.

Gardiner, C. W. (1983), *Handbook of stochastic methods*, Springer-Verlag, Berlin.

Gat, J. R. (1996), Oxygen and hydrogen isotopes in the hydrologic cycle, *Annual Review of Earth and Planetary Sciences*, *24*(1), 225–262, doi:10.1146/annurev.earth.24.1.225.

Ginn, T. R. (1999), On the distribution of multicomponent mixtures over generalized exposure time in subsurface flow and reactive transport: Foundations, and formulations for groundwater age, chemical heterogeneity, and biodegradation, *Water Resources Research*, *35*(5), 1395–1407.

Ginn, T. R., H. Haeri, A. Massoudieh, and L. Foglia (2009), Notes on Groundwater Age in Forward and Inverse Modeling, *Transport in Porous Media*, *79*(1), 117–134, doi:10.1007/s11242-009-9406-1.

Godsey, S. E., W. Aas, T. a. Clair, H. a. de Wit, I. J. Fernandez, J. S. Kahl, I. a. Malcolm, C. Neal, M. Neal, S. J. Nelson, S. a. Norton, M. C. Palucis, B. L. Skjelkvå le, C. Soulsby, D. Tetzlaff, and J. W. Kirchner (2010), Generality of fractal 1/f scaling in catchment tracer time series, and its implications for catchment travel time distributions, *Hydrological Processes*, *24*(12), 1660–1671, doi:10.1002/hyp.7677.

Gomez, J. D., and J. L. Wilson (2013), Age distributions and dynamically changing hydrologic systems: Exploring topography-driven flow, *Water Resources Research*, *49*(3), 1503–1522, doi:10.1002/wrcr.20127.

Guan, H., A. J. Love, C. T. Simmons, J. Hutson, and Z. Ding (2010), Catchment conceptualisation for examining applicability of chloride mass balance method in an

area with historical forest clearance, *Hydrology and Earth System Sciences*, *14*(7), 1233–1245, doi:{10.5194/hess-14-1233-2010}.

Haria, A., and P. Shand (2004), Evidence for deep sub-surface flow routing in forested upland Wales: implications for contaminant transport and stream flow generation, *Hydrology and Earth System Sciences*, *8*(3), 334–344.

Haria, A. H., and P. Shand (2006), Near-stream soil water-groundwater coupling in the headwaters of the Afon Hafren, Wales: Implications for surface water quality, *Journal of Hydrology*, *331*(3-4), 567–579, doi:10.1016/j.jhydrol.2006.06.004.

Harman, C., and M. Kim (2014), An efficient tracer test for time-variable transit time distributions in periodic hydrodynamic systems, *Geophysical Research Letters*, *41*(5), 1567–1575, doi:10.1002/2013GL058980.Abstract.

Harman, C. J. (2014), Time-variable transit time distributions and transport: Theory and application to storage-dependent transport of chloride in a watershed, *Water Resources Research*, doi:10.1002/2014WR015707.

Harman, C. J., P. S. C. Rao, N. B. Basu, G. S. McGrath, P. Kumar, and M. Sivapalan (2011), Climate, soil, and vegetation controls on the temporal variability of vadose zone transport, *Water Resources Research*, *47*(10), n/a–n/a, doi:10.1029/2010WR010194.

Heidbuechel, I., P. A. Troch, S. W. Lyon, and M. Weiler (2012), The master transit time distribution of variable flow systems, *Water Resources Research*, *48*, doi:{10.1029/2011WR011293}.

Hooper, R. P., and C. A. Shoemaker (1986), A comparison of chemical and isotopic hydrograph separation, *Water Resources Research*, *22*(10), 1444–1454, doi:10.1029/WR022i010p01444.

Hornberger, G., T. Scanlon, and J. Raffensperger (2001), Modelling transport of dissolved silica in a forested headwater catchment: the effect of hydrological and chemical time scales on hysteresis in the concentration-discharge relationship, *Hydrological Processes*, *15*(10), 2029–2038, doi:{10.1002/hyp.254}.

Hrachowitz, M., C. Soulsby, D. Tetzlaff, I. A. Malcolm, and G. Schoups (2010), Gamma distribution models for transit time estimation in catchments: Physical interpretation of parameters and implications for time-variant transit time assessment, *Water Resources Research*, *46*, doi:{10.1029/2010WR009148}.

Hrachowitz, M., H. Savenije, T. A. Bogaard, D. Tetzlaff, and C. Soulsby (2013), What can flux tracking teach us about water age distribution patterns and their temporal dynamics?, *Hydrology and Earth System Sciences*, *17*(2), 533–564, doi:{10.5194/hess-17-533-2013}.

Ingraham, N. L. (1998), Chapter 3 - isotopic variations in precipitation, in *Isotope Tracers in Catchment Hydrology*, edited by J. J. McDonnell and C. Kendall, pp. 87 – 118, Elsevier, Amsterdam, doi:http://dx.doi.org/10.1016/B978-0-444-81546-0.50010-0.

Jankovic, I., A. Fiori, and G. Dagan (2009), The impact of local diffusion on longitudinal macrodispersivity and its major effect upon anomalous transport in highly heterogeneous aquifers, *Advances in Water Resources*, *32*(5), 659–669, doi:{10.1016/j.advwatres.2008.08.012}.

Kennedy, C. D., C. Bataille, Z. Liu, S. Ale, J. VanDeVelde, C. R. Roswell, L. C. Bowling, and G. J. Bowen (2012), Dynamics of nitrate and chloride during storm events in agricultural catchments with different subsurface drainage intensity (Indiana, USA), *Journal of Hydrology*, *466*, 1–10, doi:{10.1016/j.jhydrol.2012.05.002}.

Kirby, C., M. Newson, and K. Gilman (1991), *Plynlimon research: the first two decades*, 109, Inst. of Hydrol., Wallingford, U.K.

Kirby, C., C. Neal, H. Turner, and P. Moorhouse (1997), A bibliography of hydrological, geomorphological, sedimentological, biological and hydrochemical references to the Institute of Hydrology experimental catchment studies in Plynlimon, *Hydrology and Earth System Sciences*, *1*(3), 755–763.

Kirchner, J., X. Feng, and C. Neal (2000), Fractal stream chemistry and its implications for contaminant transport in catchments, *Nature*, *403*(6769), 524–527, doi:{10.1038/35000537}.

Kirchner, J., X. Feng, and C. Neal (2001), Catchment-scale advection and dispersion as a mechanism for fractal scaling in stream tracer concentrations, *Journal of Hydrology*, *254*(1-4), 82–101, doi:{10.1016/S0022-1694(01)00487-5}.

Kirchner, J. W. (2003), A double paradox in catchment hydrology and geochemistry, *Hydrological Processes*, *17*(4), 871–874, doi:10.1002/hyp.5108.

Kirchner, J. W. (2009), Catchments as simple dynamical systems: Catchment characterization, rainfall-runoff modeling, and doing hydrology backward, *Water Resources Research*, *45*(2), doi:10.1029/2008WR006912.

Kirchner, J. W., and C. Neal (2013), Universal fractal scaling in stream chemistry and its implications for solute transport and water quality trend detection., *Proceedings of the National Academy of Sciences of the United States of America*, *110*(30), 12,213–8, doi:10.1073/pnas.1304328110.

Kirchner, J. W., D. Tetzlaff, and C. Soulsby (2010), Comparing chloride and water isotopes as hydrological tracers in two Scottish catchments, *Hydrological Processes*, *24*(12), 1631–1645, doi:10.1002/hyp.7676.

Kreft, A., and A. Zuber (1978), On the physical meaning of the dispersion equation and its solutions for different initial and boundary conditions, *Chemical Engineering Science*, *33*(11), 1471 – 1480, doi:http://dx.doi.org/10.1016/0009-2509(78)85196-3.

Laio, F., A. Porporato, L. Ridolfi, and I. Rodriguez-Iturbe (2001), Plants in water-controlled ecosystems: active role in hydrologic processes and response to water stress - II. Probabilistic soil moisture dynamics, *Advances in Water Resources*, *24*(7), 707–723, doi:{10.1016/S0309-1708(01)00005-7}.

Likens, G. (2013), *Biogeochemistry of a Forested Echosystem*, 3 ed., Springer, New York.

Liu, F., M. Williams, and N. Caine (2004), Source waters and flow paths in an alpine catchment, Colorado Front Range, United States, *Water Resources Research*, *40*(9), doi:{10.1029/2004WR003076}.

Maher, K. (2011), The role of fluid residence time and topographic scales in determining chemical fluxes from landscapes, *Earth and Planetary Science Letters*, *312*, 48–58, doi:10.1016/j.epsl.2011.09.040.

Marc, V., and M. Robinson (2007), The long-term water balance (1972-2004) of upland forestry and grassland at Plynlimon, mid-Wales, *Hydrology and Earth System Sciences*, *11*(1), 44–60, doi:10.5194/hess-11-44-2007.

McDonnell, J. J., K. McGuire, P. Aggarwal, K. J. Beven, D. Biondi, G. Destouni, S. Dunn, A. James, J. Kirchner, P. Kraft, S. Lyon, P. Maloszewski, B. Newman, L. Pfister, A. Rinaldo, A. Rodhe, T. Sayama, J. Seibert, K. Solomon, C. Soulsby, M. Stewart, D. Tetzlaff, C. Tobin, P. Troch, M. Weiler, A. Western, A. Worman,

and S. Wrede (2010), How old is streamwater? Open questions in catchment transit time conceptualization, modelling and analysis, *Hydrological Processes*, *24*(12, SI), 1745–1754, doi:{10.1002/hyp.7796}.

McGlynn, B., J. McDonnell, M. Stewart, and J. Seibert (2003), On the relationships between catchment scale and streamwater mean residence time, *Hydrological Processes*, *17*(1), 175–181, doi:{10.1002/hyp.5085}.

McGuire, K., J. McDonnell, M. Weiler, C. Kendall, B. McGlynn, J. Welker, and J. Seibert (2005), The role of topography on catchment-scale water residence time, *Water Resources Research*, *41*(5), doi:{10.1029/2004WR003657}.

McGuire, K. J., and G. E. Likens (2011), *Historical roots of forest hydrology and biogeochemistry*, vol. 216, chap. 1, pp. 3–26, Springer-Verlag, Heidelberg, Germany.

McGuire, K. J., and J. J. McDonnell (2006), A review and evaluation of catchment transit time modeling, *Journal of Hydrology*, *330*(3-4), 543–563, doi:{10.1016/j.jhydrol.2006.04.020}.

McGuire, K. J., M. Weiler, and J. J. McDonnell (2007), Integrating tracer experiments with modeling to assess runoff processes and water transit times, *Advances in Water Resources*, *30*(4), 824–837, doi:{10.1016/j.advwatres.2006.07.004}.

McMillan, H., D. Tetzlaff, M. Clark, and C. Soulsby (2012), Do time-variable tracers aid the evaluation of hydrological model structure? A multimodel approach, *Water Resources Research*, *48*(5), doi:10.1029/2011WR011688.

Nauman, E. (1969), Residence time distribution theory for unsteady stirred tank reactors, *Chemical Engineering Science*, *24*(9), 1461 – 1470, doi:http://dx.doi.org/10.1016/0009-2509(69)85074-8.

Neal, C. (2004), The water quality functioning of the upper River Severn, Plynlimon, mid-Wales: issues of monitoring, process understanding and forestry, *Hydrology and Earth System Sciences*, *8*(3), 521–532.

Neal, C., and J. Kirchner (2000), Sodium and chloride levels in rainfall, mist, streamwater and groundwater at the Plynlimon catchments, mid-Wales: inferences on hydrological and chemical controls, *Hydrology and Earth System Sciences*, *4*(2), 295–310.

Neal, C., A. Robson, P. Shand, W. Edmunds, A. Dixon, D. Buckley, S. Hill, M. Harrow, M. Neal, J. Wilkinson, and B. Reynolds (1997), The occurrence of groundwater in

the Lower Palaeozoic rocks of upland Central Wales, *Hydrology and Earth System Sciences*, *1*, 3–18.

Neal, C., B. Reynolds, M. Neal, B. Pugh, L. Hill, and H. Wickham (2001), Long-term changes in the water quality of rainfall, cloud water and stream water for moorland, forested and clear-felled catchments at Plynlimon, mid-Wales, *Hydrology and Earth System Sciences*, *5*(3), 459–476, doi:10.5194/hess-5-459-2001.

Neal, C., B. Reynolds, D. Norris, J. W. Kirchner, M. Neal, P. Rowland, H. Wickham, S. Harman, L. Armstrong, D. Sleep, A. Lawlor, C. Woods, B. Williams, M. Fry, G. Newton, and D. Wright (2011), Three decades of water quality measurements from the Upper Severn experimental catchments at Plynlimon, Wales: an openly accessible data resource for research, modelling, environmental management and education, *Hydrological Processes*, *25*(24), 3818–3830, doi:10.1002/hyp.8191.

Neal, C., B. Reynolds, J. W. Kirchner, P. Rowland, D. Norris, D. Sleep, A. Lawlor, C. Woods, S. Thacker, H. Guyatt, C. Vincent, K. Lehto, S. Grant, J. Williams, M. Neal, H. Wickham, S. Harman, and L. Armstrong (2013), High-frequency precipitation and stream water quality time series from Plynlimon, Wales: an openly accessible data resource spanning the periodic table, *Hydrological Processes*, *27*(17), 2531–2539, doi:10.1002/hyp.9814.

Neal, C., N. Christophersen, R. Neale, C. Smith, P. Whitehead, and B. Reynolds (1988), Chloride in precipitation and streamwater for the upland catchment of river Severn, Mid-Wales - some consequences for hydrochemical models, *Hydrological Processes*, *2*(2), 155–165, doi:{10.1002/hyp.3360020206}.

Neal, C., M. Robinson, B. Reynolds, M. Neal, P. Rowland, S. Grant, D. Norris, B. Williams, D. Sleep, and A. Lawlor (2010), Hydrology and water quality of the headwaters of the River Severn: Stream acidity recovery and interactions with plantation forestry under an improving pollution climate, *Science of the Total Environment*, *408*(21), 5035–5051, doi:{10.1016/j.scitotenv.2010.07.047}.

Neal, C., B. Reynolds, P. Rowland, D. Norris, J. W. Kirchner, M. Neal, D. Sleep, A. Lawlor, C. Woods, S. Thacker, H. Guyatt, C. Vincent, K. Hockenhull, H. Wickham, S. Harman, and L. Armstrong (2012), High-frequency water quality time series in precipitation and streamflow: From fragmentary signals to scientific challenge, *Science of the Total Environment*, *434*(SI), 3–12, doi:{10.1016/j.scitotenv.2011.10.072}.

Niemi, A. J. (1977), Residence time distributions of variable flow processes, *The International Journal of Applied Radiation and Isotopes*, *28*(10-11), 855 – 860, doi: 10.1016/0020-708X(77)90026-6.

Oda, T., Y. Asano, and M. Suzuki (2009), Transit time evaluation using a chloride concentration input step shift after forest cutting in a Japanese headwater catchment, *Hydrological Processes*, *23*, 2705–2713, doi:10.1002/hyp.7361.

Page, T., K. Beven, J. Freer, and C. Neal (2007), Modelling the chloride signal at Plynlimon, Wales, using a modified dynamic TOPMODEL incorporating conservative chemical mixing (with uncertainty), *Hydrological Processes*, *21*(3), 292–307, doi:10. 1002/hyp.

Penna, D., O. Oliviero, R. Assendelft, G. Zuecco, I. H. J. V. Meerveld, T. Anfodillo, V. Carraro, M. Borga, and G. D. Fontana (2013), Tracing the Water Sources of Trees and Streams: Isotopic Analysis in a Small Pre-Alpine Catchment, *Procedia Environmental Sciences*, *19*, 106–112, doi:10.1016/j.proenv.2013.06.012.

Peters, N. E., D. a. Burns, and B. T. Aulenbach (2013), Evaluation of High-Frequency Mean Streamwater Transit-Time Estimates Using Groundwater Age and Dissolved Silica Concentrations in a Small Forested Watershed, *Aquatic Geochemistry*, *20*(2-3), 183–202, doi:10.1007/s10498-013-9207-6.

Rango, A., and J. Martinec (1995), Revisiting the degree-day method for snowmelt computations, *Journal of the American Water Resources Association*, *31*(4), 657–669, doi:10.1111/j.1752-1688.1995.tb03392.x.

Rinaldo, A., and A. Marani (1987), Basin scale-model of solute transport, *Water Resources Research*, *23*(11), 2107–2118, doi:{10.1029/WR023i011p02107}.

Rinaldo, A., and I. Rodriguez-Iturbe (1996), Geomorphological theory of the hydrological response, *Hydrological Processes*, *10*(6), 803–829, doi:{10.1002/(SICI) 1099-1085(199606)10:6<803::AID-HYP373>3.0.CO;2-N}.

Rinaldo, A., A. Marani, and A. Bellin (1989), On Mass Response Functions, *Water Resources Research*, *25*(7), 1603–1617.

Rinaldo, A., A. Marani, and R. Rigon (1991), Geomorphological Dispersion, *Water Resources Research*, *27*(4), 513–525.

Rinaldo, A., G. Vodel, R. Rigon, and I. Rodriguez-Iturbe (1995), Can one gauge the shape of a basin?, *Water Resources Research*, *31*(4), 1119–1127, doi:{10.1029/94WR03290}.

Rinaldo, A., K. J. Beven, E. Bertuzzo, L. Nicotina, J. Davies, A. Fiori, D. Russo, and G. Botter (2011), Catchment travel time distributions and water flow in soils, *Water Resources Research*, *47*, doi:{10.1029/2011WR010478}.

Robinson, J. S., M. Sivapalan, and J. D. Snell (1995), On the relative roles of hillslope processes, channel routing, and network geomorphology in the hydrologic response of natural catchments, *Water Resources Research*, *31*(12), 3089–3101, doi:10.1029/95WR01948.

Rodríguez-Iturbe, I., and A. Rinaldo (1997), *Fractal River Basins: Chance and Self-Organization*, Cambridge University Press, New York.

Rodriguez-Iturbe, I., A. Porporato, L. Ridolfi, V. Isham, and D. Cox (1999), Probabilistic modelling of water balance at a point: the role of climate, soil and vegetation, *Proceedings of the Royal Society A-Mathematical Phydical and Engineering Sciences*, *455*(1990), 3789–3805.

Rouxel, M., J. Molenat, L. Ruiz, C. Legout, M. Faucheux, and C. Gascuel-Odoux (2011), Seasonal and spatial variation in groundwater quality along the hillslope of an agricultural research catchment (Western France), *Hydrological Processes*, *25*(6), 831–841, doi:{10.1002/hyp.7862}.

Ruiz, L., S. Abiven, C. Martin, P. Durand, V. Beaujouan, and J. Molenat (2002), Effect on nitrate concentration in stream water of agricultural practices in small catchments in Brittany : II. Temporal variations and mixing processes, *Hydrology and Earth System Sciences*, *6*(3), 507–513.

Russo, D., and A. Fiori (2009), Stochastic analysis of transport in a combined heterogeneous vadose zone-groundwater flow system, *Water Resources Research*, *45*, doi:{10.1029/2008WR007157}.

Saco, P., and P. Kumar (2004), Kinematic dispersion effects of hillslope velocities, *Water Resources Research*, *40*(1), doi:{10.1029/2003WR002024}.

Scanlon, T., J. Raffensperger, and G. Hornberger (2001), Modeling transport of dissolved silica in a forested headwater catchment: Implications for defining the hy-

drochemical response of observed flow pathways, *Water Resources Research*, *37*(4), 1071–1082, doi:{10.1029/2000WR900278}.

Shand, P., a. H. Haria, C. Neal, K. J. Griffiths, D. C. Gooddy, a. J. Dixon, T. Hill, D. K. Buckley, and J. E. Cunningham (2005), Hydrochemical heterogeneity in an upland catchment: further characterisation of the spatial, temporal and depth variations in soils, streams and groundwaters of the Plynlimon forested catchment, Wales, *Hydrology and Earth System Sciences*, *9*(6), 621–644, doi:10.5194/hess-9-621-2005.

Shaw, S. B., A. a. Harpold, J. C. Taylor, and M. T. Walter (2008), Investigating a high resolution, stream chloride time series from the Biscuit Brook catchment, Catskills, NY, *Journal of Hydrology*, *348*(3-4), 245–256, doi:10.1016/j.jhydrol.2007.10.009.

Smith, T., L. Marshall, B. McGlynn, and K. Jencso (2013), Using field data to inform and evaluate a new model of catchment hydrologic connectivity, *Water Resources Research*, *49*(10), 6834–6846, doi:10.1002/wrcr.20546.

Snell, J. D., and M. Sivapalan (1994), On geomorphological dispersion in natural catchments and the geomorphological unit hydrograph, *Water Resources Research*, *30*(7), 2311–2323, doi:10.1029/94WR00537.

Soltani, S. S., and V. Cvetkovic (2013), On the distribution of water age along hydrological pathways with transient flow, *Water Resources Research*, pp. n/a–n/a, doi:10.1002/wrcr.20402.

Stelzer, R. S., and G. E. Likens (2006), Effects of sampling frequency on estimates of dissolved silica export by streams: The role of hydrological variability and concentration-discharge relationships, *Water Resources Research*, *42*(7), doi:{10.1029/2005WR004615}.

Stumpp, C., G. Nützmann, S. Maciejewski, and P. Maloszewski (2009), A comparative modeling study of a dual tracer experiment in a large lysimeter under atmospheric conditions, *Journal of Hydrology*, *375*(3-4), 566–577, doi:10.1016/j.jhydrol.2009.07.010.

Svensson, T., G. M. Lovett, and G. E. Likens (2012), Is chloride a conservative ion in forest ecosystems?, *Biogeochemistry*, *107*(1-3), 125–134, doi:10.1007/s10533-010-9538-y.

Taiz, L., and E. Zeiger (2010), *Plant Physiology*, Sinauer Associates, Inc.

ter Braak, C. J. F., and J. a. Vrugt (2008), Differential Evolution Markov Chain with snooker updater and fewer chains, *Statistics and Computing*, *18*(4), 435–446, doi: 10.1007/s11222-008-9104-9.

Tetzlaff, D., C. Birkel, J. Dick, J. Geris, and C. Soulsby (2014), Storage dynamics in hydropedological units control hillslope connectivity, runoff generation, and the evolution of catchment transit time distributions, *Water Resources Research*, *50*, 969–985, doi:10.1002/2013WR014147.

van der Velde, Y., I. Heidbuchel, S. W. Lyon, L. Nyberg, A. Rodhe, K. Bishop, and P. A. Troch (2014), Consequences of mixing assumptions for time-variable travel time distributions, *Hydrological Processes*, doi:10.1002/hyp.10372.

van der Velde, Y., G. H. de Rooij, and P. J. J. F. Torfs (2009), Catchment-scale nonlinear groundwater-surface water interactions in densely drained lowland catchments, *Hydrology and Earth System Sciences*, *13*(10), 1867–1885.

van der Velde, Y., G. H. de Rooij, J. C. Rozemeijer, F. C. van Geer, and H. P. Broers (2010a), Nitrate response of a lowland catchment: On the relation between stream concentration and travel time distribution dynamics, *Water Resources Research*, *46*, doi:{10.1029/2010WR009105}.

van der Velde, Y., J. C. Rozemeijer, G. H. de Rooij, F. C. van Geer, and H. P. Broers (2010b), Field-Scale Measurements for Separation of Catchment Discharge into Flow Route Contributions, *Vadose Zone Journal*, *9*(1), 25–35, doi:{10.2136/vzj2008.0141}.

van der Velde, Y., J. C. Rozemeijer, G. H. de Rooij, F. C. van Geer, and H. P. Broers (2010c), Field-Scale Measurements for Separation of Catchment Discharge into Flow Route Contributions, *Vadose Zone Journal*, *9*(1), 25–35, doi:{10.2136/vzj2008.0141}.

van der Velde, Y., J. C. Rozemeijer, G. H. de Rooij, F. C. van Geer, P. J. J. F. Torfs, and P. G. B. de Louw (2011), Improving catchment discharge predictions by inferring flow route contributions from a nested-scale monitoring and model setup, *Hydrology and Earth System Sciences*, *15*(3), 913–930, doi:{10.5194/hess-15-913-2011}.

van der Velde, Y., P. J. J. F. Torfs, S. E. A. T. M. van der Zee, and R. Uijlenhoet (2012), Quantifying catchment-scale mixing and its effect on time-varying travel time distributions, *Water Resources Research*, *48*, doi:{10.1029/2011WR011310}.

van Ommen, H., R. Dijksma, J. Hendrickx, L. Dekker, J. Hulshof, and M. Vandenheuvel (1989), Experimental assessment of preferential flow paths in a field soil, *Journal of Hydrology*, *105*(3-4), 253–262, doi:{10.1016/0022-1694(89)90107-8}.

Vrugt, J., C. T. Braak, C. Diks, B. Robinson, J. Hyman, and D. Higdon (2009), Accelerating Markov chain Monte Carlo simulation by differential evolution with self-adaptive randomized subspace sampling, *International Journal of Nonlinear Sciences & Numerical Simulation*, *10*(3), 271–288.

Weiler, M., B. L. McGlynn, K. J. McGuire, and J. J. McDonnell (2003), How does rainfall become runoff? a combined tracer and runoff transfer function approach, *Water Resources Research*, *39*(11), n/a–n/a, doi:10.1029/2003WR002331.

Wosten, J., J. Bouma, and G. Stoffelsen (1985), Use of soil survey data for regional soil-water simulation-models, *Soil Science Society of America Journal*, *49*(5), 1238–1244.

Xu, G., H. Magen, J. Tarchitzky, and U. Kafkafi (1999), Advances in Chloride Nutrition of Plants, *Advances in Agronomy*, *68*, 97–150, doi:10.1016/S0065-2113(08)60844-5.

Zimmer, M. a., S. W. Bailey, K. J. McGuire, and T. D. Bullen (2013), Fine scale variations of surface water chemistry in an ephemeral to perennial drainage network, *Hydrological Processes*, *27*(24), 3438–3451, doi:10.1002/hyp.9449.

Acknowledgements

At the end of my studies, I wish to thank those who provided any kind of support to my Ph.D. research and education. These include: the ICEA department, the School of Civil and Environmental Engineering Sciences and the International Center of Hydrology "Dino Tonini", for providing equipment and financial support; Enrica Belluco and Giulia Passadore, for general support; researchers from Wageningen University (Sjoerd van der Zee, Ype van der Velde and Remko Uijlenhoet), for the data on the Hupsel Brook catchment; researchers from the Hubbard Brook Ecosystem Study (John Campbell, Mark Green, Scott and Amey Bailey, Don Buso and Gene Likens), for data on Hubbard Brook Experimental Forest and productive discussions; Jim Kirchner, for advising me on the Hafren catchment study, and the UK Center for Ecology and Hydrology, for the data on the Plynlimon catchments; Aldo Fiori, for reviewing the early version of this manuscript; JP Gannon, Ype van der Velde and Ciaran Harman, for useful and productive discussions on hydrology and travel times; Kevin McGuire, for supervising my research during the 7 months at Virginia Tech; my family and friends, for their constant moral support. Finally, I wish to thank my supervisors Andrea Rinaldo and Gianluca Botter for their utterly global support and for being a positive example of academic education and research.